Genetic Characterization of *Plasmodium berghei* Apicoplast Proteins

D i s s e r t a t i o n

zur Erlangung des akademischen Grades
d o c t o r r e r u m n a t u r a l i u m
(Dr. rer. nat.)
im Fach Biologie

eingereicht an der
Mathematisch-Wissenschaftlichen Fakultät I
der Humboldt-Universität zu Berlin

von
Dipl.-Biol. Joana Haußig

Präsident der Humboldt-Universität zu Berlin:
Prof. Dr. Jan-Hendrik Olbertz

Dekan der Mathematisch-Wissenschaftlichen Fakultät I:
Prof. Stefan Hecht PhD

Gutachter/innen:
1. Prof. Dr. Kai Matuschewski
2. Prof. Dr Susanne Hartmann
3. Prof. Dr. Frank Seeber

Tag der mündlichen Prüfung: 22.03.2013

Acknowledgements

I would like to express my very great appreciation to Prof. Dr. Kai Matuschewski for giving me the opportunity to write my thesis with him. It was truly a pleasure to work in your laboratory and without your advice, support, constructive suggestions, discussions and patience this dissertation would not have been possible! I would also like to express my gratitude for the possibility to go to various conferences and especially for the encouragement and support to take part in the Biology of Parasitism Summer Course in Woods Hole. This really was a once in a lifetime experience and provided me with a lot of enthusiasm.

I am particularly grateful for the supervision by Dr. Taco Kooij. Thanks for taking so much time for explanations and answering my questions. Your support, advice, encouragement, patience and humor were deeply appreciated.

I would like to thank Jan Burgold for the collaboration on the immunological experiments and Julius Hafalla for sharing pre-publication results.

Special thanks to Carolin Nahar for assistance on the initial animal experiments and Manuel Rauch for taking care of the cell culture. Your lab management was highly appreciated.

I would also like to acknowledge the assistance of the Flow Cytometry Core Facility at the Deutsches Rheuma-Forschungszentrum (Berlin) in the parasite cloning experiments.

A very big thanks to all past and present members of the Matuschewski lab for support, discussions, advice and company. You provided a great working atmosphere and I really enjoyed all the fun times we had together.

A special thanks to Ann-Kristin Mueller and Markus Ganter. You have been there right from the start, for discussions, advice, sharing their enthusiasm, and great friendship.

I would also like to thank the whole Levashina lab for the new input in our seminars and helpful discussions.

A big thanks to everyone that made the Biology of Parasitism Course possible and especially the whole class of 2010. I had an awesome, unforgettable time there and found true friends from all over the world.

Special thanks to my friends Philip, Julia, Giulia and Miguel for the highly appreciated help with the final proofreading.

This dissertation would not have been possible without the extraordinary support from my parents. I would like to thank them, all rest of my family and specially my grandmothers, for their amazing support, encouragement and interest in my work.
I am truly grateful for all my friends that have accompanied me along the way. A special thanks to Nasi, Caro, Jane and Fee for almost two decades of great friendship. Sabrina, Julia and Christian for always being there for encouragement and spending great times together. I would also like to thank my flamenco class and my Portuguese friends for making the time here in Berlin such an amazing experience.
Dear Philip, thanks for everything!!!

Summary

Malaria is caused by *Plasmodium*, an obligate intracellular eukaryotic pathogen that belongs to the phylum *Apicomplexa*. Apicomplexan parasites harbor an unusual plastid organelle, termed apicoplast. Several metabolic pathways, such as fatty acid biosynthesis type II, the non-mevalonate pathway of isoprenoid biosynthesis and iron-sulfur [Fe-S] cluster biosynthesis localize to the apicoplast. Because this unique organelle is indispensable for parasite growth it is a validated and attractive drug target. Using the rodent malaria parasite *Plasmodium berghei*, two different aspects of apicoplast protein functions were analyzed in this study. Firstly, a previously uncharacterized *Plasmodium* apicoplast protein, *Plasmodium*-specific Apicoplast protein important for Liver Merozoite formation (PALM), was investigated. It was shown that PALM localizes to the apicoplast and is expressed throughout the *Plasmodium* life cycle. Three independent *palm*$^{-}$ knockout parasite lines were generated by targeted gene deletion. Phenotypic analysis of these knockout lines revealed the importance of PALM for transition from liver- to blood-stage parasites. While the resulting knockout mutants developed normally for most of the life cycle, merozoite release into the blood stream and the ability to establish an infection was severely impaired. The presence of a signature blood-stage antigen, merozoite surface protein 1, indicated that *palm*$^{-}$ knockout parasites are arrested at a very late time point in liver-stage development. Experimental immunization of mice with *palm*$^{-}$ sporozoites elicited unprecedented potent and long-lasting protection against malaria re-infection. Immune profiling in old *palm*$^{-}$-immunized mice revealed persistence of antigen-specific IFNγ-secreting CD8^{+} T cells in the target organ, *i.e.* the liver. The results indicate that a tailor-made arrest in the final steps of hepatic merozoite formation could be an improvement over first-generation early liver-stage genetically arrested parasites (GAPs).

Secondly, the six nuclear-encoded components of the apicoplast [Fe-S] cluster biosynthesis pathway were systematically targeted by experimental genetics. The genes of plastid localized sulfur utilization factors (SUFs) were refractory to gene deletion, suggesting that they might be essential for parasite blood-stage development. In contrast, it was possible to ablate the gene encoding the nitrogen fixation factor U (NifU)-like scaffold protein (NFUapi). The resulting parasites were able to complete the entire life cycle, indicating redundant or non-essential, auxiliary functions of NFUapi. Together, my studies show that the *Plasmodium* apicoplast harbors previously unrecognized targets for anti-malaria intervention strategies.

Zusammenfassung

Malaria wird durch den einzelligen Parasiten *Plasmodium* verursacht. Hierbei handelt es sich um einen obligat intrazellulären, eukaryotischen Erreger, der zum Phylum der *Apicomplexa* gehört. *Apicomplexa* zeichnen sich durch das einzigartige Vorhandensein eines ungewöhnlichen Plastids, genannt Apicoplast, aus. Mehrere Stoffwechselwege wie zum Beispiel die Fettsäurebiosynthese Typ II, nicht-Mevalonat Biosynthese von Isoprenoiden und die [Fe-S]-Cluster Biosynthese wurden im Apicoplast lokalisiert. Die Exklusivität dieser Organelle und ihre metabolische Notwendigkeit für das Parasitenwachstum haben sie als attraktives pharmakologisches Ziel bestätigt. In dieser Arbeit wurden, unter Anwendung des Nagetier-Malariaerregers *Plasmodium berghei*, zwei verschiedene Aspekte von Apicoplast Proteinfunktionen untersucht. Zum Ersten wurde ein bislang unbeschriebenes *Plasmodium* Apicoplast Protein, Plasmodium-*specific Apicoplast protein important for Liver Merozoite formation* (PALM), charakterisiert. Es konnte gezeigt werden, dass PALM im Apicoplast lokalisiert ist und über den gesamten Lebenszyklus hinweg exprimiert wird. Drei voneinander unabhängige *palm*$^-$ Parasitenlinien, wurden durch zielgerichtete Gendeletion generiert. Die phänotypische Analyse dieser Knockout-Parasiten offenbarte die Bedeutung von PALM für den Übergang von Leber- zu Blutstadienparasiten. Die PALM Knockout-Mutanten entwickelten sich während eines Großteils des Lebenszyklus normal, jedoch war die Abgabe von Merozoiten in den Blutstrom und die Fähigkeit eine Blutstadien-Infektion zu etablieren signifikant beeinträchtigt. Die Anwesenheit eines charakteristischen Blutstadienantigens, merozoite surface protein 1 (MSP1), wies darauf hin, dass *palm*$^-$ Parasiten zu einem sehr späten Zeitpunkt der Leberstadienentwicklung arretiert sind. Experimentelle Immunisierung von Mäusen mit *palm*$^-$ Sporozoiten bewirkte einen starken und langanhaltenden Schutz gegen Reinfektion mit Malaria. Immunologische Analysen in alten *palm*$^-$ immunisierten Mäusen wiesen die Persistenz von Antigen-spezifischen IFNγ-sekretierenden CD8$^+$ T-Zellen im Zielorgan (der Leber) nach. Diese Ergebnisse lassen darauf schließen, dass Parasiten mit einem Arrest in den finalen Schritten der Bildung von Leberstadien-Merozoiten einen Vorteil gegenüber genetisch attenuierten Parasiten der ersten Generation haben, die in der frühen Leberstadienentwicklung arretiert sind.

Zum Zweiten wurden die sechs Nucleus-kodierten Komponenten der [Fe-S] Cluster Biosynthese im Apicoplast systematisch durch experimentelle Genetik analysiert. Die

Gene der im Plastid lokalisierten *sulfur utilization factors* (SUFs) konnten nicht deletiert werden, was darauf hindeutet, dass sie möglicherweise eine essenzielle Rolle in der Blutstadientwicklung der Parasiten spielen könnten. Im Gegensatz dazu konnte das Gen, welches das *nitrogen fixation factor U (NifU)-like scaffold* Protein (NFUapi) kodiert, deletiert werden. Die resultierenden Parasiten konnten den gesamten Lebenszyklus durchlaufen, was auf eine redundante oder nicht-essenzielle Funktion von NFUapi hindeutet. Insgesamt zeigen meine Studien, dass bisher unbekannte Ziele im *Plasmodium* Apicoplast für Interventionsstrategien gegen Malaria geeignet sind.

Table of contents

1 Introduction

1.1 *Plasmodium* and related apicomplexan parasites

Plasmodium, the etiologic agent of malaria, is an obligate intracellular eukaryotic pathogen that belongs to the phylum *Apicomplexa*. Their complex life cycle includes a vertebrate host and an insect vector, typically mosquitoes of the genus *Anopheles*.

Five *Plasmodium* species are known to infect humans, namely *P. falciparum*, *P. vivax*, *P. ovale*, *P. malariae*, and *P. knowlesi*. In 2010, about 216 million cases of malaria were reported, most of them in sub-Saharan Africa (WHO, 2011). *P. falciparum* is the deadliest *Plasmodium* species to humans, often causing deaths in children under the age of five, pregnant women and non-immune adults (WHO, 2011). All clinical malaria symptoms are caused by the blood-stage phase of infection. They include fever, anemia, coma, respiratory distress, and renal dysfunction (Beeson and Brown, 2002; Marsh et al., 1995). *P. vivax* is the most common species outside Africa and is difficult to control and treat because dormant liver stages, termed hypnozoites, can lead to relapses of malaria. Primaquine is currently the only available curative drug targeting this stage and preventing relapses (Cogswell, 1992; Wells et al., 2010).

The impact of *Plasmodium* on mankind is highlighted by the fact that malaria parasites have imposed strong selective forces on the human genome in endemic regions. Balanced polymorphisms, such as sickle cell anemia and hemoglobinopathies, confer protection against malaria. This has led to significant co-adaptation of human populations in malaria endemic regions with malaria parasites (Driss et al., 2011).

There are dozens of *Plasmodium* species, however, that do not infect humans, but infect a variety of hosts, such as primates (*P. reichenowi*), rodents (*P. berghei*), birds (*P. gallinaceum*), and reptiles (*P. mexicanum*) (Martinsen et al., 2008).

The phylum *Apicomplexa* also includes various other parasites of medical and veterinary importance, such as *Toxoplasma gondii*, *Theileria* spp., *Babesia* spp., and *Cryptosporidium* spp. (Fig. 1.1).

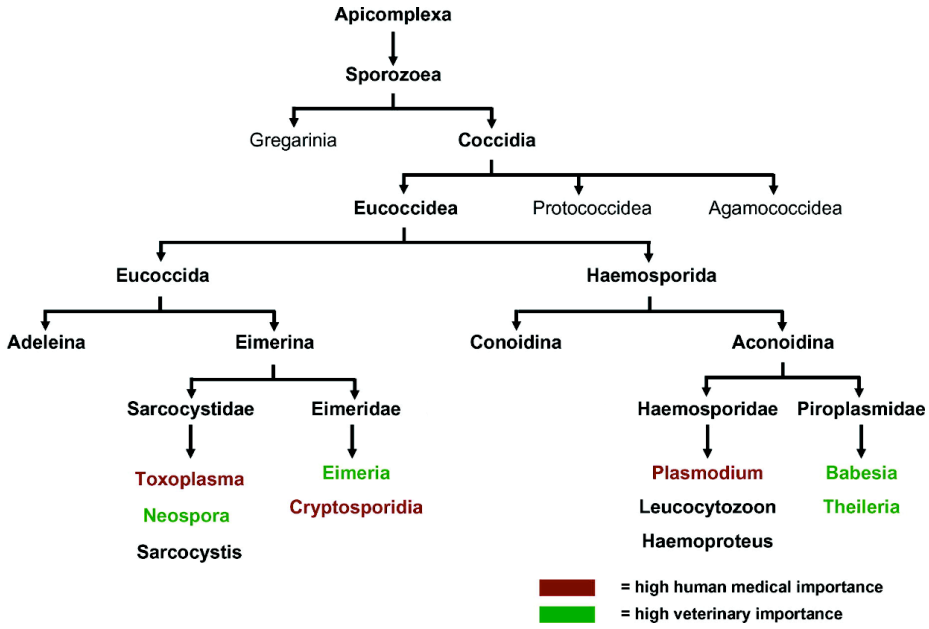

Figure 1.1: Phylogenetic tree of the *Apicomplexa*.

Phylogenetic tree of the phylum *Apicomplexa*. Selected parasites of human or veterinary importance are highlighted in red and green, respectively. Modified from (Beck et al., 2009).

Infection with *Toxoplasma gondii* is one of the most common parasitic infections of humans and other warm-blooded animals. The definitive hosts of *T. gondii* are cats, where sexual recombination occurs. *T. gondii* infection is common in humans and most infections are asymptomatic. However, under certain circumstances the parasite can cause a devastating disease, for example in immunosuppressed individuals or when congenitally acquired. Toxoplasmosis is acquired by ingestion of oocysts or bradyzoites in the host tissue. After ingestion, the parasites penetrate intestinal epithelial cells, multiply in the intestine and then spread throughout the organism where they are able to infect virtually any nucleated cell (Hill et al., 2005).

Protozoa of the genus *Babesia* infect a wide range of wild and domestic animals, causing fatal diseases, especially in domestic ones. Additionally, cases of human babesiosis have sporadically been diagnosed, mainly in North America and Europe (Hunfeld et al., 2008). *Babesia* is transmitted by ixodid ticks. During a tick bite sporozoites are directly injected into the bloodstream where they infect erythrocytes. Infection causes a host-mediated pathology and erythrocyte lysis, resulting in anemia and, occasionally, organ failure (Hunfeld et al., 2008).

Theileria are intracellular protozoa, which infect wild and domestic ruminants. Like *Babesia*, they are transmitted by ticks, however, in the mammalian host, parasites infect leukocytes and erythrocytes. The schizont stages of certain *Theileria* species

induce a lymphoma-like phenotype in infected host leukocytes by inducing proliferation of the infected cells (Bishop et al., 2004).

Cryptosporidiosis most commonly affects neonatal calves. However, infections can also occur in many other mammals and birds. Some *Cryptosporidium* species, e.g. *C. hominis* and *C. parvum*, are infectious to humans. Cryptosporidiosis is one of the most common causes of infectious diarrhea. In immunodeficient or immunosuppressed individuals it can cause a chronic, life-threatening diarrhea. Transmission occurs through the ingestion of infectious oocysts with contaminated water or food (Chako et al., 2010).

1.2 The *Plasmodium* life cycle

Plasmodium is transmitted to the vertebrate hosts during the bites of infectious female *Anopheles* mosquitoes (Fig. 1.2).

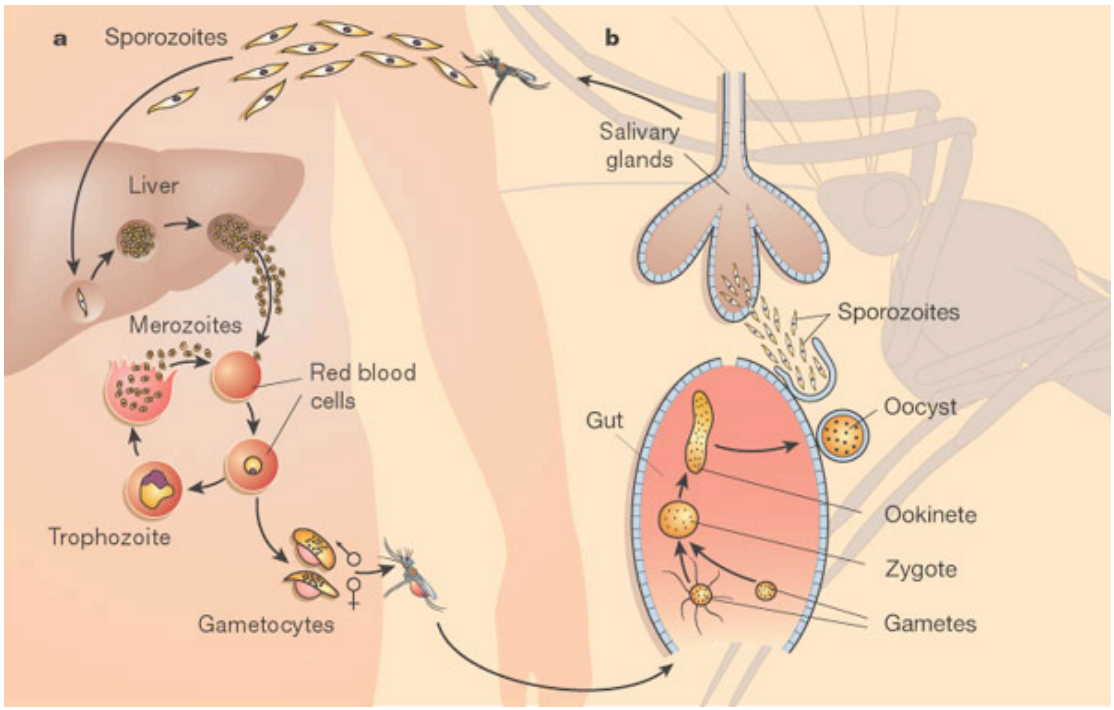

Figure 1.2: *Plasmodium* life cycle.

Schematic overview of the *Plasmodium* life cycle in the human host (a) and the mosquito vector (b). For details see main text in section 1.2. From (Wirth, 2002).

During blood feeding, sporozoites are injected into the host dermis where they rapidly migrate through the skin and enter a blood capillary (Amino et al., 2006).

Approximately 15 minutes after the mosquito bite, the first wave of migrating sporozoites has left the bite site and moved into the general circulation (Sidjanski and Vanderberg, 1997). Sporozoite migration is dependent on their ability to move by substrate-dependent locomotion, called gliding motility, that relies on the parasite's actomyosin motor (Amino et al., 2008; Menard, 2001).

Some sporozoites appear to transform in the skin (Gueirard et al., 2010), but recent studies showed that this process does not contribute to blood-stage infection (Voza et al., 2012).

Interestingly, sporozoites are highly infectious to the vertebrate host only after migration into the mosquito salivary glands (Vanderberg, 1975). In a screen using suppression subtractive cDNA hybridization, genes that are upregulated in infective sporozoites (UIS) were identified (Matuschewski et al., 2002). Some *UIS* genes were later shown to be crucial to establish infection in the vertebrate host (Mueller et al., 2005a; Mueller et al., 2005b; Zhang et al., 2010).

Once in the liver, sporozoites pass the liver sinusoidal barrier by transmigration through Kupffer cells (Frevert et al., 2005; Frevert et al., 2006; Frevert et al., 2008b; Ishino et al., 2005a; Ishino et al., 2004).

Sporozoites traverse several hepatocytes by breaching their plasmamembranes before finally taking residence in a suitable hepatocyte (Frevert et al., 2005; Mota et al., 2001). Final target cell entry coincides with the formation of a replication-competent niche, termed the parasitophorous vacuole (PV), which originates from the host cell plasma membrane (Sibley, 2011). The parasitophorous vacuole membrane prevents fusion of the developing parasite with endosomal compartments, thus providing a safe environment for liver-stage development.

Upon successful invasion of a hepatocyte, a central spherical bulb forms around the nucleus, and the two distal ends of the sporozoite retract (Jayabalasingham et al., 2010). The trophozoite then grows extensively, and multiple rounds of DNA replication occur. During this time the parasite organelles are also replicated (Stanway et al., 2011). Through this process, called schizogeny, and the following invaginations of the parasite plasma membrane thousands of first-generation merozoites are formed, which are then released into the blood stream in vesicles, termed merosomes (Sturm et al., 2006). The parasite development in the liver takes 5 to 7 days in *Plasmodium* species infecting humans, but only about two days in rodent malaria species. After being released in the pulmonary microvasculature (Baer et al., 2007), free merozoites quickly invade red blood cells, thus initiating a

malaria blood-stage infection. The subsequent fast rounds of asexual replication through schizogeny within host erythrocytes allow the parasite population to multiply exponentially. Infection of erythrocytes is the exclusive phase that causes all clinical manifestations of malaria (Haldar et al., 2007). The various erythrocytic parasite stages can be diagnosed microscopically in Giemsa-stained thin blood smears. Ring stages, trophozoites, schizonts, merozoites, and gametocytes can be distinguished. A fraction of blood-stage parasites develops into sexual stages in a process that is not yet completely understood (Kooij and Matuschewski, 2007). Parasites are transmitted to the insect vector by ingestion of gametocytes by a mosquito during a blood meal.

Exflagellation of male microgametes in the mosquito midgut is triggered by a mosquito-derived molecule, xanthurenic acid, in addition to a drop of temperature and a change in pH (Billker et al., 1998; Billker et al., 1997). The male microgametes then fertilize female macrogamete forming zygotes, which are the only diploid stages of the otherwise haploid parasites. After zygote formation meiosis takes place and genetic recombination occurs (Sinden and Hartley, 1985). Zygotes develop into motile ookinetes, which then leave the blood bolus by penetration of the peritrophic matrix that encloses the blood meal and traverse the epithelial layer of the mosquito midgut. After egress from the basal side of the epithelium ookinetes encounter the midgut basal lamina where they transform into sessile extracellular oocysts (Siden-Kiamos and Louis, 2004). The oocysts start growing, and through sporogeny, a process that takes 10 to 14 days, hundreds of haploid sporozoites are formed (Matuschewski, 2006).

When this development is completed, sporozoites are released into the hemocoel and migrate to the salivary glands (Matuschewski, 2006). Once mature sporozoites reach the salivary glands they are infectious and can be transmitted to a new vertebrate host by mosquito bite.

.

1.3 Rodent malaria models

Malaria research greatly relies on animal models, as studies with human *Plasmodium* species are very limited for ethical reasons. Human *Plasmodium* spp. are inaccessible for *in vivo* investigations because access to organs such as liver, lungs and spleen is not possible. Laboratory research with human *Plasmodium* species is restricted to culture of blood stages, mosquito infections via membrane feedings and

infection of primary human hepatocytes, therefore, it is currently not possible to reproduce the whole parasite life cycle. This limits research on host immune responses, parasite adaptations and mechanisms of disease. To overcome these limitations and to complement studies on human malaria, several animal models are available, e.g. avian, primate and rodent malaria models. The murine models are the most widely used, as they are more closely related to the human species than the avian models (Martinsen et al., 2008). They are also cheaper, easier to handle, and arising less ethical concerns than primate models.

The rodent *Plasmodium* species *P. berghei*, *P. yoelii*, *P. chabaudi* and *P. vinckei* were initially isolated from thicket rats in Central Africa and have been adapted to grow in laboratory rodents, principally mice and rats (Carlton et al., 2001). The different species and laboratory strains differ in various aspects, such as their preferences to infect reticulocytes or mature erythrocytes. In addition, lethal and non-lethal strains can be distinguished (Wykes and Good, 2009).

Apart from the great advantage that the whole parasite life cycle can be reproduced and analyzed in the laboratory, rodent malaria parasites offer the possibility of easier and faster genetic modifications than *P. falciparum* (Janse et al., 2006c). Genetic manipulation of mosquitoes (Blandin et al., 2009), mice (Kordes et al., 2011) and malaria parasites (Mueller et al., 2005a) allows the investigation of specific gene functions from the host and the parasite perspectives. In addition, the generation of fluorescent parasite lines has opened the possibility to visualize the parasites live in the vertebrate host (Amino et al., 2007).

The importance of murine malaria models is highlighted by their wide applications, such as immunopathogenesis (Lamb et al., 2006), vaccine development (Khan et al., 2012), drug discovery (Fidock et al., 2004), drug resistance (Carlton et al., 2001), host-parasite interactions (Franke-Fayard et al., 2010) and placental malaria (Hviid et al., 2010).

Recently, progress was achieved in the use of humanized mouse models to study blood-stage and liver-stage development of *P. falciparum* in mice (Legrand et al., 2009; Vaughan et al., 2012). However, to date no model allows the combined study of liver- and blood-stage development in one system. This would be of great value to study the safety of whole-organism vaccines, efficacy of drugs, and biology of dormant liver stages of *P. vivax*, for instance (Vaughan et al., 2012).

One of the most controversially discussed topics is the relevance of murine models for the investigation of cerebral malaria (CM), a life-threatening complication of *P.*

falciparum infection (Hunt et al., 2010; White et al., 2010). *P. berghei* ANKA in combination with susceptible strains of mice, such as C57BL/6, replicates many aspects seen during human CM and is accepted as the best available model of experimental cerebral malaria (ECM) (de Souza et al., 2010). Infection of susceptible strains of mice leads to the development of fatal cerebral pathology, with clinical signs including ataxia, fitting, respiratory distress and coma (de Souza and Riley, 2002). Human CM and murine ECM share several common features such as cytokine production, reduced blood flow, and increased lactate production in the brain (Hunt et al., 2010). However, there are also marked differences such as the sequestration of parasitized erythrocytes in human CM, in contrast to the accumulation of leukocytes and platelets in the venules and capillaries of the brain in the murine model (White et al., 2010).

The model system always needs to be carefully chosen according to the research question asked and it has to be kept in mind that results of studies with animal models cannot be simply extrapolated to the human pathogens. Despite the differences between human and rodent malaria parasites, rodent malaria models have proven to be invaluable for malaria research.

1.4 Apicoplast- the plastid of *Apicomplexa*

1.4.1 The *Plasmodium* apicoplast

Plasmodium contains three classes of DNA, the nuclear genome, the mitochondrial genome, and a 35kb circular genome. The 35kb circular DNA was shown to encode a genome similar to that of plant plastids (Williamson et al., 1994; Wilson et al., 1996). The plastid-like DNA was shown to localize to a membrane-bound organelle in *T. gondii*, which then was termed “apicoplast” (Kohler et al., 1997; McFadden et al., 1996). Most parasites of the genus *Apicomplexa* studied so far contain an apicoplast with the exceptions of *Cryptosporidium parvum* (Zhu et al., 2000) and *Gregarina niphandrodes* (Toso and Omoto, 2007). The apicoplast of *Plasmodium* and *Toxoplasma* is essential for parasite growth (Fichera and Roos, 1997; He et al., 2001; McConkey et al., 1997) and has attracted attention as a drug target.

The apicoplast is thought to originate from a complex event of secondary endosymbiosis, i.e. it is derived from two serial endosymbiotic events (Kalanon and

McFadden, 2010). The primary endosymbiosis resulted from a eukaryote that engulfed and retained a photosynthetic cyanobacterium bounded by two membranes, which led to the lineages of Glaucocystphytes, red algae and Viridiplantae. The second endosymbiosis led to the engulfment of this eukaryote by a second eukaryote, which then gave rise to the Chromalveolates, including *Plasmodium* spp., *Toxoplasma gondii*, *Cryptosporidium* spp., *Theileria* spp. and *Babesia* spp. It has initially been debated if the apicoplast is of red (Waller et al., 2003; Williamson et al., 1994) or green algal origin (Funes et al., 2002; Kohler et al., 1997). More recently, the red algal origin is favored (Janouskovec et al., 2010). For instance, the plastid genome phylogenies of *Chromeria velia*, a recently described photosynthetic alveolate, is closely related to apicomplexan parasites (Moore et al., 2008).

The process of secondary endosymbiosis gave rise to the four membranes surrounding the apicoplast (McFadden et al., 1996). The current model suggests that the outermost membrane is derived from the phagotrophic digestive vacuole that engulfed the red alga and is connected to the ER membrane (Cavalier-Smith, 2000). The second outermost membrane is called periplastid membrane and is derived from the plasma membrane of the red alga. The two inner membranes are called inner and outer membrane and originate from the inner and outer membrane of the primary plastid, respectively (Kalanon and McFadden, 2010).

The 35kb circular plastid genome of *Plasmodium* encodes an inverted tandem repeat encompassing large- and small- subunit rRNA genes, 17 ribosomal proteins, a complete set of tRNAs, three subunits of a bacterial-type RNA polymerase, translation elongation factor Tu (EF-Tu), a member of the Clp family of molecular chaperones, SufB, and a few orphan open reading frames (Wilson et al., 1996). As a consequence, almost all apicoplast proteins are encoded in the nucleus. As in plant chloroplasts (Martin et al., 1998) this probably happened through gene transfer from the endosymbiont to the host (Huang et al., 2004; Waller et al., 1998). This requires an import machinery that allows specific targeting to the apicoplast and transport through the four membranes into the apicoplast.

Generally, targeting to the apicoplast occurs by a N-terminal bipartite leader sequence consisting of a signal peptide (SP) and a transit peptide (TP)/ apicoplast targeting signal (ATS) (Waller et al., 1998). The SP mediates the entry into the secretory pathway and, most likely, is cleaved off during the co-translational import (Waller et al., 2000). The TP is necessary to direct the protein to the apicoplast. It is overall positively charged and enriched in certain amino acids (Foth et al., 2003a).

Experiments testing randomly scrambled sequences as TP showed that rather than a consensus sequence, an appropriate amino acid composition is sufficient for correct targeting (Tonkin et al., 2008). Furthermore, a chaperone-binding site can be critical for efficient and accurate targeting (Foth et al., 2003a). A stromal processing peptidase (SPP) has been proposed to cleave the TP in *P. falciparum* (van Dooren et al., 2002). However, a recent screen based on mRNA abundance over the cell cycle and on phyletic abundance in *Toxoplasma* identified new apicoplast-targeted proteins that lack this bipartite leader sequence (Sheiner et al., 2011).

At present, 3 bioinformatics programs are available to predict targeting to the apicoplast. Two of them, PATS (Zuegge et al., 2001) and PlasmoAP (Foth et al., 2003a) are optimized for *P. falciparum* sequences. Recently, another program was published, ApicoAP (Cilingir et al., 2012a), that predicts apicoplast targeting for *P. falciparum*, *P. yoelii*, *T. gondii* and *B. bovis*. Using PlasmoAP in a genome-wide screen, 466 candidate proteins for apicoplast targeting were identified in *P. falciparum* (Foth et al., 2003a). This set of putative apicoplast proteins was of great importance for reconstruction of several metabolic pathways that are thought to be present in the apicoplast (Ralph et al., 2004) and also explained why this organelle is essential for parasite survival.

At present, the molecular mechanisms of protein translocation through the four apicoplast membranes is poorly understood. The first membrane is probably overcome by the co-translation import into the ER that is mediated by the SP, as the outermost apicoplast membrane is connected to the ER membrane (McFadden, 1999). The periplastid membrane probably is traversed with the help of an apicoplast-localized ER-associated degradation (ERAD) system (Kalanon et al., 2009; Sommer et al., 2007; Spork et al., 2009). As the two innermost apicoplast membranes are derived from the cyanobacterium, engulfed during primary endosymbiosis, the translocation through these membranes is predicted to be mediated by the translocon of outer envelope of chloroplast (TOC) and the translocon of inner envelope of chloroplast (TIC). So far, two TIC components (Kalanon et al., 2009; van Dooren et al., 2008), but no TOC components have been described in apicoplasts.

In *Plasmodium*, each parasite contains one apicoplast that changes its size and shape during the life cycle (Fig. 1.3). In studies using GFP as a reporter, it was shown that in erythrocytic stages the apicoplast develops from a small punctate

organelle in merozoites and ring stages to a complex branched structure in schizonts (Waller et al., 2000) (Fig. 3.1).

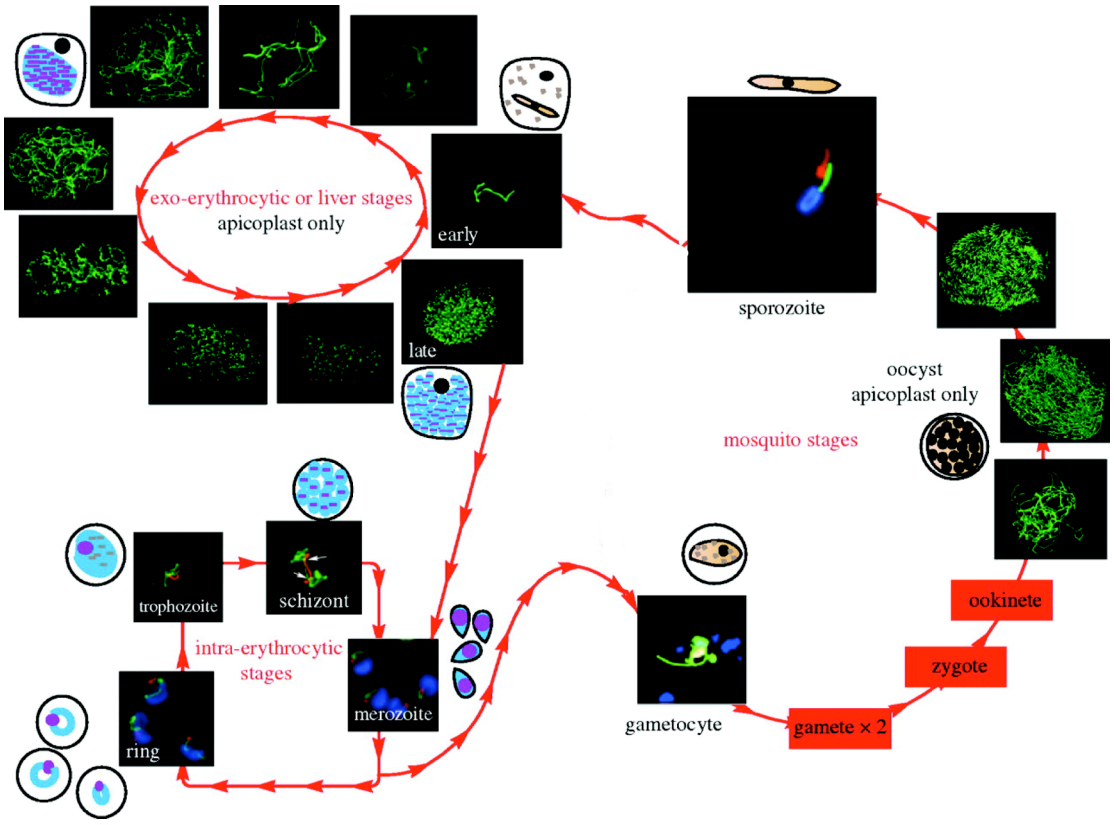

Figure 1.3: Apicoplast morphology during the *Plasmodium* life cycle.
In the non-erythrocytic stages of the parasite, green denotes apicoplast and red denotes mitochondrion. In the intra-erythrocytic stages and the gametocyte, green denotes mitochondrion and red denotes apicoplast. Blue denotes nucleus in all stages. Modified from (Lim and McFadden, 2010).

During gametocytogenesis, the apicoplast stays round or slightly elongated (Okamoto et al., 2009). The male microgametes do not contain an apicoplast or mitochondrion (Okamoto et al., 2009), which is consistent with the maternal inheritance of these organelles (Creasey et al., 1994). In oocysts the apicoplast again displays a branched structure and after segregation into sporozoites can be seen as a round or slightly elongated structure (Fig. 1.3). Similar to asexual blood stages, in liver stages the apicoplast expands from a small dot in early to a complex reticulate structure in later stages (Stanway et al., 2009). The apicoplast and the mitochondrion are tightly associated throughout most life-cycle stages (Okamoto et al., 2009; Stanway et al., 2011; van Dooren et al., 2005). This might be important for

the heme biosynthesis pathway, which is shared between the two organelles (Sato et al., 2004; van Dooren et al., 2006).

Recently, a novel trafficking pathway in *P. falciparum* was proposed for the localization of glutathione peroxidase-like thioredoxin peroxidase, which is localized to the apicoplast, the mitochondrion, and the cytosol (Chaudhari et al., 2012). The authors suggest that a common pathway for the dual localization of a single gene product, such as the primitive endoplasmic reticulum- Golgi route, may have been retained as opposed to optimization for individual organellar import pathways.

Like all plastids, the apicoplast cannot be created *de novo*. Therefore, this organelle and its genome have to be divided and segregated into every parasite during replication. To date, little is known about the molecules involved in this process in *Plasmodium*. However, it could be shown that in a tightly regulated process the apicoplast divides prior to the mitochondrion in asexual blood stages and liver stages (Stanway et al., 2011; van Dooren et al., 2005).

1.4.2 *Plasmodium* apicoplast pathways and drug targets

Since the apicoplast is not photosynthetically active, its essentiality must be based on other pathways. With the help of *in silico* analysis and expanding experimental work various pathways could be mapped to the apicoplast (Ralph et al., 2004; Seeber and Soldati-Favre, 2010). The bacterial origin of the apicoplast renders it a good drug target, because it harbors pathways that either are not present in humans and animals or some enzymes differ substantially. Here, a brief overview of the currently known *Plasmodium* apicoplast pathways is given.

<u>DOXP pathway of isoprenoid synthesis</u>

Isoprenoids are a group of highly diverse natural compounds that play key roles in a variety of processes in *Plasmodium*, including protein prenylation and carotenoid biosynthesis (van der Meer and Hirsch, 2012). The precursors for isoprenoids are isopentenyl diphosphate (IPP) and dimethylallyl diphosphate (DMAPP). Their products are also needed for the transfer of glycosylphosphatidyl inositol (GPI)-anchors of membrane-bound proteins, such as merozoite surface proteins (Davidson and Gowda, 2001; Gowda et al., 1997; Orlean, 1990).

In mammals, yeast, higher plants, and archaebacteria, IPP is generated through the mevalonate pathway, which starts with the synthesis of mevalonate from acetyl-CoA. In bacteria and plants an alternative pathway is used for IPP production, which does not use mevalonate as a precursor (Rohmer et al., 1993). This pathway was also shown to be located in the apicoplast (Jomaa et al., 1999). The non-mevalonate pathway uses pyruvate and glyceraldehydes 3-phosphate (GA3P) as substrates to generate 1-deoxy-D-xylulose 5-phosphate (DOXP), which then is converted to 2-C-methyl-erythritol 4-phosphate (MEP). IPP is then generated from MEP after several consecutive enzyme reactions. For this reason the non-mevalonate pathway of isoprenoid biosynthesis is also called DOXP pathway. Attempts to delete DOXP reductoisomerase (Dxr) in *P. falciparum* were unsuccessful, strongly suggesting that this pathway is essential for blood-stage parasites (Odom and Van Voorhis, 2010).
Fosmidomycin is an inhibitor of the DOXP reductoisomerase (DXR) (Jomaa et al., 1999). Recently, it was shown that fosmidomycin might also act on a second enzyme of the DOXP pathway, methylerythritol phosphate cytidyltransferase (IspD), downstream of DXR (Zhang et al., 2011). Fosmidomycin is successfully used to treat malaria blood-stage infection (Borrmann et al., 2004). However, it does not act on *T. gondii*, although the DOXP pathway including DXR is present there. This difference has been attributed to the poor uptake of the drug (Nair et al., 2011). It is still a matter of debate if fosmidomycin acts on *P. berghei* liver stages, as contradictory results have been published recently (Baumeister et al., 2011; Nair et al., 2011).
In a recent paper the DOXP pathway of isoprenoid biosynthesis was suggested to be the sole reason for the essentiality of this pathway in *P. falciparum* blood stages (Yeh and DeRisi, 2011). The authors treated *P. falciparum* blood-stage cultures with azithromycin, a drug that acts on the apicoplast and eventually leads to parasite death. They were able to rescue parasite death by supplementation with IPP, the precursor for isoprenoid biosynthesis. However, it remains unclear what happens to other nuclear-encoded apicoplast proteins and if some of them might still be able to fulfill (part of) their functions if they are not targeted to the apicoplast. If this were the case, there might be other essential pathways in *Plasmodium* blood stages that are simply not affected by azithromycin treatment.

Type II fatty acid synthesis

Plasmodium has a high demand for lipids and phospholipids as it harbors various additional organelles that are membrane-bound, e.g. the apicoplast, micronemes and

rhoptries (Palacpac et al., 2004). It also requires membranes during schizogeny for thousands of daughter parasites.

The eukaryotic fatty acid synthase type I (FASI) combines all enzymatic steps in one large cytoplasmic multifunctional enzyme (Leibundgut et al., 2008). The bacterial type II pathway of fatty acid synthesis (FASII) was the first pathway assigned to the apicoplast (Waller et al., 1998). The fatty acid chain elongation step of FASII consists of the cycling of the growing fatty acyl moiety through four key enzymes: β-ketoacyl-acyl carrier protein (ACP) synthase I/II (FabB/F), β-ketoacyl ACP reductase (FabG), β-hydroxyacyl-ACP dehydratase (FabZ), enoyl-ACP reductase (FabI) (Ralph et al., 2004; Waller et al., 1998). Acyl carrier protein (ACP) serves to shuttle the growing fatty acids between the enzymes and successive cycles through the elongation pathway typically lead to the formation of fatty acyl ACPs of about 12 carbons (Upadhyay et al., 2009).

For a long time the FASII pathway was thought to be essential for *Plasmodium* blood stages, because triclosan, a drug inhibiting bacterial FabI (Stewart et al., 1999), inhibited growth of asexual blood stages (Surolia and Surolia, 2001). However, it could be shown that triclosan does not target the *Plasmodium* FabI, and its efficacy on blood stages is probably an off-target effect (Yu et al., 2008). Additional proof was generated by targeted gene deletions of the enzymes involved in this pathway (Vaughan et al., 2009; Yu et al., 2008). Theses studies showed that in *Plasmodium* FASII is only essential for liver stages. Ablation of these enzymes resulted in late liver-stage arrested parasites, whereas development of blood and mosquito stages remained unaffected. It is unclear if this is due to the requirement of unique fatty acids during liver-stage schizogeny that only the parasite can synthesize or simply the quantity of lipids required for membrane biogenesis to form tens of thousands of infectious merozoites (Tarun et al., 2009). Several studies have now identified inhibitors of the FAS II pathway validating this pathway as a drug target for causative treatment (Goodman and McFadden, 2007).

Lipoic acid biosynthesis

Lipoic acid is an essential cofactor of multienzyme-complexes in the apicoplast and mitochondrion of *Plasmodium*, such as the apicoplast pyruvate dehydrogenase (PDH). In *Plasmodium,* the mitochondrion can salvage lipoic acid. *De novo* lipoic acid biosynthesis is confined to the apicoplast and depends on the supply of octanoyl-acyl carrier protein (ACP), an intermediate of fatty acid biosynthesis, which is transferred

by LipB (Thomsen-Zieger et al., 2003; Wrenger and Muller, 2004). However, disruption of the *LipB* gene had no detrimental effect on parasite growth (Gunther et al., 2007). Despite the great decrease of lipoic acid, the apicoplast PDH still showed lipoylation. It was shown that LipB function can be compensated for by a lipoic acid protein ligase, which is dually targeted to the apicoplast and mitochondrion (Gunther et al., 2007).

Efforts to generate *LipA* knockout mutants in *Plasmodium* were so far unsuccessful, suggesting that the protein is essential for the survival of the malaria parasites (Gunther et al., 2009).

Heme biosynthesis

Heme is an important prosthetic group of proteins such as cytochromes (Meunier et al., 2004). Although a lot of heme is released during parasite digestion of hemoglobin during blood stage development and even has to be polymerized into non-toxic hemozoin crystals (Sullivan et al., 1996), heme *de novo* biosynthesis appears to be essential for *Plasmodium* (Ramya et al., 2007; Surolia and Padmanaban, 1992).

The biosynthesis of heme in *Plasmodium* is split between the apicoplast and the mitochondrion (Ralph et al., 2004; Sato et al., 2004; van Dooren et al., 2006). This stands in contrast to animals and plants, where the heme biosynthesis takes place exclusively either in the mitochondrion or mainly in the plastid, respectively (Heinemann et al., 2008; Tanaka and Tanaka, 2007). Heme biosynthesis in *Plasmodium* starts in the mitochondrion from glycine and succinyl-CoA and the pathway later continues in the mitochondrion (Sato et al., 2004; Varadharajan et al., 2002).

[Fe-S] cluster biogenesis

The apicoplast of *Plasmodium* also harbors the SUF (sulfur utilization factor) system for [Fe-S] cluster biogenesis, which will be described in more detail below (chapter 1.7.2).

Thanks to the bacterial origin of the apicoplast, many housekeeping functions also differ from the host and therefore present good drug targets. The application of antimalarials, targeting these pathways, benefits enormously from the extensive research on these processes in bacteria. Antibiotics targeting DNA replication (e.g. ciprofloxacin), RNA transcription (e.g. rifampicin) and protein translation (e.g.

azithromycin, clindamycin) have been shown to effectively act on *Plasmodium* and other *Apicomplexa* (Ralph et al., 2001; Seeber, 2003). Interestingly, drugs targeting the apicoplast housekeeping functions cause the so-called “delayed-death” phenotype. This phenotype was observed for the first time in *T. gondii* after treatment with clindamycin and describes the phenomenon that treatment with some antibiotics does not kill the treated parasites directly, but causes them to produce progeny that are unable to complete a replicative life cycle (Fichera et al., 1995; Pfefferkorn et al., 1992). This is probably due to the distribution of nonfunctional apicoplasts into the progeny (Fichera and Roos, 1997).

1.5 Liver-stage genetically arrested parasites (GAPs) in *Plasmodium*

The first successful malaria vaccine strategy, using radiation-attenuated sporozoites (RAS), was developed 45 years ago and has since remained the benchmark for malaria vaccine development (Nussenzweig et al., 1967). RAS are capable of establishing a normal hepatocyte infection including parasite vacuole formation. However, they then fail to grow and replicate. Immunization with at least three doses of RAS induces protracted, often sterile, protection in murine malaria models (Nussenzweig et al., 1967), non-human primates (Gwadz et al., 1979), and humans (Clyde, 1975; Hoffman et al., 2002).

Several decades later a new benchmark was set in the form of genetically attenuated parasites (GAPs) (Mueller et al., 2005b). Since then, a wide range of GAPs have been generated that arrest at different points of liver stage development (Fig. 1.4).

GAPs can assist malaria research in at least three ways: (1) phenotypic analysis of mutants can hint at possible function(s) of the missing protein, unraveling previously unknown mechanisms of parasite development. (2) attenuated parasites inform anti-malaria vaccine strategies, as they can be used to analyze the immunological mechanisms involved in protection against parasites. (3) GAPs might be used as whole-organism vaccines. To achieve the latter, however, extensive research and optimization is still needed to ensure safety and efficacy. This includes generation of parasites with a complete arrest without breakthrough infections, which might be achieved by simultaneous deletion of various genes. Production processes, storage and routes of administration of *Plasmodium* whole-organism vaccines are currently under investigation (Hoffman et al., 2010; Ploemen et al., 2012).

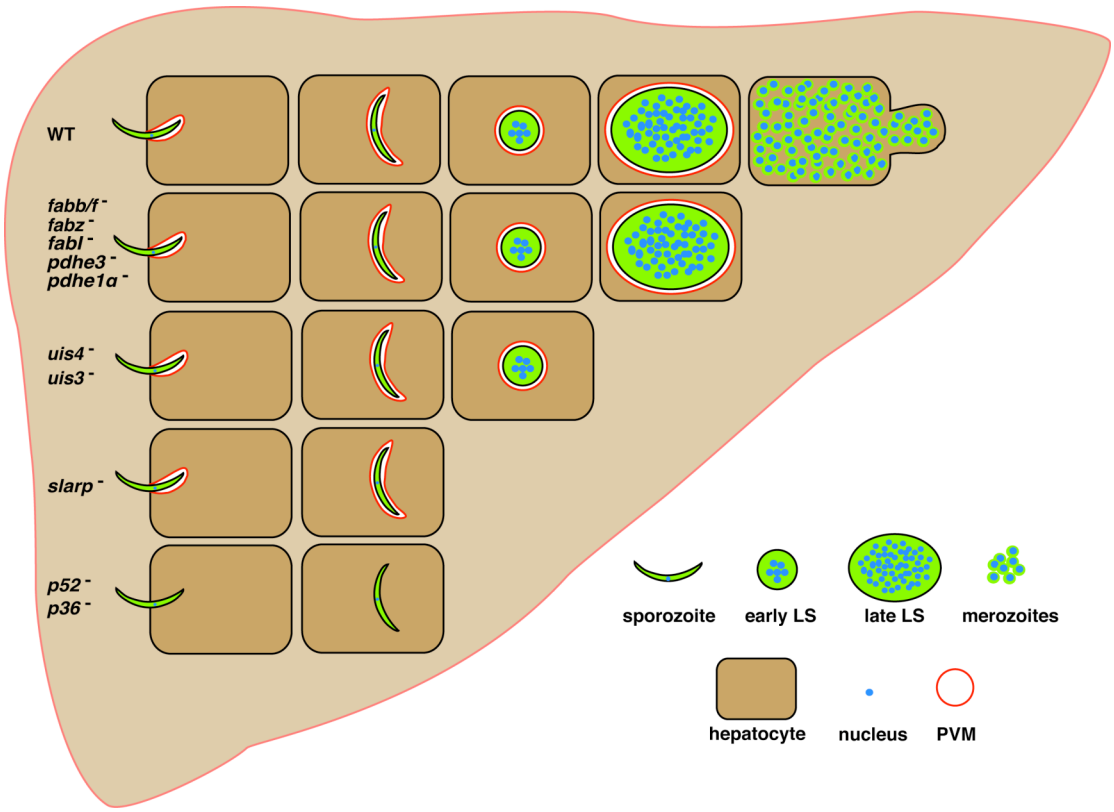

Figure 1.4: Developmental arrest in liver stages of rodent genetically attenuated parasites (GAPs).

WT sporozoites invade hepatocytes by formation of a parasitophorous vacuole (PV) (red). Subsequently sporozoites round up into early liver stages and nuclei (blue) start to divide. The parasite grows and nuclear division progresses in late liver stages. Liver-stage development is finalized by merozoite formation and release of merozoites in merosomes. GAPs are arrested at different time points of this development. Modified from (Vaughan et al., 2010).

The parasites with the earliest arrest in liver-stage development are ***Pbp36***$^{-}$ and ***Pbp52***$^{-}$ (= *Pbp36p*$^{-}$) mutants (Ishino et al., 2005b; van Dijk et al., 2005). Ishino and colleagues generated these mutants and described them as having an extremely elevated cell traversal rate and a very low infection rate in hepatoma cells. In the few cases, where early liver stages were formed, they were much smaller than WT liver stages (Ishino et al., 2005b). However, Dijk and colleagues showed that *Pbp52*$^{-}$ (= *Pbp36p*$^{-}$) parasites are able to traverse and infect hepatocytes as well as WT parasites. *Pbp52*$^{-}$ parasites arrest early in liver stage development, fail to maintain a parasitophorous vacuole (PV) and most of them can no longer be detected at 24 hours after hepatocyte invasion (van Dijk et al., 2005). However, occasional

breakthrough blood-stage infections were observed both with *Pbp36*$^{-}$ and *Pbp52*$^{-}$ parasites (Ishino et al., 2005b; van Dijk et al., 2005).

Double knockout mutants of *p52* and *p36* have been generated in *P. yoelii* (Labaied et al., 2007), *P. berghei* (Annoura et al., 2012) and *P. falciparum* (VanBuskirk et al., 2009). In *P. yoelii p52*$^{-}$/*p36*$^{-}$ mutants are completely attenuated. In *P. berghei* and *P. falciparum*, however, it was shown that occasionally parasites are able to develop fully and, in the case of *P. berghei*, establish blood-stage infection in mice (Annoura et al., 2012).

By deletion of sporozoite and liver stage asparagine-rich protein (SLARP), a key regulator of sporozoite gene expression and liver-stage development, another early arrested parasite was generated. ***Pbslarp***$^{-}$ sporozoites productively invade hepatocytes by forming a parasitophorous vacuole (PV), but subsequent remodeling of the parasitophorous vacuole membrane (PVM) is impaired as a consequence of drastic down-regulation of genes encoding PVM-resident proteins (Silvie et al., 2008). This results in the inability of the parasites to establish a blood-stage infection. Immunization with these mutants only confers limited protective immunity in mice (Silvie et al., 2008). However, in the Balb/c model ***Pyslarp***$^{-}$ (=*Pysap1*$^{-}$) parasites confer sterile protection (Aly et al., 2008).

The first GAPs were generated by knocking out two parasitophorous vacuole membrane (PVM) proteins, upregulated in infective sporozoites gene 3 (*UIS3*) (Mueller et al., 2005b) and upregulated in infective sporozoites gene 4 (*UIS4*) (Mueller et al., 2005a). ***Pbuis3***$^{-}$ mutants are arrested early in liver-stage development and are impaired to develop to liver-stage trophozoites (Mueller et al., 2005b). In the C57BL/6 model these parasites are completely attenuated and confer sterile protection against re-infection after three immunizations. Similarly, ***Pbuis4***$^{-}$ parasites are also arrested early in development and confer sterile protection against re-infection after 3 immunizations. However, occasional breakthrough infections of blood-stage parasites were observed with this mutant. ***Pbuis3***$^{-}$***/uis4***$^{-}$ double-knockout mutants were also generated and showed a similar phenotype and protective efficacy as the single- knockouts (Jobe et al., 2007).

Several late liver-stage arrested GAPs were subsequently generated by deletion of genes involved in the type II fatty acid biosynthesis. *FABB/F* was deleted in *P. yoelii* and *P. berghei*, *FABZ* in *P. yoelii* and *FABI* in *P. berghei* and *P. falciparum.* ***Pyfabb/f***$^{-}$ parasites are smaller than WT parasites at 44 hours after invasion of sporozoites into hepatocytes, show abnormal progression of nuclear division, lack

expression of the merozoite signature protein merozoite surface protein 1 (MSP1) and are tightly arrested in the Balb/c model (Vaughan et al., 2009). In sharp contrast, ***Pbfabb/f***$^{-}$ mutants were able to establish blood-stage infections in all sporozoite-injected C57BL/6 mice (Annoura et al., 2012). ***Pyfabz***$^{-}$ show the same complete arrest in late liver-stage development as ***Pyfabb/f***$^{-}$ *in vivo* (Vaughan et al., 2009). ***Pbfabl***$^{-}$ parasites show impaired nuclear division in late liver stages and most parasites lack expression of MSP1 at 60 hours after sporozoite invasion *in vitro (Yu et al., 2008)*. However, *in vivo* breakthrough blood-stage infections were regularly observed in C57BL/6 mice (Yu et al., 2008). Taken together, deletion of genes involved in the type II fatty acid biosynthesis cause defects in late liver-stage development with varying degrees of attenuation in different models.

In *P. yoelii*, knockouts of the apicoplast **pyruvate dehydrogenase (PDH) subunits E1α** and **E3** were generated. These mutants can infect hepatocytes, but fail to form mature schizonts and initiate blood-stage infections (Pei et al., 2010).

Parasites missing liver-specific protein 1 (LISP1) develop liver stage merozoites, but do not rupture the parasitophorous vacuole membrane (PVM) efficiently. Nevertheless, ***Pblisp1***$^{-}$ parasites are able to establish a blood stage infection in Wistar rats and therefore do not display an attenuation phenotype in the stricter sense (Ishino et al., 2009).

A different kind of GAP was generated by conditional knockout of ***P. berghei*** **cGMP-dependent protein kinase (*Pb*PKG)** in sporozoites. Here, the targeted gene is not only essential for liver-stage development, but also in blood stages. Through conditionally knocking out the gene only in sporozoites, this limitation was circumvented. These mutant parasites are arrested late in liver-stage development, only rarely form merosomes *in vitro* and do not establish blood-stage infections *in vivo*, except for breakthroughs of WT parasites where PKG was not excised.

Most GAPs have been generated in the rodent malaria parasites *P. berghei* and *P. yoelii*, as transgenic parasites are generated faster and mutant parasites can be analyzed throughout the whole parasite life cycle. However, for some GAPs there are discrepancies between the two models in terms of attenuation phenotype, as for *p52*$^{-}$/*p36*$^{-}$ parasites (Annoura et al., 2012; Labaied et al., 2007), and protective potency, as for *slarp*$^{-}$ parasites (Aly et al., 2011; Silvie et al., 2008). In the past years the first *P. falciparum* GAPs were generated (Mikolajczak et al., 2011; van Schaijk et al., 2008; VanBuskirk et al., 2009).

Studies to elucidate the immunological mechanisms of protection against GAPs

revealed that protection is mainly mediated by IFNγ-producing $CD8^+$ T lymphocytes (Jobe et al., 2007; Mueller et al., 2007). In the *P. berghei*/ C57BL/6 model, persistence of *uis3*$^-$ parasites is crucial for protective efficacy, as primaquine treatment completely abolished protection (Mueller et al., 2007).

As different parasite species, mouse strains and immunization protocols were used for studies using GAPs as whole-organism vaccines, comparison of protective efficacy in these studies is not easily achieved. Generally, sterile protection is more easily achieved in the *P. yoelii*/ Balb/c model than the *P. berghei*/ C57BL/6 model (Doolan and Hoffman, 2000; Ngonseu et al., 1998). A recent study using the *P. yoelii*/ Balb/c model showed that late arrested *fabb/f*$^-$ parasites mount superior antimalarial immunity compared to early arrested *sap1*$^-$ parasites, suggesting enhanced protection of late liver-stage arrested GAPs due to a broader set of presented antigens (Butler et al., 2011). The longevity of protection with whole-organism vaccines against *Plasmodium* re-challenge was assessed for up to 1 year (Douradinha et al., 2011; Douradinha et al., 2007; Jobe et al., 2007; Nganou-Makamdop et al., 2012). Again a variety of different parasite species, mouse strains and immunization protocols were used.

1.6 Loss-of-function studies of *Plasmodium* apicoplast genes

To date, various apicoplast genes have been deleted in *Plasmodium* (Fig. 1.5). They include genes involved in the type II fatty acid biosynthesis (Vaughan et al., 2009; Yu et al., 2008) and two subunits of the pyruvate dehydrogenase complex (Pei et al., 2010), highlighting the importance of fatty acid biosynthesis for late liver-stage development.

The lipoic acid synthesis pathway has been targeted by disruption of the ***PfLipB*** gene. Loss of *LipB* did not negatively affect parasite growth despite a drastic loss of lipoic acid (Gunther et al., 2007). It was shown that LipB function can be compensated for by a lipoic acid protein ligase, which is dually targeted to apicoplast and mitochondrion (LplA2) (Gunther et al., 2007).

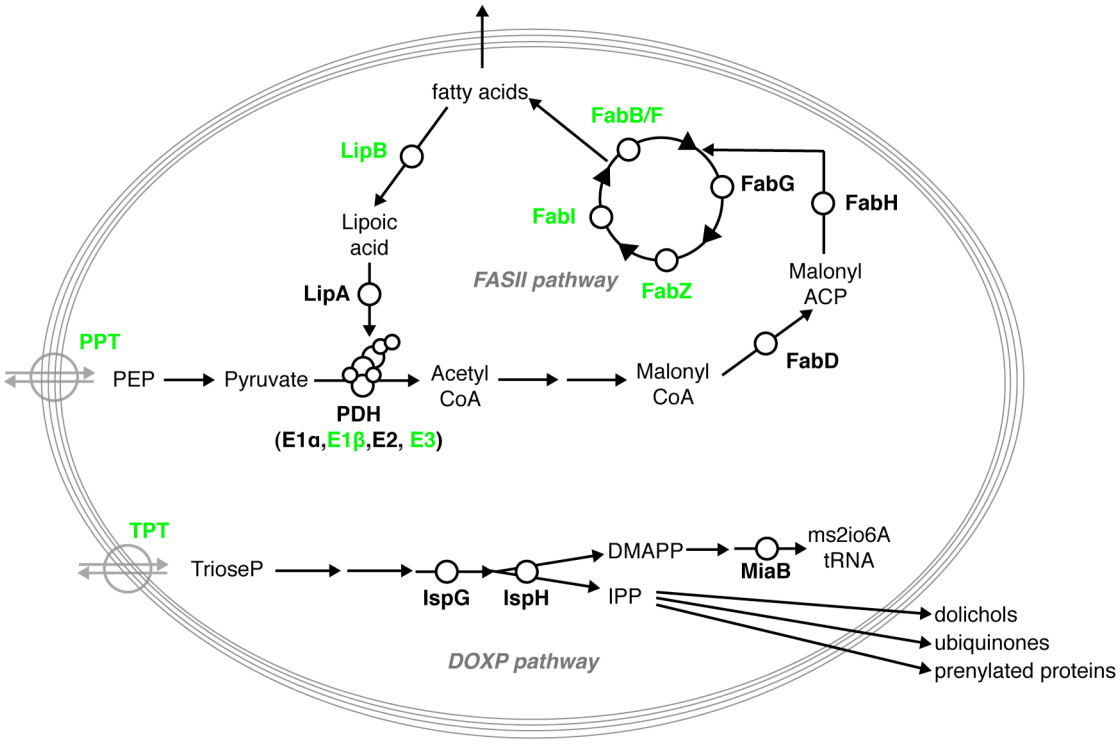

Figure 1.5: Overview of *Plasmodium* apicoplast knockout mutants.

Shown is an overview of apicoplast localized biosynthesis pathways that have been targeted for gene deletions in *Plasmodium*. Apicoplast enzymes successfully targeted by transfection plasmids are depicted in green. For references see section 1.5 and 1.6. (PPT= phospho-enolpyruvate transporter, PEP= phospho-enolpyruvate, PDH= pyruvate dehydrogenase, CoA= coenzyme A, FabD= malonyl-CoA:ACP transacylase, ACP= acyl carrier protein, FabH= b-ketoacyl-ACP synthase III, FabG= β-ketoacyl-ACP reductase, FabZ= β-hydroxyacyl-ACP dehydratase, FabI= trans-2-enoyl-ACP reductase, FabB/F= β-ketoacyl-acyl-carrier-protein synthase, LipB= lipoate protein ligase, LipA= lipoate synthase, TPT= triose phosphate transporter, TrioseP= triose-phosphate, IspG= GcpE; 4-hydroxy-3-methyl-but-2-enyl-diphosphate (HMBPP)-synthase, IspH= LytB; HMBPP-reductase, DMAPP= dimethylallyl pyrophosphate, IPP= isopentenyl pyrophosphate, MiaB= (Dimethylallyl)adenosine-tRNA-methylthiotransferase), DOXP= 1-deoxy-D-xylulose-5-phosphate).

In a recent study, two apicoplast sugar phosphate transporters, triose phosphate transporter (TPT) and phospho-enolpyruvate transporter (PPT), were targeted by gene deletion (Banerjee et al., 2012). ***PbTPT*** $^{-}$ parasites only survived a few cycles of blood-stage replication. In contrast, ***PbPPT***$^{-}$ parasites developed similar to the WT in the blood stages. However, the absence of PPT led to defects in mosquito and liver-stage development (Banerjee et al., 2012).

At large, the generation of apicoplast gene knockout mutants helps to reveal the importance of the various apicoplast pathways for different life cycle stages of *Plasmodium*. This is of enormous value to understand the apicoplast physiology and to evaluate potential druggable targets in the apicoplast. Only a small fraction of the

proteins that are likely targeted to the apicoplast have been functionally assigned. Therefore, it is highly likely that additional pathways and molecules with important functions will be identified.

1.7 [Fe-S] cluster biogenesis

1.7.1 Overview on biogenesis of [Fe-S] clusters

Iron-sulfur [Fe-S] clusters are inorganic cofactors that constitute one of the most ancient and ubiquitous prosthetic groups. Proteins containing [Fe-S] clusters are involved in numerous biological processes, such as mitochondrial oxidative phosphorylation (Bych et al., 2008), photosynthesis (Sakurai and San Pietro, 1985), DNA replication (Klinge et al., 2007), DNA repair (Porello et al., 1998), ribosome biogenesis (Kispal et al., 2005) and regulation of gene expression (Haile et al., 1992). Accordingly, the list of [Fe-S] cluster-containing proteins is continuously expanding. Although early *in vitro* studies suggested a spontaneous assembly of [Fe-S] clusters (Malkin and Rabinowitz, 1966), *in vivo* [Fe-S] clusters are not formed spontaneously, but need a rather complex machinery involving numerous proteins for their assembly. Bacteria harbor the ISC (iron-sulfur cluster) and the SUF (sulfur utilization factor) systems for assembly of [Fe-S] clusters. In *E. coli* the ISC system is thought to mediate housekeeping functions, whereas the SUF system was shown to be especially important under stress conditions such as iron starvation (Lill, 2009; Outten et al., 2004). Deletion of either of the operons alone is not lethal (Takahashi and Tokumoto, 2002; Tokumoto and Takahashi, 2001).

The NIF (nitrogen fixation) system is only present in nitrogen-fixing bacteria such as *Azotobacter vinelandii* and is generally exclusively for the maturation of nitrogenase (Johnson et al., 2005b; Zheng et al., 1993). However, Nif-like components are also found in many species that do not fix nitrogen (Ali et al., 2004; Angelini et al., 2008; Leon et al., 2003; Touraine et al., 2004).

In eukaryotes, [Fe-S] biogenesis machineries are thought to have evolved from their bacterial counterparts that had been acquired by endosymbiosis (Muhlenhoff and Lill, 2000). Different systems of [Fe-S] cluster assembly are required for biogenesis in distinct cellular compartments, namely the ISC (iron-sulfur cluster) system in the

mitochondrion and the SUF (sulfur utilization factor) system in plastids (Fig. 1.6). The mitochondrial ISC proteins were found to supply [Fe-S] clusters not only to the mitochondrial [Fe-S] proteins, but also to [Fe-S] proteins in the cytosol (Kispal et al., 1999), where the CIA (cytosolic iron-sulfur protein assembly) machinery is responsible for the maturation of cytosolic [Fe-S] proteins (Sharma et al., 2010).

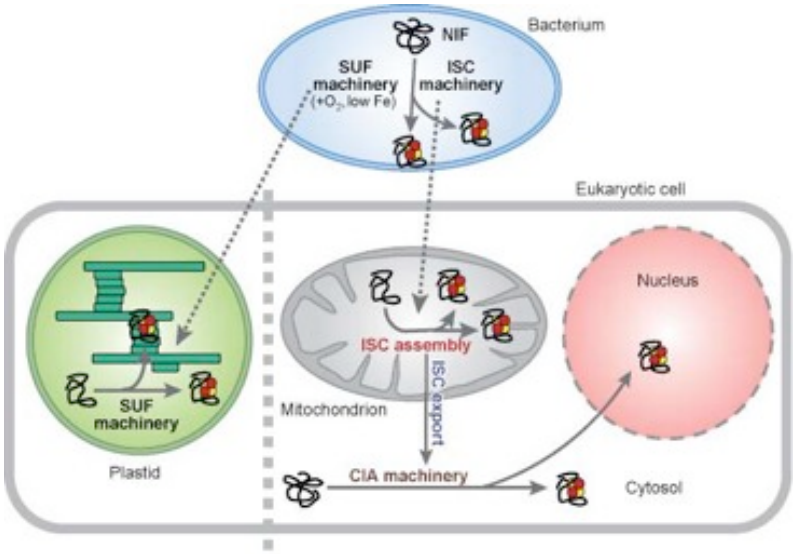

Figure 1.6: Eukaryotic machineries for the biogenesis of [Fe-S] cluster proteins and their putative evolutionary origin.

The ISC (iron-sulfur cluster) assembly machinery of mitochondria was likely inherited from α-proteobacteria. The SUF (sulfur utilization factor) machinery of plastids in plant cells was probably aquired by endosymbiosis of a photosynthetic bacterium. Maturation of cytosolic and nuclear [Fe-S] proteins requires the mitochondrial ISC assembly machinery, a mitochondrial ISC export system, and the cytosolic iron-sulfur protein assembly (CIA) machinery. The bacterial NIF (nitrogen fixation) system is specialized for the assembly of nitrogenase in nitrogen-fixing bacteria. Small red and yellow circles depict [Fe-S] clusters. From (Lill and Muhlenhoff, 2006).

In spite of the differences between bacteria and eukaryotes, the basic principles of [Fe-S] clusters biogenesis seem to be conserved (Fig.1.7). In a first step the [Fe-S] cluster is assembled *de novo* onto a scaffold protein. For this step sulfur is mobilized from cysteine by a cysteine desulfurase (IscS, SufS, NifS) (Hidese et al., 2011). The iron source is mostly unknown. In a second step the [Fe-S] cluster is transferred from the scaffold protein to a target apoprotein and assembled into the polypeptide chain. The most common [Fe-S] clusters are rhombic [2Fe-2S] or cubic [4Fe-4S], however more complex structures have been described that can also include other heavy metals (Johnson et al., 2005a).

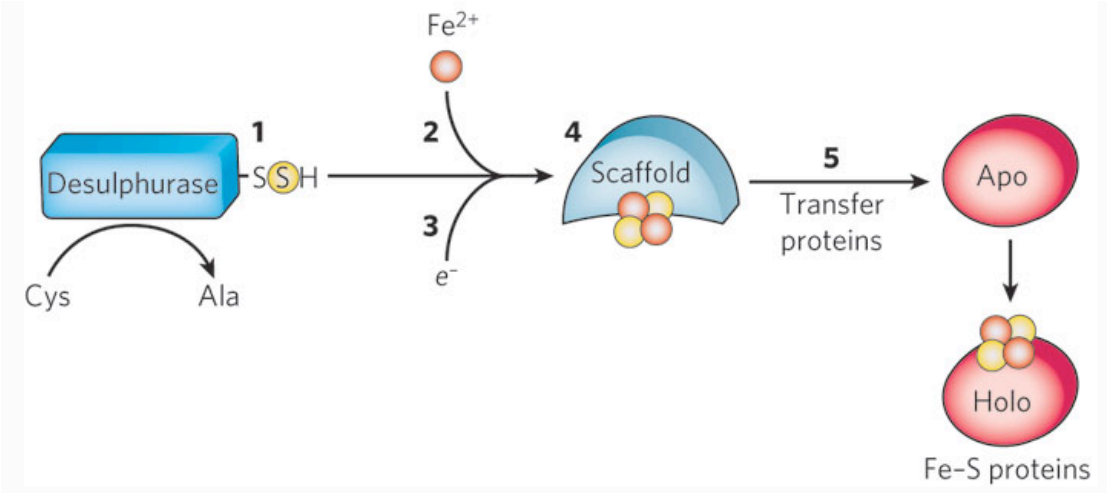

Figure 1.7: Principles of [Fe-S] cluster biogenesis.

Numbers in the figures correspond to the following steps: (1) a desulfurase acquires sulfur for the [Fe-S] cluster from cysteine, converting the cysteine to alanine. (2) An iron donor delivers iron to the scaffold protein. (3) Electrons are needed for the reduction of S^0 (present in cysteine) to sulphide (S^{2-}, present in [Fe-S] clusters). (4) The [Fe-S] cluster is assembled on scaffold proteins and then (5) transfer proteins load the [Fe-S] cluster from the scaffold proteins to apoproteins converting them to holoproteins. From (Lill, 2009).

Because most studies on the SUF system were conducted in bacteria the functions of SUF proteins will be briefly exemplified for *E. coli*. The SUF system in *E.coli* consists of 6 genes organized in the *sufABCDSE* operon (Takahashi and Tokumoto, 2002). SufS acts as cysteine desulfurase that provides the sulfur for the [Fe-S] cluster and SufE has been shown to interact with SufS to enhance its activity up to 50-fold (Loiseau et al., 2003; Outten et al., 2003). SufBCD forms a functional complex serving as a [Fe-S] scaffold (Chahal et al., 2009; Wollers et al., 2010) and also enhancing SufS function (Outten et al., 2003). SufC was shown to contain ATPase activity in *Erwinia chrysanthemi* (Nachin et al., 2003) and the crystal structure of *E. coli* SufC confirmed it to be an ABC-type ATPase (Kitaoka et al., 2006). SufA interacts with SufBCD to accept Fe-S clusters formed *de novo* on the SufBCD complex (Chahal et al., 2009).

As mentioned earlier, proteins showing similarity with the NifU protein of *Azotobacter vinelandii* can be found in many other species in the mitochondria as well as plastids (Leon et al., 2003). NifU-like proteins seem to act as scaffolds for [Fe-S] cluster biosynthesis (Tong et al., 2003; Touraine et al., 2004). However, their specific roles may vary in different organisms and localizations. For instance in humans, mutations in *NFU1* lead to defects in the maturation of a subset of mitochondrial [Fe-S]

proteins, which causes a fatal disease (Navarro-Sastre et al., 2011). In contrast, *Saccharomyces cerevisiae* mitochondrial NFU1 is involved in [Fe-S] cluster biogenesis, but is not an essential protein (Schilke et al., 1999).

1.7.2 [Fe-S] cluster biogenesis in the apicoplast of *Apicomplexa*

Compared to bacteria, yeast and plants, relatively little is known about [Fe-S] cluster biosynthesis in *Apicomplexa*. In *Plasmodium* components of the SUF, ISC and CIA system have been identified by bioinformatics analysis (Ellis et al., 2001; Seeber, 2002; Seeber and Soldati-Favre, 2010). As it is the case for other eukaryotes, the ISC system localizes to the mitochondrion and the SUF system to the apicoplast (Seeber, 2002) (Fig. 1.8). In *Plasmodium*, all components of the Suf system are nuclear-encoded, except for SufB, which is encoded in the apicoplast genome (Wilson et al., 1996).

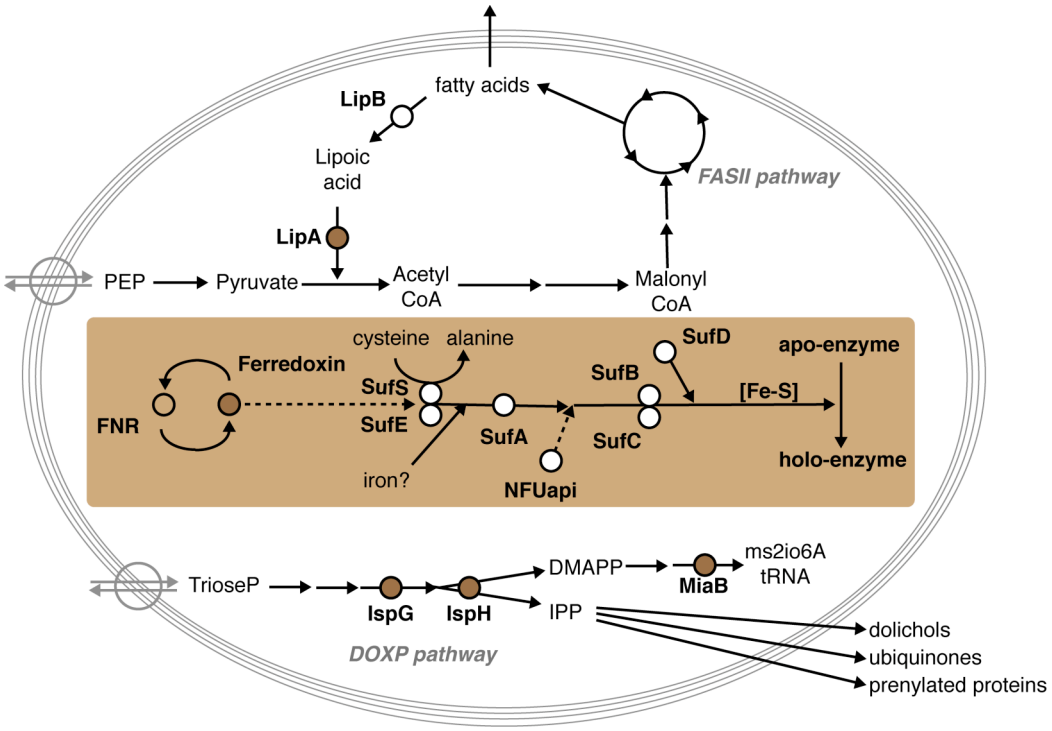

Figure 1.8: Overview of *Plasmodium* apicoplast-resident proteins containing a [Fe-S] cluster or involved in the biosynthesis of [Fe-S] clusters.

Shown is an overview of the principal apicoplast localized biosynthesis pathways: fatty acid synthesis (FASII pathway), non-mevalonate isoprenoid synthesis (DOXP pathway), lipoic acid synthesis and [Fe-S] cluster synthesis (highlighted in brown), with their respective precursors and products. Apicoplast proteins that contain a [Fe-S] cluster are depicted as brown circles.

A recent biochemical study has focused on the *P. falciparum* plastid SUF system and provided evidence that SufC is localized to the apicoplast (Kumar et al., 2011). In bacteria and plants, SufC interacts with SufB (Nachin et al., 2003; Rangachari et al., 2002; Xu et al., 2005), which could be confirmed in *P. falciparum* (Kumar et al., 2011). Furthermore, ATPase activity of recombinant *Pf*SUFB and *Pf*SUFC proteins provided compelling evidence for the evolutionary conservation of the plastid SUF system between plants and apicomplexan parasites (Kumar et al., 2011). In *Arabidopsis thaliana*, SUFB and SUFC display ATPase activity (Xu et al., 2005), whereas the bacterial SufB seems to lack this activity.

In *Plasmodium* [Fe-S] cluster-containing proteins in the apicoplast are involved in pathways such as mevalonate-independent isoprenoid biosynthesis, lipoic acid metabolism and biogenesis of [Fe-S] clusters itself (Fig. 1.8). Because some proteins are involved in pathways that are essential for parasite growth, such as the DOXP pathway of isoprenoid biosynthesis (Yeh and DeRisi, 2011), [Fe-S] cluster assembly is likely to be essential for parasite survival.

1.8 Aims of this thesis

After transmission by infectious *Anopheles* mosquito bites, malaria parasites undergo an intra-hepatic expansion phase in the vertebrate host that leads to the formation of thousands of infectious merozoites. The pre-erythrocytic phase is clinically silent and provides an excellent target for antimalarial vaccines. Hence, a better understanding of liver-stage biology is highly desirable, but remains challenging as liver stages have the most limited experimental accessibility in the *Plasmodium* life cycle.

The aim of this thesis was to characterize genes that are important for liver-stage development and to demonstrate their significance by applying targeted gene deletions in the rodent malaria parasite *Plasmodium berghei*. If possible, a late liver-stage arrested parasite line should be generated. This should allow to test if a later developmental arrest would lead to a broader range of presented antigens and could mount superior protective immune responses compared to early arrested parasites.

Most *Apicomplexa* harbor a plastid organelle termed apicoplast. The apicoplast harbors various pathways that are not present in humans, such as the DOXP pathway of isoprenoid biosynthesis and the SUF system of [Fe-S] cluster biogenesis. [Fe-S] cluster biogenesis in the apicoplast of *Plasmodium* is hypothesized to be

essential for parasite development. However, no experimental data are available yet. As part of this thesis, systematic targeted gene deletions should be attempted to unravel the role of the various genes involved [Fe-S] cluster biogenesis in the apicoplast and also to estimate which of them might be considered as potential drug targets.

In general, these experiments will help to further characterize the importance of the apicoplast for parasite development and survival and identify new key players in *Plasmodium* liver-stage development.

2 Materials and methods

2.1 Materials

2.1.1 Organisms and cell lines

female NMRI and C57BL/6 mice	Charles River Laboratories, Germany
Anopheles stephensi	Nijmegen, Netherlands
Plasmodium berghei ANKA-GFP-507cl	referred to as WT ANKA-GFP (Janse et al., 2006b)
Plasmodium berghei ANKA Bergreen	(Kooij et al., 2012)
Plasmodium berghei ANKA	referred to as WT ANKA Prof. Dr. Chris Janse, LUMC Leiden, Netherlands
Huh7 human hepatoma cells	Prof. Dr. Ralf Bartenschlager, Universitätsklinikum Heidelberg, Germany
E. coli XL-1blue	Stratagene, Germany

2.1.2 Laboratory equipment

<u>Centrifuges:</u>	
Bench centrifuge, 5424	Eppendorf, Germany
Megafuge1.OR	Heraeus, Germany
Cooled bench centrifuge 5415R	Eppendorf, Hamburg
<u>Incubators:</u>	
Incubator, for cells, Thermo scientific	Heraeus, Germany
Incubator, for *P. berghei* transfection	Mytrom, Germany
Incubator for bacteria, Thermo scientific	Heraeus, Germany
Incubator, Shaker for bacteria, Innova40	Eppendorf, Germany
Incubator for Mosquitoes	Mytrom, Germany
<u>Microscopes:</u>	
Binoculars, M80, MZ10F	Leica, Germany
Leica DM2500	Leica, Germany
Confocal laser scanning microscope, TSP-SP1	Leica, Germany
Agarose gel casting apparatus, Horizon11.14	Biometra, Germany
Amaxa Electroporator	Amaxa, Germany
Axiovert, 200M, with XL-3 incubator	Zeiss, Germany
Electrophoresis power supply	Amersham Pharmacia Biotech/ GE Healthcare, Germany
FACS Diva	BD Biosciences, Germany
Flow cytometers LSRII and Fortessa	BD Biosciences, Germany
Gel documentation system, Gel Doc 2000	BIORAD, Germany
Heating block, Thermo Scientific	Eppendorf, Germany

Micropipette (Gilson)	Abimed, Germany
Mosquito cages	BioQuip Products Inc, USA
Nanodrop ND 1000	peQLab, Germany
Neubauer counting chamber	Marienfeld, Germany
PCR Thermocycler, MJ-mini	BIORAD, Germany
PCR Thermocycler, StepOnePlus	Applied Biosystems, USA
pH-meter	Mettler Toledo, Germany
Photometer, GeneQuant pro	Amersham, Germany
Sterile hood, Herasafe KS12	Heraeus, Germany
Vortex-Genie2	Scientific Industries, USA

2.1.3 Consumables

6-well and 24-well plates	Greiner bio-one, Germany
8-well chamber slides, LabTek	Nunc, Fischer, Germany
CellTrics filters	Partec, Germany
Cover slips	Roth, Germany
Cryo-freezing tubes	Greiner bio-One, Germany
Electroporation cuvettes	Amaxa, Germany
Eppendorf tubes, 1.5 ml	Eppendorf, Germany
Falcon blue cap (50 mL and 15 mL)	Greiner Bio-One, Germany
Filter paper	Schleier and Schuel, Germany
Forceps	Neolab, Germany
Glass slides, clear	Menzel, Germany
Microscope oil	Zeiss, Germany
Needles, sterile	Braun, Germany
Neubauer counting chamber	Roth, Germany
Nitrocellulose membrane, Hybond	Amersham, Germany
Pasteur pipettes	Roth, Germany
PCR tubes	Greiner Bio-One, Germany
Petri-dishes	Sarstedt, Germany
Poly-L-Lysins Coated Cover slips	BD, BioCoad, Belgium
Pipettes tips	Brand GMBH, Germany
Serological pipettes (10 and 25 ml)	Greiner Bio-One, Germany
Sterile filter (0.2 and 0.4 mm)	Millipore, Ireland
Sterile filtration units (500 ml)	Nalgene®, USA
Syringes, 1ml	Roth, Germany
Syringes, insuline	Braun, Germany
Tissue culture flasks (50 and 250 ml)	Greiner Bio-One, Germany
Whatman™ 3MM paper	Whatman, UK

2.1.4 Reagents

Standard reagents were obtained from Merck, Sigma and Roth, unless otherwise indicated.

Agarose	Invitrogen, Germany
dNTP-mix	Fermentas, Germany
DRAQ5	Axxora/Enzo Life Sciences,

	Germany
Evans Blue	Sigma-Aldrich, Germany
Fibrous Cellulose Powder	Whatman, United Kingdom
Fluoromount-G	Southern Biotech, USA
Gentamycin	Invitrogen, Germany
Giemsa stain	VWR, Germany
Heparin	Ratiopharm, Germany
Hepes	Merck/Calbiochem, Germany
Hoechst 33342	Invitrogen, Germany
human T-cell Nucleofector™ solution	Amaxa, Lonza, Germany
Isofluran	Baxter, Germany
Ketamin (10%) (=Ketavet)	Pfizer, Germany
LB-agar powder (Lennox L Agar)	Invitrogen, Germany
Nycodenz	Axis Shield, Norway
Para-formaldehyde	Serva, Germany
PCR-buffer set	Roche, Germany
Percoll	GE Healthcare, Germany
Power SYBR®Green PCR Master Mix	Applied Biosystems, Germany
SYBR Safe DNA Gel stain	Invitrogen, Germany
SYBR Green PCR Mastermix	Applied Biosystems, Germany
Xylazin (= Rompun 2%)	Bayer, Germany

antibiotics:

ampicillin	Roth, Germany
azithromycin	Pfizer, Germany
fosmidomycin	Sigma-Aldrich, Germany
penicillin/streptomycin, liquid	Invitrogen, Germany

2.1.5 Commercial Kits

DNAse Turbo	Ambion, Germany
HiSpeed Plasmid Midi Kit	Qiagen, Germany
Human T Cell Nucleofactor Kit	Lonza, Germany
QIAamp DNA-Blood Mini Kit	Qiagen, Germany
QIAquick PCR Purification Kit	Qiagen, Germany
QIAprep Spin Miniprep Kit	Qiagen, Germany
Rapid DNA Dephos & Ligation Kit	Roche, Germany
RETROscript	Ambion,Germany
RNeasy Mini Kit	Qiagen, Germany

Southern blot kits and reagents from Roche, Germany:

PCR DIG Probe synthesis kit; Cat. No. 11 636 090 910
DIG Wash and block buffer set; Cat. No. 11 585 762 001
DIG Easy Hyb; Cat. No. 11 603 558 001
DIG Luminescent Detection kit; Cat. No. 11 363 514 910

2.1.6 Enzymes

Restriction endonucleases	New England Biolabs, Germany
T4-DNA-ligase	Fermentas, Germany
Taq DNA polymerase	Fermentas, Germany
Phosphatase	Roche, Germany
Platinum *Taq* DNA polymerase (HF)	Invitrogen, Germany
ProteinaseK	Invitrogen, Germany

2.1.7 Media, solutions, buffers, markers

6x loading dye	Fermentas, Germany
1kb DNA-Ladder	Fermentas, Germany
Antibiotic-Antimycotic (Anti-anti)	Gibco Invitrogen, Germany
DMEM 41966	Gibco Invitrogen, Germany
FCS (Fetal Calf Serum), certified (USA)	Gibco Invitrogen, Germany
FCS	Gibco Invitrogen, Germany
HBSS, w/o Ca and Mg	Gibco Invitrogen, Germany
Lysing buffer (BD Pharm Lyse™)	BD Biosciences, Germany
PBS, sterile solution	Gibco Invitrogen, Germany
PBS, tablets	Gibco Invitrogen, Germany
Perm/Wash™ buffer	BD Biosciences, Germany
RPMI Medium 1640 w/HEPES	Gibco Invitrogen, Germany
SOC	Invitrogen, Germany
Trypsin-EDTA	Invitrogen, Germany

Ampicillin stock solution	100mg/ml ampicillin in ddH_2O
LB-Agar	LB-medium, 15g/l Bacto-agar
Luria Broth- (LB-) medium	10g/l Bacto- tryptone, 5g/l Bacto-yeast extract, 5g/l NaCl, add to ddH_2O pH 7.5; autoclaved
giemsa staining solution	10% Giemsa solution in H_2O
hepatocyte cell culture medium	450ml DMEM, 50ml FCS SA, 5ml penicillin/streptomycin or anti-anti
mosquito breeding water	1 ‰ sea salt in ddH_2O
mosquito dissecting medium	3% Bovine albumin serum in RPMI
mosquito feeding solution	10g sucrose, 20µg pABA; ad 100ml ddH_2O
3 M NaAc solution	24,06 g ad 100 ml ddH_2O; pH 4,8
Nycodenz-stock solution	5µM Tris pH 7.5 (1M stock), 3mM KCL (250mM stock), 0.3mM EDTA (0.5 M stock) and 110.4g Nycodenz (27.6 g/100 ml), dissolved in 400ml dH_2O, autoclaved
P. berghei freezing solution	Glycerin, Alsever's Solution (1:9)

P. berghei culture medium (transfection)	160ml RPMI-medium 1640, 25mM HEPES, L-Glutamin (Gibco); 40ml FCS USA (heat inactivated 30min at 56°C), 50µl gentamycin (50mg/ml), sterile filtered
100 x Pyrimethamin- stock solution	7mg Pyrimethamin /ml in DMSO
50 x TAE-Puffer	2M Tris, 250mM sodium acetate, 0,5mM EDTA; pH 7,8
TBST	20mM Tris pH 7,6; 137mM NaCl; 0,1% Tween
Tris / HCl, pH 6,8	0,5M Tris / HCl, pH 6,8
Tris / HCl, pH 8,8	1,5M Tris / HCl, pH 8,8

2.1.8 Antibodies

α-ACP (rabbit)	(Friesen et al., 2010)
α-HSP70 (mouse)	(Tsuji et al., 1994)
α-*Py*MSP1 (mouse)	Prof. Dr. Anthony Holder, NIMR London, UK
α-c-Myc (clone 9E10) (mouse)	Santa Cruz Biotechnology, Germany
α-UIS4 (rabbit)	Dr. Georgina Montagna, MPIIB Berlin, Germany

α-CD8 (clone 53.6-7), α-CD4 (clone GK1.5), α-CD11a (clone M17/4), α-CD3 (145-2C11), α-CD28 (37.51), α-IL-2 (JES6-5H4), α-TNF (MP6-XT22) and α-IFNγ (XMG1.2) were purchased from eBiosciences.

Donkey α-mouse IgG Alexa Fluor 488/ 546, donkey α-rabbit IgG Alexa Fluor 488/ 546, goat α-mouse IgG Alexa Fluor 488/ 546 and goat α-rabbit IgG Alexa Fluor 488g/ 546 were purchased from Invitrogen.

2.1.9 Peptides

P1 (KIYNRNIVNRLLGDA) (Boscardin et al., 2006)
S and T peptides correspond to immunodominant *Plasmodium* $CD8^+$ T cell epitopes (Hafalla et al., unpublished data).

2.1.10 *Plasmodium* targeting vectors

b3D.DT^H.^D	Prof. Dr. Andy Waters, University of Glasgow, Scotland
pBART-SIL6	(Kooij et al., 2012)
pBAT (intermediate construct)	(Kooij et al., 2012)

2.1.11 Oligonucleotides

All oligonucleotides were ordered from Eurofins MWG Operon.

Table 2.1: Primer list.

Primer Name	Primer Sequence (REase sites bold)	REase[a]	Purpose[b]	Target	Sense[c]
PbPALM-F2-BamHI	TTT**GGATCC**TTTTGACGTATGCATTAATCTAGC	BamHI	TV	5'PALM	F
PbPALM-R1-EcoRI	TTT**GAATTC**TGCCTATATTCTGCCCATAGC	EcoRI	TV	5'PALM	R
PbPALM-F7-HindIII	TTT**AAGCTT**TTCGCAAAAATATGGATGCAAC	HindIII	TV	3'PALM	F
PbPALM-R6-KpnI	ATT**GGTACC**TTACTTTTCCTACCTAAACCTTTTTTG	KpnI	TV	3'PALM	R
PbPALM-F1	CCAGCCTCAATAGATAAACAGTTC		GT	5'PALM	F
PbPALM-R2	GATGGTTGTGCTGCATTCTG		GT	5'PALM	R
PbPALM-F6	AAATGATCCAATATTCTCTTGCAG		GT	3'PALM	F
PbPALM-R7	CCCCCTACATACAGGAGCAG		GT	3'PALM	R
PbPALM-F3-NotI	TTT**GCGGCCGC**TTTTGACGTATGCATTAATCTAGC	NotI	TV	PALM	F
PbPALM-R3-PshAI	TTA**GACATATGTC**CATTTGCATTCCTATTATTATCTTCTATG	PshAI	TV	PALM	R
PbPALM-F5-EcoRI	ATT**GAATTC**TTAACTCCAACGATGATATAGAGG		TV	PALM	F
PbPALM-R5-Blunt	AATGGCGGCTAAAATATTTCCATCATGCTTCTTATATATATTATC		TV/RT-PCR	PALM	R
PbPALM-F4	TCCTTTGTAATAAAACTTTCTTTGTGG		GT	PALM	F
PbPALM-R4	TTATCAATATCAAAAATGGTCAAATGG		GT	PALM	R
TV-5'NFU-F	TAT**CCGCGG**TTTTTCCTATAAATGTGTGTGTAATGC	SacII	TV	5'NFU	F
TV-5'NFU-R	AAA**GATATC**ACTCACAAAAATAAGCACATGATTG	EcoRV	TV	5'NFU	R
TV-C-NFU-F	AAA**CCGCGG**CGTGTAGCTCAAATAGTGTAACTG	SacII	TV	C-NFU	F
TV-C-NFU-R	TAA**GATATC**ATTTTCAAAATTAACAGTTAATGTTGGAAA	EcoRV	TV	C-NFU	R
TV-3'NFU-F	TAT**AAGCTT**CAGCGGCTAGTCAATCTAATC	HindIII	TV	3'NFU	F
TV-3'NFU-R	TAA**GGTACC**GTTCATTTAAAACACCAGCGAG	KpnI	TV	3'NFU	R
GT-5'NFU-F	ATTTTTTCTCTGGTTTTCATTTATATTTC		GT	5'NFU	F
GT-5'NFU-R	TTGTTTTATTTCTGTGTGCATTAACC		GT	5'NFU	R
GT-C-NFU-F	GCCCCAAATTACAAATAGATAATGG		GT	C-NFU	F
GT-3'NFU-F	GAAAATGAAGATAAGGAAGTAAATATACC		GT	3'NFU	F
GT-3'NFU-R	TAATATACATAAATGTTATTGGGATCTTTTG		GT	3'NFU	R
TV-5'SUFA-F	TTT**CCGCGG**TTTTAGTTTATTATATTTCACAATTTGCAC	SacII	TV	5'SUFA	F
TV-5'SUFA-R	AAA**GATATC**ATAATGAGGGGTAAATGAACCAG	EcoRV	TV	5'SUFA	R
TV-3'SUFA-F	TTT**AAGCTT**TTGTATGGTCCCCTATATGAATTTG	HindIII	TV	3'SUFA	F
TV-3'SUFA-R	TTT**GGTACC**GATGCATTTTTGTTAAGTTTGTGC	KpnI	TV	3'SUFA	R
GT-5'SUFA-F	TTCATCTCCTTTTGGCTATTTTG		GT	5'SUFA	F
GT-5'SUFA-R	TAAAGCCAGCGTATCTCAAG		GT	5'SUFA	R
GT-3'SUFA-F	GAAAAAATGTGGTTGTGGAAAATCC		GT	3'SUFA	F
GT-3'SUFA-R	AAAATGGAGAAAACAGGGTTACG		GT	3'SUFA	R
TV-5'SUFC-F	TTT**CCGCGG**ATGCTTATCCATTTTGCTTGG	SacII	TV	5'SUFC	F
TV-5'SUFC-R	TAA**GATATC**GTGTCACATGTTGTATTTCCTTTC	EcoRV	TV	5'SUFC	R
TV-3'SUFC-F	ATT**AAGCTT**ATTTATTGCATGCCCTTGTTTTG	HindIII	TV	3'SUFC	F
TV-3'SUFC-R	TTT**GGTACC**TGCTTACACAATTATCTCTTTTTGG	KpnI	TV	3'SUFC	R
GT-5'SUFC-F	TTGCTATCTATTGTTATCATATTTCTTG		GT	5'SUFC	F
GT-5'SUFC-R	CTAGCCAAAATTGTCCTCGC		GT	5'SUFC	R
GT-3'SUFC-F	AATCTGATGGATATGCACAATTTG		GT	3'SUFC	F
GT-3'SUFC-R	AAAATCATCGCCATATTCTATATTACC		GT	3'SUFC	R
TV-5'SUFD-F	TAT**CCGCGG**CATATTTTTTGTTCTTTTTCCTATTCACC	SacII	TV	5'SUFD	F
TV-5'SUFD-R	AAA**GATATC**CATTAAAGCTATCCAAAAGAAAGTG	EcoRV	TV	5'SUFD	R
TV-3'SUFD-F	TTT**AAGCTT**TATTCCATGCAGCACATTGG	HindIII	TV	3'SUFD	F
TV-3'SUFD-R	TTT**GGTACC**GCCTGTGAAGCTCAATTTCG	KpnI	TV	3'SUFD	R
GT-5'SUFD-F	TCGAACCCATGCGAACTTAC		GT	5'SUFD	F
GT-5'SUFD-R	TTCGTTGCTTCTTTTCTTTTCAC		GT	5'SUFD	R
GT-3'SUFD-F	TTCTTGAACATGTGCCTGATG		GT	3'SUFD	F
GT-3'SUFD-R	AGGACCATGCAAAGGACCTC		GT	3'SUFD	R
TV-5'SUFE-F	TTT**CCGCGG**TGTGCCATTATCGCATTACAG	SacII	TV	5'SUFE	F
TV-5'SUFE-R	AAA**GATATC**AAAAGGCCTACATAACATTCCAG	EcoRV	TV	5'SUFE	R
TV-3'SUFE-F	TTT**AAGCTT**GAATACAATGCATGCTATATAATGC	HindIII	TV	3'SUFE	F
TV-3'SUFE-R	TAT**GGTACC**TTTTAATGCAAAAATGCACAAGG	KpnI	TV	3'SUFE	R
GT-5'SUFE-F	CTGGCGTTTTGTGTCCATTAC		GT	5'SUFE	F
GT-5'SUFE-R	TAATTTTGTGCGAATGATCGAC		GT	5'SUFE	R
GT-3'SUFE-F	CTAATTTGTCCTTGTTTCGTTGTC		GT	3'SUFE	F
GT-3'SUFE-R	TGTAACAATAAAATAAGACGGTTGG		GT	3'SUFE	R
TV-5'SUFS-F	TTT**CCGCGG**GATTTTGCCTTTTTCAAGAATATGG	SacII	TV	5'SUFS	F
TV-5'SUFS-R	ATA**GATATC**CTCATTATTCATATTCCCACAAATTTG	EcoRV	TV	5'SUFS	R
TV-3'SUFS-F	AAA**AAGCTT**ATCATTTGTGTGTGCTCATACG	HindIII	TV	3'SUFS	F
TV-3'SUFS-R	AAA**GGTACC**ATTCTCCATGCAAAGCAAAAATAC	KpnI	TV	3'SUFS	R
GT-5'SUFS-F	CATAAGCGAGCCACACATTG		GT	5'SUFS	F
GT-5'SUFS-R	TATATGTCCTTTATAAATTGTACGTGTG		GT	5'SUFS	R
GT-3'SUFS-F	TCAGGACACCACTGTGCATC		GT	3'SUFS	F
GT-3'SUFS-R	TTGTTTGATTTTCACACGCTTTG		GT	3'SUFS	R

Table 2.1 continued

5'HSP70rev	CAATTTGTTGTACATAAAATAGGCAG	GT	vector	R
5'DHFRrev	ATGAAATACCGCTCCATTTTTCC	GT	vector	R
mCherryRev	CCCTCCATGTGAACCTTGAAG	GT	vector	R
TgRevPro	CGCATTATATGAGTTCATTTACACAATCC	GT	vector	R
TgForw	CCCGCACGGACGAATCCAGATGG	GT	vector	F
mCherryRev	CCCTCCATGTGAACCTTGAAG	GT	vector	R
PbHSP70-F	GCTAACGCAAAAGCAAAGC	RT-PCR	HSP70	F
PbHSP70-R	TCGGTAAAAGCTACATAGGATG	RT-PCR	HSP70	R
mGAPDH-for	CGTCCCGTAGACAAAATGGT	qPCR	mGAPDH	F
mGAPDH-rev	TTGATGGCAACAATCTCCAC	qPCR	mGAPDH	R
*Pb*18SrRNA-for	AAGCATTAAATAAAGCGAATACATCCTTAC	qPCR	18SrRNA	F
*Pb*18SrRNA-rev	GGAGATTGGTTTTGACGTTTATGTG	qPCR	18SrRNA	R

[a] Restriction endonuclease (REase) sites in primer sequence.
[b] TV and GT indicate primers designed for the generation of transfection vectors and genotyping, respectively. RT-PCR and qPCR indicate primers used for reverse transcription PCR and quantitative real-time PCR, respectively.
[c] Forward (F) and reverse (R) sense primers.

2.1.12 Software and databases

Primer design was performed with Primer3 (http://frodo.wi.mit.edu/) and OligoCalc (Kibbe, 2007). SerialCloner 2.1 (Serial Basics) and EnzymeX (Nucleobytes Inc.) were used for DNA sequence analysis and plasmid design. DNA and amino acid sequence alignments were done with ClustalW2 (Larkin et al., 2007) and MUSCLE (Edgar, 2004).

PlasmoDB (Aurrecoechea et al., 2009), EupathDB (Aurrecoechea et al., 2007), OrthoMCL (Chen et al., 2006) and BLAST (Altschul et al., 1990) were used for DNA and amino acid sequence retrieval and search for gene orthologs.

In silico prediction of cellular localization of proteins was done with PlasmoAP (Foth et al., 2003a), ApicoAP (Cilingir et al., 2012a), MitoProt (Claros and Vincens, 1996) and PlasMit (Bender et al., 2003a).

Flow cytometry analysis was performed with FlowJo™ software . Statistical analysis was done with GraphPad Prism version 5.0c (GraphPad Software, Inc.). Image and data processing was done with Adobe® Illustrator, Adobe® Photoshop, ImageJ (US National Institute of Health, Bethesda), GraphPad Prism version 5.0c (GraphPad Software, Inc.), Microsoft® Excel and Microsoft® Powerpoint. The bibliography was managed with EndNote (Thomson Reuters).

2.2 Methods

2.2.1 Microbiological methods

2.2.1.1 Culture of *E. coli* on agar plates

To obtain clonal colonies of *E. coli*, liquid cultures were spread with glass beads on agar plates containing ampicillin. These were incubated over night at 37°C and kept at 4°C for long-term storage.

2.2.1.2 Culture of *E. coli* in liquid medium

For liquid culture of *E. coli*, 3ml (for mini-preps) or 50ml (for midi-preps) of LB-medium containing 1:1000 ampicillin stock solution were inoculated with cells from one colony on a agar plate or from glycerol-stock. Cultures were incubated over night at 37°C and 230rpm.

2.2.1.3 Long-term storage of *E. coli*

800µl of overnight liquid bacteria culture was mixed with 300µl 80% glycerol in cryo-tubes and stored at -80°C.

2.2.1.4 Transformation of *E. coli*

Competent *E.coli* XL1 blue cells were thawed for 10min on ice. Per transformation reaction 0.68*µ*l β-Mercaptoethanol was added to 35*µ*l of cells and incubated for 10min on ice. 5*µ*l ligation reaction was added to the cells and kept on ice for 30min. Heatshock was performed at 42°C for 45s. Cells were kept on ice for 2min and then 100*µ*l pre-warmed SOC medium was added and bacteria were spread with glass beads on pre-warmed LB agar plates containing ampicillin. Plates were incubated over night at 37°C.

2.2.2 Molecular biological methods

2.2.2.1 Agarose gel electrophoresis

Agarose gel electrophoresis was performed to separate DNA molecules, according to their charge, size and conformation. Gels were typically prepared with 1% agarose in 1x TAE buffer. The solution was boiled in a microwave to dissolve the agarose and after cooling down, 12*µ*l SYBR Safe green (10µg/ 100ml) was added. The DNA samples were loaded in 1x loading dye. 3 to 5*µ*l of 1kb ladder was loaded and DNA fragments were separated at about 100V for 40-60 min. Ultraviolet light was used to visualize the separated DNA molecules in a gel documentation system.

2.2.2.2 Isolation of recombinant plasmids

Plasmids were isolated from *E. coli* over night liquid cultures using the QIAprep Spin Miniprep Kit (Qiagen) or, for large scale-preparation of transfection plasmids, the HiSpeed Plasmid Midi Kit (Roche) according to the manufacturer's protocol.

2.2.2.3 DNA purification by ethanol precipitation

Plasmids for transfection of parasites were purified by precipitation using 0.1x volumes of sodium acetate (pH 4.8) and 2.5 x volumes of 100% ethanol. After a 5min incubation at -80ºC, the precipitated DNA was collected by centrifugation for 10min at maximum speed (13,000 rpm) at 4ºC. The DNA pellet was washed two times with ice-cold 70% ethanol and centrifuged for 5min at 4ºC. The air-dried DNA pellet was then dissolved in an appropriate volume of ddH_2O.

2.2.2.4 DNA purification using the PCR purification kit

For purification of PCR fragments and digestion preparations, the PCR purification kit (Qiagen) was used according to the manufacturer' protocol. PCR fragments were analyzed by agarose gel electrophoresis.

2.2.2.5 Amplification of DNA sequences by polymerase chain reaction (PCR)

PCR was used to amplify specific DNA sequences for molecular cloning and parasite genotyping. Platinum *Taq*-Polymerase was employed for amplification of fragments used for expression cloning and *Taq*-Polymerase was used for analytical PCR. Due

to the high AT content of *Plasmodium* DNA, the annealing temperature was typically 55°C and the extension temperature was 60ºC. PCR composition and conditions were further set according to the primers, polymerase and amplification targets. PCR products were purified with the QIAquick PCR Purification Kit (Qiagen) following the manufacturer's protocol if used for molecular cloning.

Standard PCR program:

Step 1: Denaturation	94ºC, 5min
Step 2: Denaturation	94ºC, 30s
Step 3: Annealing	55ºC, 30s
Step 4: Elongation	60ºC, 2-5min
Cycling between steps 2-4	35 cycles
Step 5: Elongation	60ºC, 10min
Step 7: store	4ºC, ∞

2.2.2.6 Restriction endonuclease reactions

DNA was digested with restriction endonucleases purchased from New England Biolabs. For test-digests of recombinant plasmids, typically, 1µl of DNA from a Mini or Midi plasmid preparation was digested for 1h at 37°C and analyzed by agarose gel electrophoresis.

2.2.2.7 Ligation of DNA fragments

DNA ligations were performed using the Rapid Ligation Kit (Roche) according to the manufacturer's protocol.

2.2.2.8 Construction of *Plasmodium* targeting vectors

For generation of *PALM-mCherry-myc* parasites fragments of the C-terminal coding region and 3' untranslated region (UTR) of *PALM* were amplified from gDNA using gene-specific primers: PbPALM-F5-EcoRI and PbPALM-R5-Blunt (C-terminal fragment, 422bp), and PbPALM-F7-HindIII and PbPALM-R6-KpnI (3' fragment, 545bp). Fragments were cloned into a vector (pBAT intermediate construct) (Kooij et al., 2012), which contains the *mCherry* coding region fused to a quadruple *c-myc* tag sequence and the pyrimethamine-resistant *Toxoplasma gondii* dihydrofolate

reductase/thymidylate synthetase cassette. The resulting plasmid, pPbPALM-mCherry-myc, was linearized with *EcoRI* and *Acc65I* and to minimize transfection with partially digested plasmid ampicillin resistance cassette was cut with *ScaI*.

In order to generate *palm*$^{-}$ parasites, fragments of the 5'UTR and part of the N-terminal coding region and of the 3'UTR were amplified from gDNA using the following primer combinations: PbPALM-F2-BamHI and PbPALM-R1-EcoRI (5' fragment, 587bp), and PbPALM-F7-HindIII and PbPALM-R6-KpnI (3' fragment, 545bp). PCR fragments were cloned into the B3D vector. The resulting plasmid, pPbPALM-KO, was linearized with *BamHI* and *Acc65I*. In addition, the plasmid backbone was cut with *SapI* to minimize transfection with partially digested plasmid. This plasmid was used to transfect *P. berghei* ANKA parasites and a clone, termed ANKA-GFP, which expresses GFP under the control of the constitutive *PbEF1a* promoter (Janse et al., 2006b).

For a third *palm*$^{-}$ parasite line, termed *palm*$^{-}$*-NT-tag*, fragments of the 5'UTR including part of the N-terminal coding region corresponding to the apicoplast targeting signal and of the 3'UTR were amplified from gDNA using the following primer combinations: PbPALM-F3-NotI and PbPALM-R3-PshAI (5' fragment, 700bp), and PbPALM-F7-HindIII and PbPALM-R6-KpnI (3' fragment, 545bp). PCR fragments were cloned into a targeting vector (pBAT intermediate construct) (Kooij et al., 2012), which contains the *mCherry* coding region fused to a quadruple *c-myc* tag sequence and the pyrimethamine-resistant *Toxoplasma gondii* dihydrofolate reductase/thymidylate synthetase cassette. The resulting plasmid, pPbPALM-KO2, was linearized with *NotI* and *ScaI*., and cut with *SapI* to minimize transfection with partially digested plasmid.

For targeted gene deletion of the *P. berghei SUF* and *NFUapi* genes, fragments of the 5'UTR and of the 3'UTR were amplified using gene-specific primers (see chapter 2.1.10) from gDNA. PCR fragments were cloned into the *berghei* adaptable recyclable transfection vector (pBART-SIL6) (Kooij et al., 2012), which contains drug-selectable and high-expressing GFP cassettes. First, the 3'UTR homologous sequences were cloned following restriction digestion of vector and insert with *HindIII* and *KpnI*. Then, the 5'UTR homologous sequences digested with *SacII* and *EcoRV* were cloned into *SacII* and *PvuII* linearized vector, thus removing the mCherry-3xMyc tag from the original vector. The resulting plasmids were linearized with *SalI* and *ScaI* and used to transfect *P. berghei* ANKA parasites.

2.2.2.9 Determination of DNA concentration

DNA concentration was determined using the Nanodrop ND 1000.

2.2.2.10 DNA sequencing

When coding gene regions were amplified for generation of gene-tagging vectors, correct PCR amplification was verified by DNA sequencing (MWG), in order to avoid unwanted mutations or frame-shifts and to ensure subsequent functionality.

2.2.2.11 Isolation of mRNA

Isolation of parasite mRNA was performed with the RNeasy Mini Kit (Qiagen). Collected parasite cells were kept in 350µl RTL buffer with 3.5µl β-mercaptoethanol, in RNAse free tubes and stored at –80°C. After mRNA isolation, samples were eluted in H_2O and subsequently processed to cDNA or stored at –80°C. An additional DNAse treatment was applied with Turbo DNAse to avoid gDNA contamination of samples. For mRNA isolation filter tips were used to avoid RNase contamination of the sample.

2.2.2.12 Complementary DNA (cDNA) synthesis and reverse transcription PCR (RT-PCR)

RT-PCR was used to confirm inactivation of *PALM*. Total RNA was isolated from livers excised from infected mice at 44h after infection using the RNeasy Mini kit (Qiagen) following the manufacturer's protocol. To remove contaminating genomic DNA, RNA samples were treated with Turbo-DNA-free (Ambion). After clearance of gDNA contamination was confirmed by PCR, cDNA was synthesized by a two-step PCR reaction using oligo dT primers (Ambion). For the detection of PALM transcripts, cDNA samples were tested using gene specific primers PbPALM-F6 and PbPALM-R5 (260bp). Primers specific for heat shock protein 70 (HSP70, PbHSP70-F and PbHSP70-R, 164bp) were used to control cDNA load.

2.2.2.13 Southern blot analysis

Genotyping of knockout parasite lines was confirmed by Southern blot analysis using the PCR DIG Probe Synthesis kit and the DIG Luminescent Detection kit (Roche), according to the manufacturer's protocol.

In short, gDNA of blood-stage parasites was isolated and 1-5µg of gDNA were precipitated and dissolved in 10-50µL of water. Digestion of gDNA was performed over night at 37°C in a reaction volume of 25-40µl. Digested gDNA was run on a 0.8% agarose gel o/n at 15-20V. The gel was stained with SYBR safe and a picture of the gel was taken with a ruler next to it. The DNA in the agarose gel was depurinated in 0.5M HCl for 10min and then denatured in 0.5M NaOH/ 1.5M NaCl for 30min. The DNA was blotted on a Hybond-N membrane for a few hours or over night. Hybridization and probe detection was performed using DIG Easy Hyb and DIG Luminescent Detection kit (Roche) according to the manufacturer's protocol.
Probe synthesis was done with the PCR DIG Probe synthesis kit (Roche).
For genotyping of WT ANKA-GFP and *palm*$^{-}$ ANKA-GFP primers PbPALM-F2-BamHI and PbPALM-R1-EcoRI, and PbPALM-F7-HindIII and PbPALM-R6-KpnI were used for amplification of the 5' and 3' probes, respectively. The 5' probe was annealed to *EcoRI*-digested gDNA resulting in bands of 8.2kb (ANKA GFP) and 3.6kb (*palm*$^{-}$ ANKA-GFP). The 3' probe was annealed to *KpnI*-digested gDNA resulting in bands of 1.5kb (WT ANKA-GFP) and 5.3kb (*palm*$^{-}$ ANKA-GFP).
For analysis of the clonal *nfu*$^{-}$ parasite line primers TV-3'NFU-F and TV-3'NFU-R were used for amplification of the hybridization probe. The hybridization probe was annealed to *NdeI*-digested gDNA resulting in bands of 2.2kb (WT) and 7.0kb (*nfu*$^{-}$).

2.2.3 *Plasmodium berghei* methods

2.2.3.1 Rearing of *Anopheles stephensi* mosquitoes

Mosquitoes were raised in a 14h light /10h dark cycle, at 75 % humidity and kept at 28°C or 20°C for uninfected and infected mosquitoes, respectively. Adult mosquitoes were fed with sucrose solution and mosquito breading solution.

2.2.3.2 Mosquito infection with *P. berghei*

Mosquitoes were infected 2 to 6 days after hatching. Mosquitoes were starved for several hours prior to blood meal feeding. A drop of tail-blood was analyzed for male gametocyte exflagellation and mice were only used for blood-meal, if at least three

exflagellation centers (each corresponding to one male gametocyte) could be observed per microscopic field. The mice were anesthetized with 80-100µl ketamin/ xylazinhydrochlorid. Infected mice were placed on top of mosquito cages and mosquitoes were allowed to feed for about 30min. After blood meal, the mosquitoes were kept in incubators at 20°C to ensure optimal parasite development.

2.2.3.3 Exflagellation assay of male gametocytes

In order to characterize the functionality of mutant parasites or to obtain optimal mosquito infection rates, exflagellation of male gametocytes can be tested *ex vivo*. A drop of tail-blood is placed onto a cover slip and examined with the 40x objective using a bright-field microscope. The drop in temperature induces the exflagellation process after about 10min (Billker et al., 1997). Exflagellation centers per microscopic field were then counted.

2.2.3.4 Analysis of *Plasmodium* mosquito-stage development

Blood-feeding and mosquito dissection were performed as described previously (Vanderberg, 1975). In order to determine infectivity, and quantify midgut and salivary gland associated sporozoites, infected mosquitoes were dissected at days 10, 14 and 17-21 after feeding, respectively. Oocysts of GFP-expressing parasites and non-fluorescent parasites were counted in isolated midguts using a fluorescent microscope or a bright-field microscope, respectively. Midguts and salivary glands were grinded with plastic pestles to liberate sporozoites. After two washing steps, sporozoites were counted in a Neubauer chamber using a bright-field microscope.

2.2.3.5 Giemsa-stained blood smears and determination of parasitemia

Giemsa staining of *Plasmodium* blood stages allows the monitoring of red blood cell infection, differentiation between developmental stages and determination of the parasitemia, the percentage of erythrocytes infected with *Plasmodium*.

One drop of tail-blood from an infected mouse was smeared on a glass slide. The slide was fixed in methanol for a few seconds and then stained in Giemsa solution for 5 to 20min. The slides were rinsed in water and air-dried. Microscopical analysis was performed using a 100x objective of a bright-field microscope. The number of erythrocytes in one field was determined and the number of parasites was counted in 15 to 50 fields with comparable erythrocyte density. The parasitemia was calculated

as follows: # of parasites / (# of erythrocytes per field x # of counted fields).

2.2.3.6 Infection of mice with salivary gland sporozoites

For all infections with *P. berghei* sporozoites female C57BL/6 mice were used. Sporozoites were liberated from mosquito salivary glands and injected in a maximum volume of 100µl RPMI medium into the tail-vein.

2.2.3.7 Overnight *P. berghei* culture and purification of schizonts for transfection

Transfection of *P. berghei* mature schizonts purified from parasite overnight cultures and selection of recombinant parasites was performed as described previously (Janse et al., 2006a; Waters et al., 1997).

To obtain parasites for the overnight culture, NRMI mice were infected by intraperitoneal injection of either *Plasmodium berghei* ANKA (WT ANKA) or *Plasmodium berghei* ANKA-GFP-507cl (WT ANKA-GFP) parasites. Animals with 2 to 3% parasitemia and low gametocyte density were used for the schizonts culture. The blood was harvested by heart puncture from isofluran-anesthetized animals with heparin-treated syringes. The blood was washed once in 10ml of pre-warmed transfection medium, containing 250µl heparin/PBS (200U/ml), by centrifugation at 1,000rpm for 8min at room temperature. The blood pellet was mixed with 50ml of pre-warmed transfection medium and pipetted under the final 100ml transfection culture in the Erlenmeyer vessel. The culture was incubated for 16 to 18h at gentle shaking by 77 to 80 rpm at 37°C in a mixed gas incubator at 10% O_2, 5% CO_2 and 85% N_2. The culture was monitored for schizont development by Giemsa-stained thin blood smears. When enough schizonts were detected, the culture was transferred into four 50ml tubes (35ml per tube). A 55% Nycodenz/PBS solution (27.5ml Nycodenz stock solution + 22.5ml sterile PBS) was prepared and 10ml of the Nycodenz-solution were gently pipetted under the culture suspension in each tube. The tubes were tared and centrifuged for 25min at 1,500rpm, RT, without brake. The brown interphase (30-40ml) was carefully collected with a Pasteur pipette. 20ml of culture medium from top of gradients were added to wash the schizonts by centrifugation at 1,500rpm for 8min. The supernatant was discarded and the pellet was used for electroporation.

2.2.3.8 Electroporation of *P. berghei* schizonts

The schizont pellet was resuspended in culture medium and transferred to x eppendorf tubes (1.1^7-3.10^7 parasites in 1ml for one transfection). The cells were pelleted by centrifugation for 5s at maximum speed. The supernatant was discarded, and the parasite pellet resuspended in 100µl Human T-cell Nucleofactor solution buffer, which contained 5-10µl DNA (1µg/µl final concentration. This solution was transferred to a cuvette and was transfected with the Amaxa gene pulser using protocol U33. Immediately after transfection, 50µl culture medium was added and transfected parasites were injected intravenously into the tail-vein of a naive NMRI mouse.

2.2.3.9 Positive selection of recombinant parasites

One day after transfection, the selection pressure was applied by adding the antifolate drug pyrimethamine (70 ng/ml; pH 3.6- 5.0) to the drinking water of NMRI mice. Parasitemia was monitored starting at day 8 after transfection. When parasitemia reached <1%, blood was collected by heart-puncture. Parasites were stored as blood stabilates and parasite gDNA was isolated for genotyping.

2.2.3.10 Cryostabilates for long-term storage of blood-stage parasites

100µl of blood from an infected mouse was mixed with 200µl freezing solution and stored in cryo-tubes in liquid nitrogen or at -80°C.

2.2.3.11 Isolation of parasites from infected blood

Blood of *P. berghei* -infected mice was obtained by heart-puncture. Erythrocytes were separated from leukocytes and thrombocytes by running the blood through a column filled with cotton, cellulose and glass beads (from bottom to top). The erythrocytes were eluted from the column with 1xPBS and collected in a 15ml falcon tube. Erythrocytes were pelleted by centrifugation at 1,500 rpm for 8min at room temperature. Subsequently, parasites were isolated by erythrocyte lysis, through resuspension of the erythrocyte pellet in 14ml 0.2% Saponin/ 1xPBS. The parasites were pelleted by centrifugation for 8min at 3,000 rpm, room temperature. Parasites were transferred to a 1.5ml eppendorf tube and washed once in 1xPBS by centrifugation at 7,000rpm for 3min at room temperature. The parasite pellet was

resuspended in 200µl 1xPBS and stored at –20 °C or directly used to isolate parasite gDNA.

2.2.3.12 Isolation of parasite genomic DNA

The genomic DNA was isolated from blood stage parasites for gene amplification or genotyping of transgenic parasite lines. Blood of infected mice was obtained by heart-puncture and parasites were isolated as described. The gDNA was then isolated with the QIAamp DNA-Blood Mini Kit (Qiagen) according to the manufacturer's protocol and stored at –20°C.

2.2.3.13 Genotyping of parasite populations

For genotyping of parasite populations after transfection experiments, parasite gDNA was isolated and tested by WT- and integration-specific PCR.

Integration-specific PCR amplification of the *PALM* locus to confirm the predicted deletion of PALM in *palm*$^{-}$ ANKA and *palm*$^{-}$ ANKA-GFP parasites was done using the following primers: PbPALM-F1 and TgForw (5' integration, 1261bp), TgRevPro and PbPALM-R7 (3' integration, 988bp), PbPALM-F1 and PbPALM-R2 (5' ANKA-GFP control, 799bp), and PbPALM-F6 and PbPALM-R7 (3' ANKA-GFP control, 906bp). For 5' ANKA-GFP control of *palm*$^{-}$*-NT-tag* parasites the primers PbPALM-F1 and PbPALM-R4 (904bp) were used.

Correct integration in *PALM-mCherry-myc* parasites was confirmed using the following specific primer combinations: PbPALM-F4 and mCherryRev (5' integration, 979bp), TgRevPro and PbPALM-R7 (3' integration, 988bp), PbPALM-F4 and PbPALM-R6-KpnI (5' ANKA-GFP control, 1,450bp), and PbPALM-F6 and PbPALM-R7 (3' ANKA-GFP control, 906bp).

Integration-specific PCR amplification of the *NFUapi* locus to confirm the predicted deletion of *NFUapi* was done using the following primers: 5'HSP70rev and GT-5'NFU-F (5' integration, 958bp), and GT-3'NFU-R and 5'DHFRrev (3' integration, 1,210bp). Absence of WT-specific PCR products using primers GT-5'NFU-F and GT-5'NFU-R (5' WT ANKA control, 960bp), and GT-3'NFU-F and GT-3'NFU-R (3' WT ANKA control, 702bp) were used to confirm the purity of the clonal *nfu*$^{-}$ parasite line.

Integration-specific PCR amplification of the *SUF* loci was performed as for the *NFUapi* locus with the according locus specific primers.

All primer sequences, including primers for WT-specific PCRs, are listed in section 2.1.10.

2.2.3.14 Parasite cloning by limiting parasite dilutions

Clonal parasite populations were obtained *in vivo* by intravenous injection of limiting dilutions of one parasite per recipient NMRI mice, and calculated as follows:
$7 \times 10^6 \times$ parasitemia $\times 10^{-2}$ parasites = number of parasitized erythrocytes per µl blood.
Blood was collected by heart-puncture from mice with < 1 % parasitemia and series of 6 1:10 dilutions were prepared in RPMI medium on ice. After intravenous injection of single parasites in a volume of 100µl into NMRI mice, animals were kept under pyrimethamine treatment. When the parasitemia reached >1% mice were bled by heart-puncture. Stabilates for long-term storage were prepared and gDNA was isolated. The clonality of the parasite population was confirmed by PCR with integration specific primers.

2.2.3.15 Parasite cloning by flow cytometry

Parasite cloning by flow cytometry was performed as recently described (Kenthirapalan et al., 2012).
When parasitemia of the parental population was still <1%, one drop of tail blood was collected and resuspended in 1ml of Alsever's solution in order to minimize agglutination of the blood. The samples were passed through 30µm CellTrics filters to remove cell aggregates. All sorting experiments were performed on a BD Biosciences FACSDiva using a purity sort-mask at a sorting speed of 30,000 events per second. Excitation of GFP was done at a wavelength of 488 nm, while fluorescence was detected using a band pass filter of 530/30 nm with the photomultiplier tube voltage set to its maximum sensitivity. Forward and sideward scatter gating was used to exclude small particles (such as blood platelets and debris) as well as overly large cells (predominantly leukocytes). The remaining population mainly consisted of erythrocytes and was gated for high-expressing GFP (GFP_{hi}) but low-expressing phycoerythrin (PE_{lo}) cells, thus excluding autofluorescent cells with equal GFP and PE levels, 500 of which were collected in 200µl of 20% FCS/RPMI. After sorting, the collection tube was washed with 800µl of 20% FCS/RPMI. Naive recipient NMRI mice were injected intravenously with 100µl cell

suspension containing approximately 50 parasite-infected erythrocytes. At a parasitemia of >1%, mice were bled, parasite stabilates were frozen, and parasite gDNA was isolated. FACS sorting was done in collaboration with the Flow Cytometry Core Facility at the Deutsches Rheuma-Forschungszentrum (Berlin).

2.2.3.16 Phenotypical analysis of mixed blood-stage parasites growth *in vivo*

NMRI mice were injected intravenously with 1,000 blood-stage parasites and monitored for blood stage development by daily examination of Giemsa-stained thin blood smears.

2.2.3.17 Blood-stage transfer experiment

In order to test the presence of parasites in the blood below Giemsa-stained thin blood smear detection threshold, blood-transfers were performed. C57BL/6 mice were infected by bites of mosquitoes infected with WT ANKA-GFP or *palm*$^{-}$ ANKA-GFP parasites. At day 3, 4 and 5 after infection (when parasitemia was undetectable by thin blood smears), about 30μl of tail-blood were transferred by intravenous injection into naive recipient mice. Development of blood-stage infection was monitored in the recipient mice by daily thin Giemsa-stained blood smears.

2.2.3.18 Evans Blue staining for assessment of blood-brain barrier breaching

During all experiments, mice were monitored for the development of behavioral and functional abnormalities (Lackner et al., 2006), as indicators of ECM development. Mice were classified as suffering from ECM when they were diagnosed with at least three behavioral and functional abnormalities (e.g. positional passivity, body position, limb grasping, toe pinch, etc.). Mice were immediately sacrificed upon showing sudden onset of signature symptoms of ECM, such as ataxia, paralysis, convulsions or coma. To test the integrity of the blood–brain barrier as a further indication for the susceptibility to ECM, 100μl of 2% Evans Blue were injected in saline intravenously into naive C57BL/6 mice, or mice infected with 10,000 or 100,000 *palm*-, or 10,000 WT ANKA-GFP sporozoites at day 4 after patency. After one hour, mice were sacrificed, brains prepared, and digital images taken using standardized lighting, exposure and white balance settings. This experiment was done in collaboration with Dr. Taco Kooij and Carolin Nahar.

2.2.3.19 Liver-stage development assay

P. berghei in vitro liver stages were cultured in DMEM complete medium and analyzed using standard techniques (Silvie et al., 2008). 30,000 hepatoma (HuH7) cells per well were plated in eight-well chamber slides (Nalge Nunc International). After 24h the cells were incubated with 10,000 sporozoites. First for 60min at room temperature, then at 37°C for 90–120min. Non-invaded sporozoites were washed off and medium was changed daily. At the time points indicated, infected hepatoma cultures were fixed for 10min with ice-cold methanol and blocked with PBS/10% FCS. For drug tests with azithromycin and fosmidomycin, antibiotics were added to the DMEM complete medium and were applied after washing off the sporozoites. Medium was changed daily and cells were kept in this medium until development was stopped with methanol. Controls contained DMEM complete medium with equal amounts of DMSO, when drugs were dissolved in DMSO.

2.2.3.20 Merosome development assay

Merosome formation was followed using two different methods, either by (1) seeding of 100,000 to 150,000 Huh7 hepatoma cells per well in 24-well plates and inoculation with 100,000 sporozoites per well 24h later, or by (2) seeding of 30,000 Huh7 hepatoma cells per well in eight-well Labtek chamber slides and inoculation with 10,000 sporozoites 24h later. Sporozoites were left to settle for one hour at room temperature. Sporozoite invasion occurred at 37°C for 1.5 to 2 hours. After invasion sporozoites were carefully washed off with DMEM complete medium. Culture medium was changed 24 and 48h after infection. Merosomes were harvested and counted in a Neubauer chamber 72h after infection.

2.2.3.21 Infection of mice with merosomes

Infectivity of *in vitro* cultured WT ANKA-GFP and *palm*$^{-}$ parasites was tested by intravenous injection of the complete merosome containing liver-stage culture supernatants in naive NMRI mice. All animals were monitored for parasitemia by daily Giemsa-stained thin blood smears.

2.2.3.22 Quantification of relative parasite liver infection load by real-time PCR

Plasmodium liver stages can be detected and quantified by real-time PCR (Bruna-Romero et al., 2001). For quantification of parasite liver loads, mice were immunized

twice with 10,000 *palm*$^{-}$ sporozoites and received one challenge/boost by intravenous injection of 10,000 WT sporozoites. One year after the last boost, animals were challenged by intravenous injection of 10,000 WT sporozoites. Control animals were one year old. Mice were sacrificed 41h after challenge infection, and livers were removed and homogenized. Total RNA was extracted using the RNeasy Kit (Qiagen) and used as template for cDNA synthesis with the RETROscript Kit (Ambion) according to the manufacturer's protocol. Quantitative real-time PCR was performed using the Power SYBR Green PCR Master Mix (Applied Biosystems). All reactions were performed in triplicate.

Standard qRT-PCR program:
Step 1: 95°C, 15 min
Step 2: 95°C, 15 sec
Step 3: 55°C, 15 sec
Step 4: 60°C, 45 sec
Step 5: 40 cycles between step 2 and 3
Step 6: 60°C, 45 sec

The mean C_t value of the *P. berghei 18S* ribosomal subunit (gene ID: 160641), normalized to the C_t value of mouse *GAPDH* (gene ID: 281199965) was determined with the ΔΔCt method, as described previously (Friesen et al., 2010).

2.2.3.23 Immunofluorescent assays (IFA) of *P. berghei*

To quantify liver-stage parasites, monoclonal mouse anti-*P. berghei* heat shock protein 70 (HSP70) antibodies (1:300 dilution; (Tsuji et al., 1994)) were used. Bound antibodies were detected using donkey anti-mouse IgG Alexa Fluor 488 conjugated antibodies (1:3000 dilution, Invitrogen). Nuclei were visualized with DNA-dyes Hoechst 33342 (Invitrogen) and DRAQ5 (Axxora; both 1:1000 dilution) and coverslips were mounted with Fluoromount-G (Southern Biotech). Total numbers of parasites were counted using a Leica DM2500 epifluorescence microscope.
Midguts of *PALM-mCherry-myc* infected mosquitoes were dissected at day 10 after infection and fixed with 4% paraformaldehyde with 0.0075% glutaraldehyde. Subsequently, midguts were permeabilized with 0.5% Triton X-100 and blocked with 3% bovine serum albumin. Incubation with mouse anti-myc antibodies (1:200 dilution, Santa Cruz Biotechnology) was done overnight at 4°C. Bound antibodies were

detected using donkey anti-mouse IgG Alexa Fluor 488 conjugated antibodies (1:2,000 dilution, Invitrogen).

Salivary glands of *PALM-mCherry-myc* infected mosquitoes were dissected and liberated sporozoites were settled in RPMI medium containing 3% bovine serum albumin and fixed with 4% paraformaldehyde. Subsequently, sporozoites were permeabilized with 0.1% Triton X-100 in PBS and blocked with 3% bovine serum albumin. Incubation with mouse anti-myc antibodies (1:100 dilution, Santa Cruz Biotechnology) was done overnight at 4°C. Bound antibodies were detected using donkey anti-mouse IgG Alexa Fluor 546 conjugated antibodies (1:1,000 dilution, Invitrogen).

Liver-stage *PALM-mCherry-myc* parasites were fixed and incubated with mouse anti-myc antibodies (1:1000 dilution, Santa Cruz Biotechnology). To confirm apicoplast targeting of PALM, liver-stage parasites were co-stained with rabbit anti-*P. berghei* ACP peptide antiserum (1:750 dilution;(Friesen et al., 2010)). Completion of liver merozoite formation was analyzed using rabbit anti-*P. berghei* upregulated in infectious sporozoites protein 4 (UIS4) peptide antiserum (1:2,000 dilution; kindly provided by Dr. G. Montagna, MPI-IB, Berlin) and a monoclonal mouse anti-*P. yoelii* merozoite surface protein 1 (MSP1) antibody against a 90 kDa N-terminal fragment of the protein that shares 74% identity with *P. berghei* MSP1 (1:2,000 dilution; kindly provided by Prof. Dr. A. Holder, National Institute for Medical Research, London, UK). Bound antibodies were detected using donkey anti-rabbit/mouse IgG Alexa Fluor 488/546 conjugated antibodies (1:3,000 dilution, Invitrogen).

For confirmation of expression and determination of the subcellular localization of NFUapi, fixed *nfu::tag* liver stage parasites were incubated with mouse anti-myc antibodies (1:1,000 dilution, Santa Cruz Biotechnology) and rabbit anti-*P. berghei* ACP peptide antiserum (1:750 dilution). Monoclonal mouse anti-*P. berghei* heat shock protein 70 (HSP70) antibodies (1:300 dilution;(Tsuji et al., 1994)) were used to visualize and quantify *nfu*– liver stage parasites. Bound antibodies were detected using donkey/goat anti-rabbit/mouse IgG Alexa Fluor 488/546 conjugated antibodies (1:3,000 dilution, Invitrogen).

In all experiments, with exception of sporozoite stainings, nuclei were visualized with DNA-dyes Hoechst 33342 (Invitrogen) and DRAQ5 (Axxora; both 1:1,000 dilution) and coverslips were mounted with Fluoromount-G (Southern Biotech). Images were recorded using a Leica TCS SP-1 confocal microscope.

2.2.4 Immunology methods

Lymphocyte isolations, peptide stimulations and immunological flow cytometry experiments were done in collaboration with Jan Burgold.

2.2.4.1 Immunizations with *palm*$^-$ sporozoites

For all immunization experiments age-matched female C57BL/6 mice were used. Mice were immunized with two doses of 1,000 or 10,000 *palm*$^-$ sporozoites extracted from salivary glands of infected mosquitoes. Sporozoites were injected intravenously in a volume of 100µl. For the prime/boost protocol, animals that remained malaria-free after the first immunization were given a second dose 5–7 weeks after the first immunization. Only animals that remained blood-stage parasite-negative after the first immunization and subsequent boost were used for the challenge experiments at 4–6 weeks after the last immunization. Mice were challenged with five WT ANKA-GFP-infected mosquitoes, 10,000 intravenously injected WT ANKA-GFP sporozoites, or 10 intravenously injected WT ANKA-GFP blood-stage parasites. The number of ANKA-GFP salivary gland sporozoites per mosquito used for the challenge by bite ranged from 20,000 to 70,000. At least three age-matched naive animals were included to verify infectivity of sporozoites during all challenge experiments. Parasitemia was monitored by daily Giemsa-stained thin blood smears, starting from day 3 after immunization or WT ANKA-GFP challenge until at least day 17.

To test, whether vaccine efficacy is quantifiable beyond one year, two cohorts were used. All mice received two doses of 10,000 *palm*$^-$ sporozoites given at a 51 day interval. Mice in group 1 received a challenge/boost by intravenous injection of 10,000 WT ANKA-GFP sporozoites four weeks later. Animals in group 2 were first exposed to bites of five WT-infected *Anopheles* mosquitoes one month later, followed by an additional challenge/boost by intravenous injection of 10,000 WT ANKA-GFP sporozoites another two weeks later. All mice from groups 1 and 2 remained malaria-free until the final challenge. Challenge infections were done 14 and 15 months after the final boosts for animals in groups 1 and 2, respectively, by intravenous injection of 20,000 WT ANKA-GFP sporozoites. As controls for the challenge infections, five aged (15 months old) and three young (two months old) C57BL/6 mice were used. All animals were monitored for presence of blood stage parasites by daily microscopic examination of Giemsa-stained thin blood smears until day 17 after challenge.

2.2.4.2 Isolation of liver lymphocytes

For flow cytometric analysis, mice were immunized twice with 10,000 *palm*$^-$ sporozoites and received one challenge/boost by intravenous injection of 10,000 WT sporozoites. One year after the last boost, animals were challenged by intravenous injection of 10,000 WT sporozoites. Control animals were one year old. Animals were anesthetized and livers were removed 41 hours after infection.

The livers were perfused via the portal vein with 20ml PBS/ 2% FCS (pH7.0) and gently passed through a 200-gauge stainless steel mesh. Cells were resuspended in RPMI 1640 medium containing 10%FCS/ 2%penicillin/ streptomycin (RPMI complete) and centrifuged at 1,800 rpm for 3 min. The supernatant was removed and the pellet was resuspended in ~40% Percoll solution (27.1ml HBSS (Hanks' Balanced Salt Solution) or RPMI complete, 14.2ml Percoll, 1.6ml 10x PBS, 100U/ml heparin) and centrifuged at 2,000rpm for 20min at room temperature. The supernatant was discarded and the cells were washed once with RPMI complete. The pellet was resuspended in 1ml 1x NH_4Cl lysis solution and incubated for 10min. After a washing step with RPMI complete the pellet was resuspended in 400µl medium. Cell numbers were calculated using a Neubauer chamber, and live/dead cell differentiation was performed using trypan blue.

2.2.4.3 Isolation of spleen lymphocytes

For flow cytometric analysis, mice were immunized twice with 10,000 *palm*$^-$ sporozoites and received one challenge/boost by intravenous injection of 10,000 WT sporozoites. One year after the last boost, animals were challenged by intravenous injection of 10,000 WT sporozoites. Control animals were one year old. Animals were anesthetized and spleens were removed 41 hours after infection.

Spleens were pressed through a cell strainer with 5ml RPMI complete (10% FCS/ 2% penicillin/ streptomycin). The cells were then centrifuged for 3min at 1,800rpm.

The pellet was resuspended in 1ml 1x Lysing buffer and incubated at room temperature for 10min. RPMI complete was added to obtain a total volume of 15ml and cells were centrifuged for 3min at 1,800rpm. In the end the pellet was resuspended in 1ml RPMI complete.

2.2.4.4 Surface staining of lymphocytes

For phenotypic analysis of cellular activation, cells were surface stained for CD8 (clone 53.6-7), CD4 (clone GK1.5) and CD11a (clone M17/4). Cells were resuspended in 50µl per well in a 1:150 dilution of the surface marker in 2%FCS/ PBS and incubated at 4°C for 30min. Cells were then washed twice with 2% FCS/ PBS and then centrifuged for 3min at 1,800rpm.

2.2.4.5 *Ex vivo* peptide stimulations

For the analysis of IFN-γ, IL-2, and TNF production, cells were stimulated with antibodies to CD3 (145-2C11) and CD28 (37.51), with the S and T peptides corresponding to immunodominant $CD8^+$ T cell epitopes (Hafalla *et al.*, unpublished data), or with a peptide corresponding to a conserved $CD4^+$ T cell epitope, P1 (KIYNRNIVNRLLGDA) of *P. yoelii* circumsporozoite protein (CSP) (Boscardin et al., 2006).

30µl of spleen or liver cell suspensions per well were pipetted into a 96-well-plate and centrifuged for 3min at 1,800rpm. Lymphocytes were stimulated with 200µl per well, with one of the peptides or CD3 and CD28 antibodies in a 1:5,000 dilution in RPMI and in the presence of Brefeldin A (1:5,000). All T cell stimulations were done for 5 hours and were followed by surface staining for CD8 and CD4. After fixation and permeabilization, cells were stained for intracellular IFN-γ, IL-2 and TNF.

2.2.4.6 Intracellular cytokine staining

For intracellular cytokine staining after *ex vivo* stimulation, cells were centrifuged for 3min at 1,800rpm and then fixed with 50µl 4%PFA per well for 30min at 4°C. Subsequently, cells were permeabilized 2x with 100µl 1x Perm/Wash buffer and centrifuged for 3min at 1,800rpm. For intracellular cytokine staining, cells were incubated with anti-TNF, anti-IL-2 and anti-INFγ antibodies (1:150) in 1x Perm/Wash buffer for 30min at 4°C. Cells were then washed twice with 100µl 1x Perm/Wash buffer and resuspended in 100µl 1%PFA/PBS per well.

2.2.4.7 Flow cytometry analysis

Flow cytometers LSRII and Fortessa (BD Biosciences) were used for flow cytometry analysis of surface and intracellular cytokine stained lymphocytes and data was analyzed with FlowJo™.

3 Results

3.1 *Plasmodium* apicoplast protein important for liver merozoite formation (PALM)

3.1.1 Identification of the candidate *Plasmodium* liver stage specific gene PALM

To identify *Plasmodium* genes with a specific critical function in liver merozoite formation, available data sets (Aurrecoechea et al., 2009; Tarun et al., 2008) were systematically searched for potential liver stage-specific genes of unknown functions. The attention came to a small hypothetical gene (PY01863) expressed during liver-stage development and upregulated in late liver stages (i.e. 50 hours after infection) (Tarun et al., 2008). The only additional expression data available were from a recent RNA sequencing effort of synchronous *P. falciparum* blood stages that revealed negligible *PALM* transcription levels with a slight upregulation in mature blood stages (Otto et al., 2010).

Via BLAST analysis, orthologs were readily identified in other *Plasmodium* species such as *P. berghei* (PBANKA_010110), *P. chabaudi* (PCHAS_010180), *P. falciparum* (PF3D7_0602300), *P. vivax* (PVX_113280) and *P. knowlesi* (PKH_114760), but not in any other organism. The overall amino acid sequence identities of PALM orthologs in *P. yoelii* (PY01863), *P. falciparum* (PF3D7_0602300) and *P. vivax* (PVX_113280), compared with *P. berghei* PALM (PBANKA_010110) are 88%, 50%, and 50%, respectively (Fig. 3.1 A). Using cross-species comparisons, the *Plasmodium berghei* gene was manually re-annotated, disclosing a previously unrecognized N-terminal region. Sequence analysis through PlasmoAP, a *P. falciparum* specialized, rules-based algorithm that uses amino-acid frequency and distribution to identify putative apicoplast-targeting peptides (Foth et al., 2003a), revealed a putative apicoplast-targeting sequence in all orthologs (Fig. 3.1 A, B). For these reasons and the loss-of-function analysis (see sections 3.1.11 and 3.1.14), the protein was termed '*Plasmodium* apicoplast protein important for liver merozoite formation' (PALM).

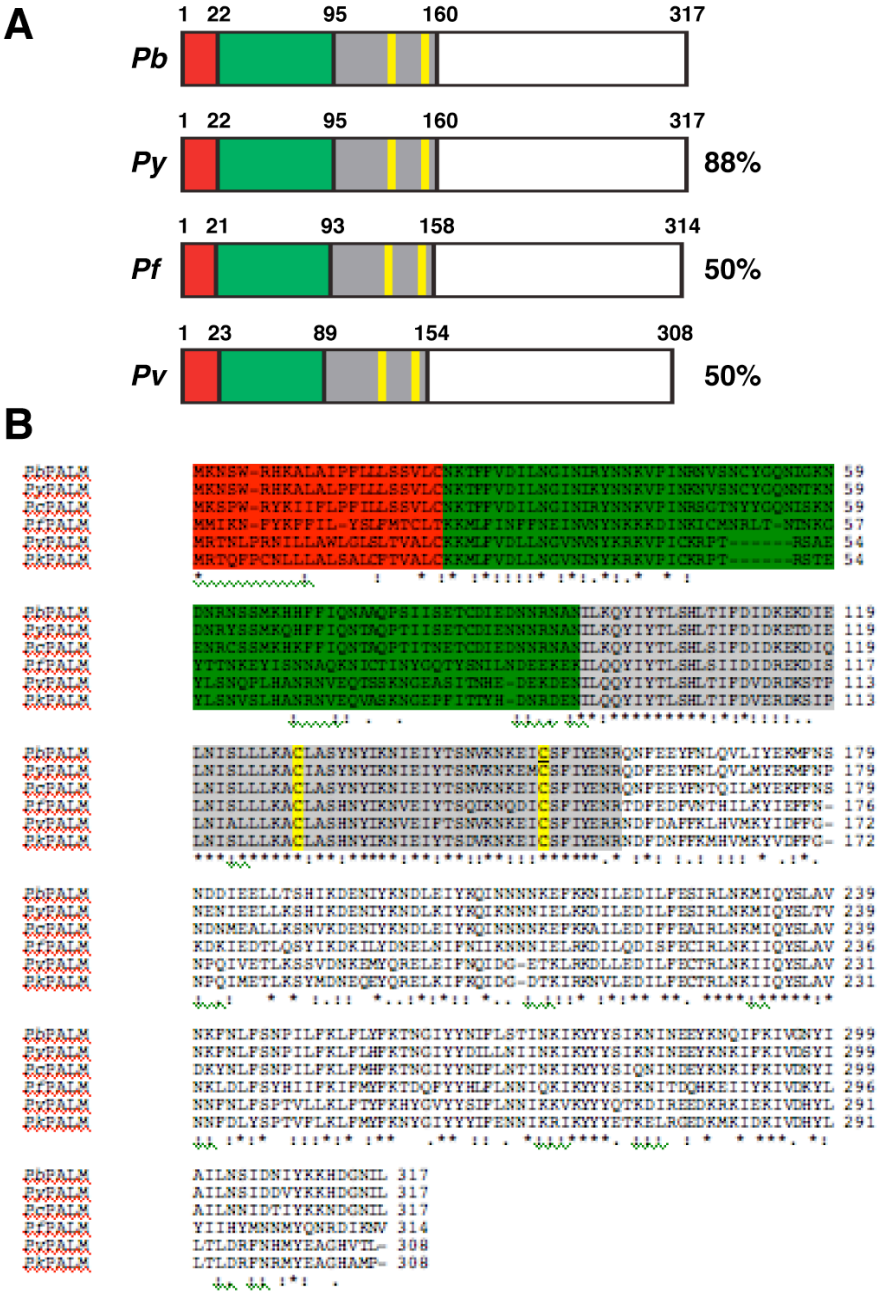

Figure 3.1: The *Plasmodium*-specific apicoplast protein important for liver merozoite formation (PALM).

(**A**) Primary structure of *Plasmodium* PALM proteins. Shown are the overall primary sequence structures and amino acid sequence identities of PALM orthologs in *P. yoelii* (PY01863), *P. falciparum* (PF3D7_0602300) and *P. vivax* (PVX_113280), compared with *P. berghei* PALM (PBANKA_010110). Signal peptide (red), apicoplast-targeting sequence (green) as predicted with PlasmoAP (Foth et al., 2003a), and the conserved domain (gray) with two conserved cysteine residues (yellow) are shown. (**B**) Sequence alignment of *Plasmodium* PALM proteins. In addition to proteins in (A), *P. chabaudi* PALM (PCHAS_010180) and *P. knowlesi* PALM (PKH_114760) are shown. Color code as in (A). * fully conserved residue, : conservation of strongly similar properties and . conservation of weakly similar properties as determined by ClustalW2 (Larkin et al., 2007).

A central, highly conserved domain that contains two strictly conserved cysteine residues is apparent in all analyzed *Plasmodium* species (Fig. 3.1 A, B). Application of a recently developed extended similarity group method (Chitale et al., 2009) predicted *P. falciparum* PALM to display potential transferase activity of uncertain specificity. However, neither functional domains nor transmembrane regions could be readily identified in *Plasmodium* PALM.

3.1.2 Generation of *PALM-mCherry-myc* parasites

The apicoplast-targeting signal prediction tool PlasmoAP revealed a high probability of PALM being targeted to the apicoplast. To confirm this *in silico* prediction and to analyze *PALM* expression *in vivo*, a parasite line was generated where the C-terminus of the endogenous *PALM* gene was linked in-frame to mCherry and a quadruple c-myc tag by a short spacer sequence (Fig. 3.2 A).

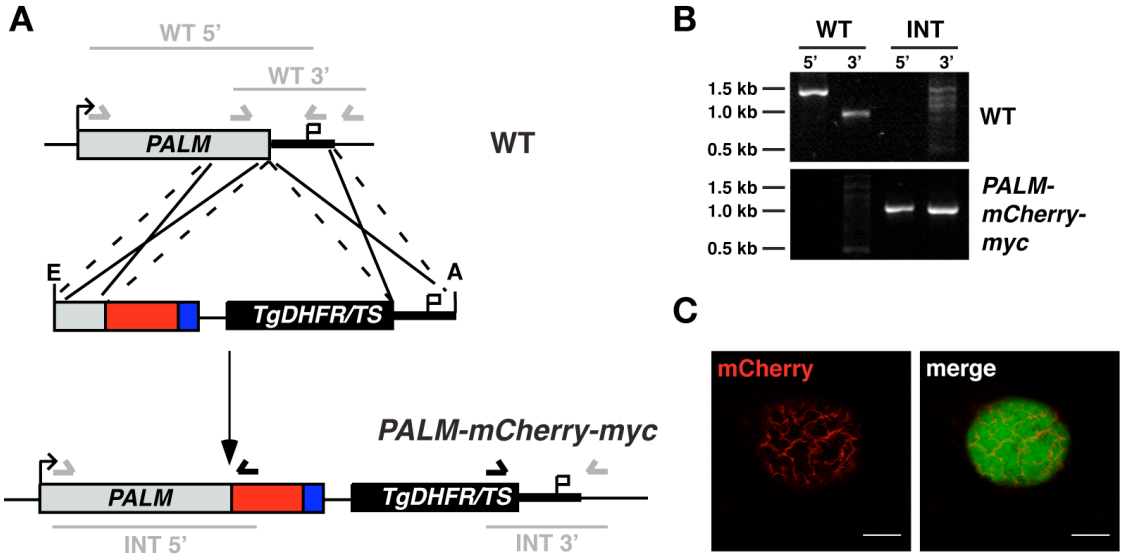

Figure 3.2: Live cell imaging of PALM in infected hepatoma cells.

(**A**) Generation of *PALM-mCherry-myc* parasites. The *PbPALM* genomic locus was targeted with a replacement plasmid containing the C-terminal *PALM* fragment (gray) fused in-frame to the *mCherry* coding sequence (red), and a quadruple *c-myc* tag (blue) and followed by the 3'UTR of *PbDHFS/FPGS*. In addition, the targeting plasmid contains the *PbDHFR/TS* positive selectable marker (black box), and a fragment of the *PALM* 3'UTR. Upon a double cross-over event, the targeting plasmid is expected to replace the endogenous *PALM* open reading frame with a C-terminally

tagged PALM fusion protein. Arrows and bars indicate specific primers and PCR fragments, respectively. (**B**) Genotyping of the *PALM-mCherry-myc* parasite line. Using integration-specific primer combinations (**A**), the successful replacement event was verified. Absence of the WT signal from *PALM-mCherry-myc* parasites confirmed the purity of the clonal population. (**C**) Hepatoma cells were infected with *PALM-mCherry-myc* sporozoites. PALM expression was visualized in late liver stages 2 days after infection. Note the branched structure of the mCherry signal. Bars, 10 μm.

For this purpose the C-terminal part and the 3'UTR of *PALM* were amplified by PCR and cloned into a targeting vector, which contains the mCherry coding region fused to a quadruple c-myc tag sequence and the pyrimethamine-resistant *T. gondii* dihydrofolate reductase/thymidylate synthetase cassette for positive selection. *Plasmodium berghei* WT ANKA-GFP parasites were transfected with the linearized plasmid and correct integration by double homologous recombination of the replacement construct was confirmed by integration specific PCR using primers PbPALM-F4 and mCherryRev (5' integration, 979 bp) and TgRevPro and PbPALM-R7 (3' integration, 988 bp) (Fig. 3.2 B). After successful integration, a clonal parasite line was generated by intravenous injection of limiting dilutions of parasites into mice. Absence of WT specific PCR products using primers PbPALM-F4 and PbPALM-R6-KpnI (5' WT ANKA-GFP control, 1450bp), and PbPALM-F6 and PbPALM-R7 (3' WT ANKA-GFP control, 906bp) confirmed the purity of the clonal *PALM-mCherry-myc* parasite line (Fig. 3.2 B).

3.1.3 *PALM-mCherry-myc* parasites exhibit normal life cycle progression

Clonal *PALM-mCherry-myc* parasites were fed to mosquitoes in two independent feedings. The infectivity at day 10 after feeding, and midgut and salivary gland sporozoite numbers at day 14 and day 17 after feeding, respectively, were assessed. Liver stage and merosome development were analyzed in cultured Huh7 cells. Finally, re-infection of mice by natural bite of *PALM-mCherry-myc* parasites infected mosquitoes showed the progression of the mutant parasites through one whole life cycle (Tab. 3.1). In all of the analyzed life cycle stages mutant parasites were indistinguishable from WT ANKA-GFP parasites (Tab. 3.1).

Table 3.1: Phenotypical analysis of *PALM-mCherry-myc* and three independent *palm*$^{-}$ clones.

		ANKA-GFP	*PALM-mCherry-myc*	*palm*$^{-}$ ANKA-GFP	*palm*$^{-}$ ANKA	*palm*$^{-}$*-NT-tag*
Infectivity[a]	Day 10	46% ± 24	38% ± 6	51% ± 6	33%	57% ± 33
# mg sporozoites[b]	Day 14	23,700 ± 8,500	15,600 ± 7,400	4,700 ± 4,400	28,8	3,300 ± 1,400
# sg sporozoites[c]	Day 17	11,900 ± 7,900 (n=3)	18,600 ± 200 (n=2)	6,100 ± 2,800 (n=7)	58,3 (n=1)	20,400 ± 6,400 (n=2)
# Liver stages[d]	24h	177 ± 65	139	139 ± 7	188	115
	48h	158 ± 72	152	120 ± 16	152	126
	72h	50 ± 38 (n=3)	41 (n=1)	98 ± 4 (n=2)	111 (n=1)	91 (n=1)
# Merosomes[e]	Method 1	810 ± 484	NA	22 ± 12	NA	NA
	Method 2	141 ± 16	84 ± 29	NA	1 ± 2	1 ± 2
# Malaria-free mice[f]	Day 6	0/9	0/3 (by bite)	82/82	10/10	20/20
	Day 10	0/9	0/3 (by bite)	62/82	3/10	6/20
	Day 14	0/9	0/3 (by bite)	60/82	3/10	5/20
Prepatency (days)[g]		3	4 (by bite)	8.7	8.4	7.9
# Mice with ECM[h]		9/9 (n=9)	NA (n=3)	5/20 (n=20)	1/7 (n=7)	0/15 (n=15)

[a] Numbers of infected midguts were determined at day 10 after the blood meal. Shown are mean numbers (± S.D.).

[b] Midgut-associated (mg) sporozoites were determined at day 14 after the blood meal. Shown are mean numbers (± S.D.).

[c] Salivary gland (sg) sporozoites were determined at day 17 after the blood meal. Shown are mean numbers (± S.D.). N is the number of independent feeding experiments from which the number of mosquito stage parasites was determined.

[d] Liver stages were immunostained with anti-*Pb*HSP70 antibodies at the indicated time points after infection of hepatoma cells. Shown are mean numbers (± S.D.). N is the number of independent experiments.

[e] Numbers of merosomes were counted in a Neubauer chamber 72 hours after infection of hepatoma cells. Shown are mean numbers of triplicate wells (± S.D.). See the methods section for the differences between the two methods used.

[f] Mice immunized twice with 10,000 *palm*$^{-}$ sporozoites were challenged with 10,000 intravenously injected WT ANKA-GFP sporozoites or in the case of *PALM-mCherry-myc* by natural bite of five infectious mosquitoes. Blood stage infection following challenge was determined by Giemsa-stained thin blood smears at indicated time points.

[g] Prepatency was determined by daily Giemsa-stained thin blood smears. Shown are mean numbers.

[h] Mice were monitored for the development of signature symptoms of experimental cerebral malaria (ECM), such as ataxia, paralysis, convulsions, and coma. N is the number of mice for which prepatency and disease development were monitored.

3.1.4 *PALM* is expressed throughout the life cycle

PALM-mCherry-myc parasites permit to follow protein expression and localization either live through the fluorescent mCherry protein tag or indirectly via antibody staining of the c-myc tag in fixed parasites. First, PALM expression was followed in live parasites. Structured, although weak, signals could be observed in *in vitro* cultured liver-stage parasites (Fig. 3.2 C). Absence of a detectable signal in any of the other life cycle stages indicated that PALM expression levels in general are low, with the exception of mature liver stages. Therefore, indirect immunofluorescence microscopy was employed using mouse anti-myc antibodies on fixed parasites, to take advantage of the quadruple myc epitope that was fused in-frame to the endogenous *PALM* open reading frame. In good agreement with the report of low levels of *PALM* transcripts in mature blood stages (Otto et al., 2010), a structured PALM signal was detected in mature asexual blood stages, but not in ring stages or trophozoites (Fig. 3.3 A). Moreover, a structured staining could be observed inside developing *Plasmodium* oocysts that segregated in mature oocysts (Fig. 3.3 B), as well as a single dot in salivary gland sporozoites (Fig. 3.3 C). During *in vitro* liver-stage development the PALM signal started as a dot at 24h after infection (Fig. 3.3 D) and developed into the typically branched structure at 48h (Fig. 3.3 E) and 65h after infection (Fig. 3.3 F).

Together, these stainings are in accordance with the structures of previously published apicoplast proteins (Stanway et al., 2009), thus suggesting the correctness of the predicted apicoplast-targeting signal.

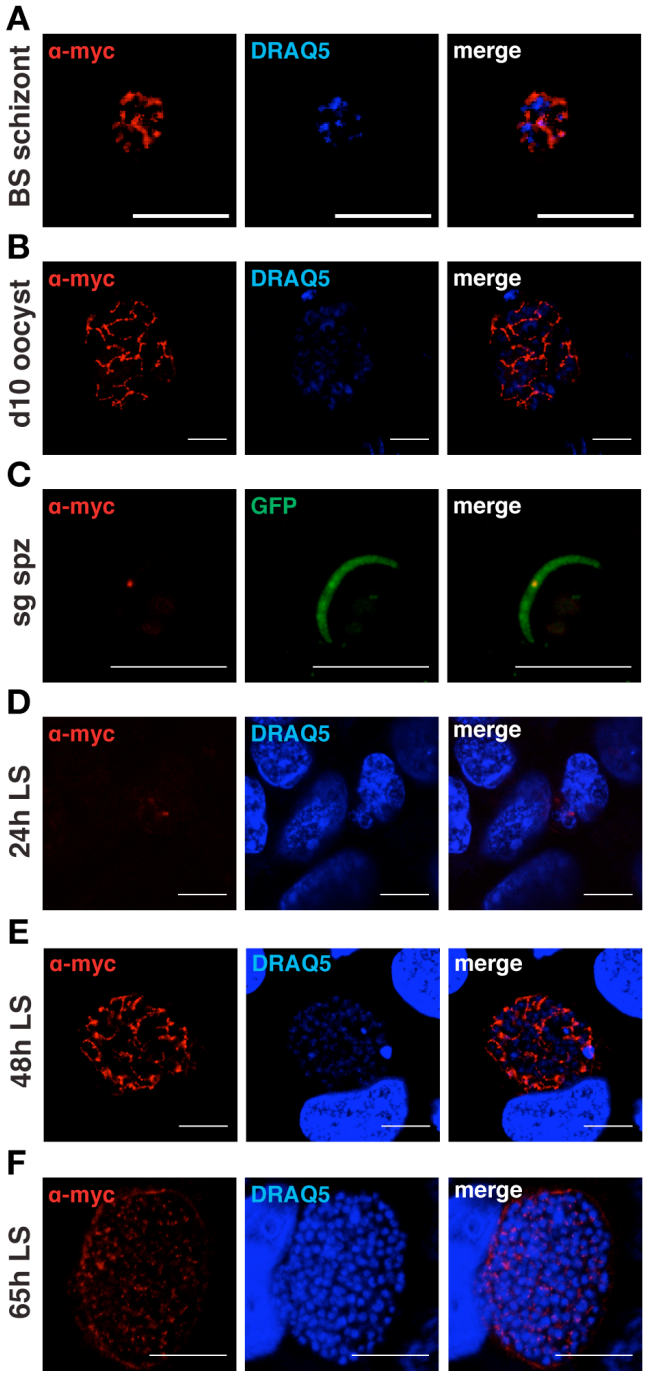

Figure 3.3: Expression of *PALM* during the *Plasmodium berghei* life cycle.

PALM-mCherry-myc parasites were used to infect mice and *Anopheles stephensi* mosquitoes. Intra- and extracellular parasite stages were fixed, permeabilized and stained with mouse anti-myc antibody (red). In replicating stages, nuclei were stained with the DNA-dye DRAQ5 (blue). The GFP signal in fixed sporozoites was used to display the extracellular parasite. (**A**) Blood-stage schizont (BS schizont) from an infected mouse. The anti-myc signal was very weak and only detectable after background subtraction in comparison with WT parasite-infected erythrocytes. Bars, 5 μm. (**B**) Oocyst fixed at day 10 after infection. Bars, 10 μm. (**C**) Salivary gland sporozoite fixed at day 17 after infection. Bars, 10 μm. Liver-stage parasites fixed at 24h (**D**), 48h (**E**) and 65h (**F**) after infection of hepatoma cells. Bars, 10 μm.

3.1.5 Subcellular localization of PALM

To further corroborate the localization of PALM to the apicoplast, liver stages, where the PALM signal is most prominent, were used for co-localization studies. Polyclonal antibodies against a signature apicoplast protein, acyl carrier protein (ACP; (Friesen et al., 2010)), were used to co-stain fixed *PALM-mCherry-myc* parasite-infected hepatocytes with a monoclonal anti-myc antibody. The staining overlapped substantially, strongly suggesting that tagged PALM is indeed transported efficiently into the apicoplast (Fig. 3.4).

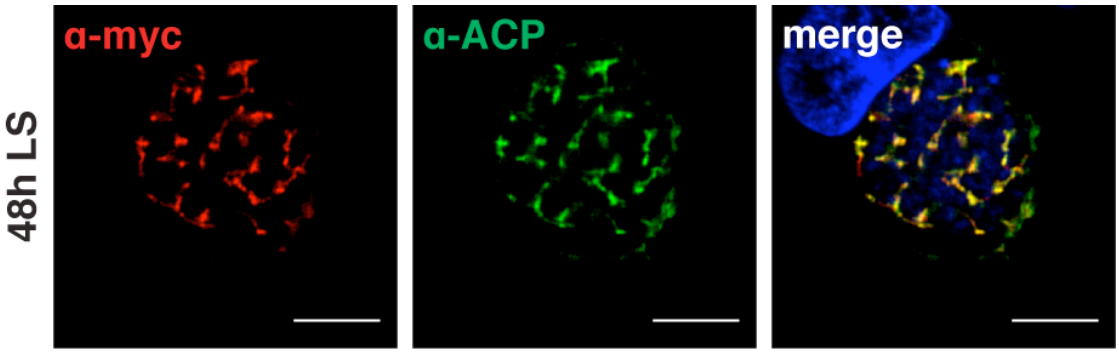

Figure 3.4: Apicoplast localization of PALM.
Co-staining of fixed, *PALM-mCherry-myc* parasite-infected hepatoma cells 48 hours after infection using anti-myc and anti-ACP antibodies. Note the substantial overlap between PALM and the signature apicoplast protein ACP.

Since in apicomplexan parasites the apicoplast and the mitochondrion are in close association (van Dooren et al., 2005), additional proof for an exclusive localization to one of the two organelles was required. Previous work established that antibiotic treatment during liver-stage development abrogated apicoplast growth and segregation (Friesen et al., 2010). Therefore the immunofluorescence assay was repeated in the presence or absence of 1μM azithromycin. Destruction of the apicoplast integrity by this treatment abolished the ACP- and PALM-positive branched structure in *in vitro* liver stages 48 hours after infection and limited the signal to a small peripheral dot (Fig. 3.5).
Combined, the co-localization of PALM with the apicoplast signature protein ACP and the disappearance of PALM-positive structures upon azithromycin treatment indicate the localization of PALM to the apicoplast.

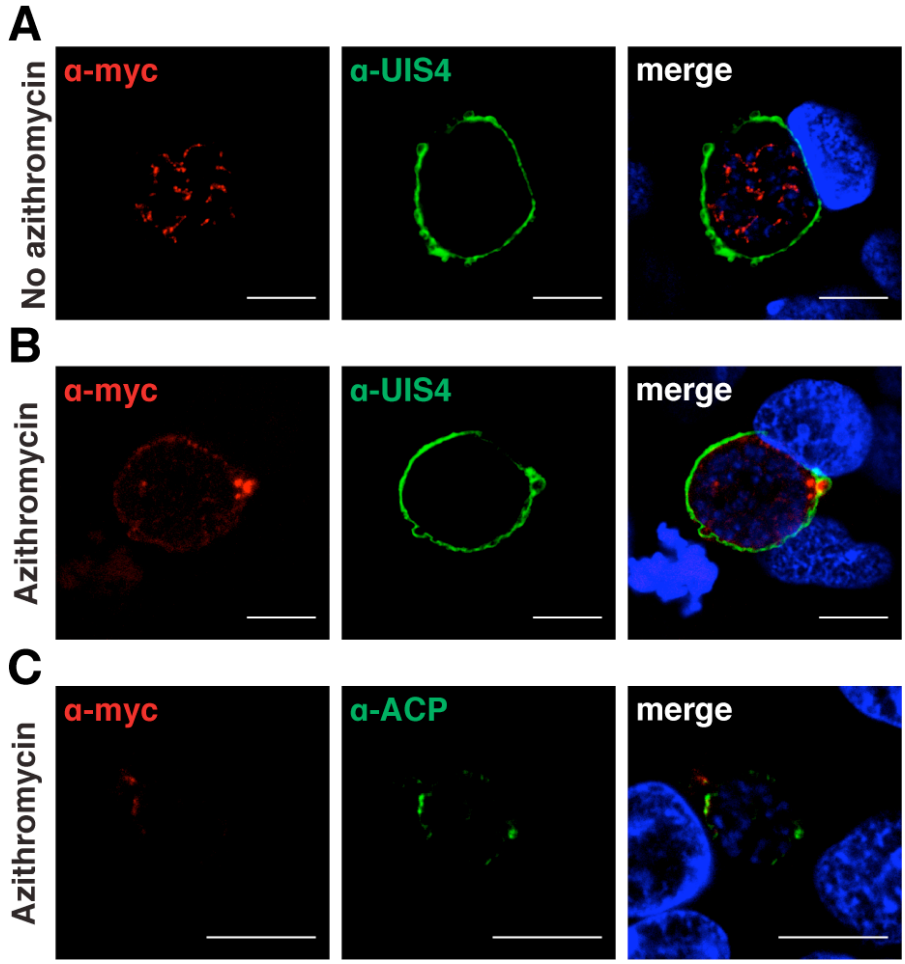

Figure 3.5: Branched PALM-positive structures disappear upon treatment with azithromycin.
(**A**) *PALM-mCherry-myc* parasite-infected hepatoma cells left untreated, fixed at 48 h after infection, and stained with antibodies specific for the myc epitope and upregulated in infective sporozoites protein 4 (UIS4), a signature protein of the parasitophorous vacuole. Note the branched PALM-positive structures. (**B**) Antibiotics treatment with 1 μM azithromycin abolishes the branched PALM-positive structures while parasites appear to remain healthy otherwise. (**C**) Antibiotics treatment with 1 μM azithromycin abolishes the branched PALM-positive structures as well as ACP-positive structures. All bars, 10 μm.

3.1.6 Generation of *palm*$^{-}$ parasites

A systematical study of the *in vivo* function of PALM was performed by generation and analysis of PALM knockout parasites. For targeted gene deletion, the *P. berghei* PALM locus was disrupted by the standard gene replacement strategy (Menard and Janse, 1997). Fragments of the 5'UTR and part of the N-terminal coding region and of the 3'UTR were amplified from gDNA. PCR fragments were cloned into the

standard transfection vector, which contains the pyrimethamine-resistant *Toxoplasma gondii* dihydrofolate reductase/thymidylate synthetase cassette. The resulting plasmid, pPbPALM-KO, was linearized and *P. berghei* WT ANKA and WT ANKA-GFP parasites were transfected (Fig. 3.6 A).

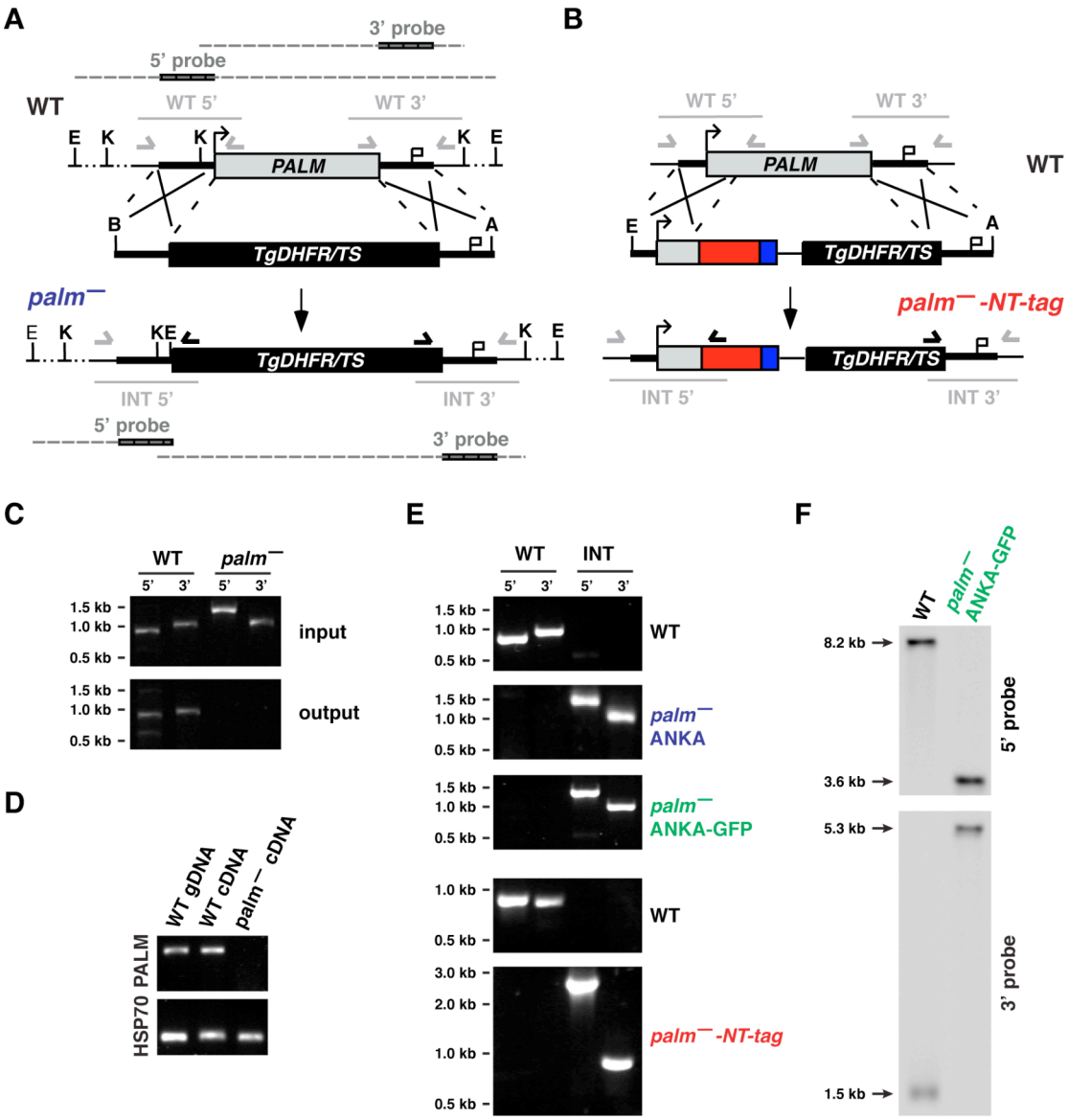

Figure 3.6: Generation of *palm*⁻ parasites.

(**A**) The *PbPALM* genomic locus was targeted with a replacement plasmid containing *PALM* 5' and 3' fragments (thick black lines) and the *DHFR/TS* positive selectable marker (black box). Upon a double cross-over event, the targeting plasmid is expected to replace the endogenous *PALM* open reading frame. Arrows and light gray solid lines indicate specific primers and PCR fragments respectively. Black bars indicate specific 5' and 3' probes; dark gray dashed lines represent *EcoRI* or *KpnI* restriction-digested fragments of WT or knockout parasite gDNA. (**B**) Alternative gene replacement vector to ablate the *PALM* locus. The *PbPALM* genomic locus was targeted with a replacement plasmid containing a *PALM* 5' fragment, containing a portion of the *PALM* open reading frame (gray box), fused to the mCherry protein

(red box) and quadruple myc tag (blue box), followed by the *DHFR/TS* positive selectable marker (black box) and the 3' flanking region (thick bar). Upon a double cross-over event, the targeting plasmid is expected to replace the endogenous *PALM* open reading frame. Arrows and bars indicate specific primers and PCR fragments respectively. (**C**) Mouse-mosquito-mouse transmission experiment starting from a mixed WT/ *palm*$^{-}$ infection (input) and resulting in a pure WT population after completion of one transmission cycle (output). Parasites were genotyped by PCR using wild-type (WT)- and replacement (INT)-specific primer pairs, as indicated in (**A**). (**D**) Parasite transcript detection in WT and *palm*- parasite-infected livers confirms the successful ablation of *PALM* in the knockout line. cDNA was prepared from liver homogenates extracted from mice at 44h after sporozoite infection. Quality of cDNA preparations and presence of parasites *in vivo* was controlled using *HSP70*-specific primers. (**E**) Genotyping of the three clonal *palm*$^{-}$ parasite lines obtained from independent transfection experiments. Using integration-specific primer combinations (**A**, **B**) the successful replacement event (INT) was verified. Absence of the WT signal from *palm*$^{-}$ parasites confirmed the purity of the clonal populations. The clonal populations *palm*$^{-}$ ANKA (blue) and *palm*$^{-}$ ANKA-GFP (green) were obtained according to design (**A**), using WT-ANKA and WT ANKA-GFP parasites as recipient lines (left); the clonal population *palm*$^{-}$*-NT-tag* (red) was obtained according to design (**C**), using WT ANKA-GFP parasites as recipient line (right). **(F**) Genotyping of the *palm*$^{-}$ ANKA-GFP parasite line used for the majority of experiments through Southern blot analysis. Probes at the 5' and 3' UTR of *PALM* were used to demonstrate the expected size shift of restriction-digested gDNA of WT and knockout parasites.

For a third knockout line fragments of the 5'UTR including part of the N-terminal coding region corresponding to the apicoplast targeting signal and of the 3'UTR were amplified from gDNA. PCR fragments were cloned into a targeting vector, which contains the mCherry coding region fused to a quadruple c-myc tag sequence and the pyrimethamine-resistant *Toxoplasma gondii* dihydrofolate reductase/thymidylate synthetase cassette. The resulting plasmid, pPbPALM-KO2, was linearized and used to transfect *P. berghei* WT ANKA-GFP parasites (Fig. 3.6 B).

3.1.7 Feeding of parental *palm*$^{-}$ population

To obtain a first indication, whether *palm*$^{-}$ parasites progress through the life cycle normally or show any sign of arrest in their development, the parental population, which consists of a mixture of WT and *palm*$^{-}$ parasites, was fed to mosquitoes. When sporozoites had colonized the salivary glands, a naive C57BL/6 mouse was infected by natural bite of mosquitoes. Five days after infection, the mouse was bled by heart puncture and parasite gDNA was isolated. PCR with WT and integration

specific primers of the parasite population before (input) and after (output) feeding revealed that only WT parasites were able to complete the transmission cycle (Fig. 3.6 C).
This finding argued for the generation of a clonal *palm*$^{-}$ population to further analyze *PALM* knockout parasites in detail.

3.1.8 Generation of three clonal *palm*$^{-}$ parasite lines

Three independent clonal *palm*$^{-}$ parasite lines were generated by intravenous injection of limiting dilutions of parasites into mice: *palm*$^{-}$ ANKA-GFP and *palm*$^{-}$*-NT-tag* following transfection of the GFP expressing WT ANKA-GFP line using vectors PbPALM-KO and PbPALM-KO2, respectively, and *palm*$^{-}$ ANKA following transfection of WT ANKA parasites with PbPALM-KO.
Inactivation of PALM in the *palm*$^{-}$ ANKA-GFP line was confirmed through RT-PCR. Total RNA was isolated from livers isolated from infected mice at 44 hours after infection and used to generate cDNA by RT-PCR. For the detection of *PALM* transcripts, cDNA samples were tested using gene specific primers PbPALM-F6 and PbPALM-R5 (260 bp). Primers specific for heat shock protein 70 (HSP70, PbHSP70-F and PbHSP70-R, 164 bp) were used to control the cDNA load (Fig. 3.6 D).
Integration-specific PCR amplification of the *PALM* locus to confirm the predicted deletion of PALM in *palm*$^{-}$ ANKA and *palm*$^{-}$ ANKA-GFP parasites was done by diagnostic PCR (Fig. 3.6 E).
Genotyping of WT ANKA-GFP and *palm*$^{-}$ ANKA-GFP gDNA was also performed by Southern blot analysis (Fig. 3.6 F).

3.1.9 Blood stage replication of *palm*$^{-}$ parasites is unaffected

PALM could be deleted in blood stages, as observed by the ability to generate the three knockout lines, and is therefore not essential for blood-stage parasites. However, this does not rule out that ablation of *PALM* could cause a growth defect of *Plasmodium berghei* blood stages. To study this, 1,000 mixed blood –stage parasites of either WT ANKA-GFP or *palm*$^{-}$ ANKA-GFP were injected intravenously into

C57BL/6 mice. The parasitemia was monitored by daily Giemsa-stained thin blood smears from day 3 to day 8 after infection. The growth curves of WT and mutant parasites were indistinguishable and equally high parasitemia was detected, indicating a normal asexual blood stage development of *palm*$^{-}$ parasites (Fig. 3.7 A).

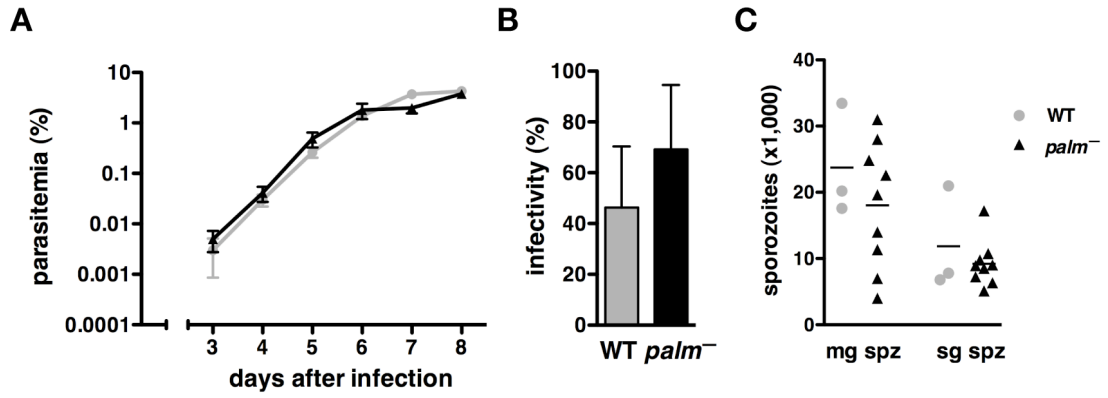

Figure 3.7: *Palm*$^{-}$ parasites display normal life cycle progression during blood-stage development and sporogony in the insect vector.

(**A**) Normal blood-stage development of *palm*$^{-}$ parasites. C57BL/6 mice were injected intravenously with 1,000 blood-stage WT ANKA-GFP or *palm*$^{-}$ ANKA-GFP parasites (n=10 each) and monitored for blood-stage development of parasites by examination of Giemsa-stained blood-smears. WT ANKA-GFP and *palm*$^{-}$ ANKA-GFP blood-stage development is indistinguishable. Shown are mean numbers (± SD). (**B**) Normal infectivity of *palm*$^{-}$ parasites. The number of mosquitoes with oocyst-infected midguts (infectivity) was determined at day 10 after the blood meal. Shown are mean numbers (± SD), for WT ANKA-GFP (feedings n=3) and for *palm*$^{-}$ ANKA-GFP (feedings n=9). (**C**) *palm*$^{-}$ parasites form normal sporozoites in the insect vector. Midgut and salivary gland sporozoites were determined at day 14 and 17, respectively, after the blood meal. Shown are mean numbers per infected mosquito. Number of feedings: WT ANKA-GFP, n=3; *palm*$^{-}$ ANKA-GFP, n=9.

3.1.10 *PALM* is dispensable for parasite transmission to the invertebrate host and development in the mosquito

The next step in the *Plasmodium* life cycle after replication in erythrocytes is the transmission of gametocytes from the vertebrate to the invertebrate host and the parasite development in the mosquito. To examine the progression of *palm*$^{-}$ parasites through this part of the life cycle, infected NMRI mice were checked for exflagellation of male microgametes under a light microscope. Male microgametes of

palm^{-} parasites displayed the typical exflagellation process after 10 to 12 minutes, similar to WT parasites (data not shown) and were fed to mosquitoes. At day 10 after feeding mosquito midguts were dissected and the percentage of oocyst-infected mosquitoes was calculated (Fig. 3.7 B). At days 14 and 17 mosquitoes were dissected to determine the number of midgut and salivary glands, respectively (Fig. 3.7 C). Infectivity and sporozoite numbers of *palm*$^{-}$ ANKA-GFP, *palm*$^{-}$ ANKA and *palm*$^{-}$*-NT-tag* parasite lines were indistinguishable from WT ANKA-GFP mosquito feedings (Tab. 3.1).

3.1.11 *In vitro* liver stage and merosome development of *palm*$^{-}$ parasites is severely impaired

As the abundance of *PALM* transcripts is highest in late liver stages, this part of the *Plasmodium* life cycle was of particular interest. In the *Plasmodium berghei* model liver-stage development can either be studied *in vitro* by infection of hepatoma cells with salivary gland sporozoites or *in vivo* by injection of freshly dissected salivary gland sporozoites or transmission through the bites of *Plasmodium* infected mosquitoes.

First, liver-stage development of *palm*$^{-}$ parasites was studied *in vitro* (Fig. 3.8). To this end, Huh7 hepatoma cells were seeded in 8-well Labtec slides and the next day each well was infected with 10,000 freshly dissected sporozoites. Development of the parasites was stopped at various time-points and the parasites were stained with anti-HSP70 antibodies. This allowed the comparison of the number of parasites at the indicated time-points between WT and *palm*$^{-}$ infected hepatoma cells. At 24 and 48 hours after infection WT and mutant parasite numbers were indistinguishable. However, at 72 hours after infection, when most WT parasites typically have been released into the supernatant as merosomes, *palm*$^{-}$ parasites remained inside the host cells as seen by the clearly higher parasite numbers (Fig. 3.8 A). This was also reflected in strikingly lower merosome numbers in the supernatant of *palm*$^{-}$ infected cells (Fig. 3.8 B). Remarkably, when the whole merosome-containing supernatants were injected into mice, *palm*$^{-}$ merosomes were infectious and capable of inducing a blood-stage infection (Fig. 3.8 C). The delay in parasite appearance in Giemsa-stained blood smears of *palm*$^{-}$ parasites compared to WT is most likely a consequence of the significantly lower merosome numbers injected.

These findings indicated that the vast majority of *palm*$^{-}$ parasites is trapped inside the host cells and only very few, if any, knockout parasites are able to develop fully into infectious merozoites.

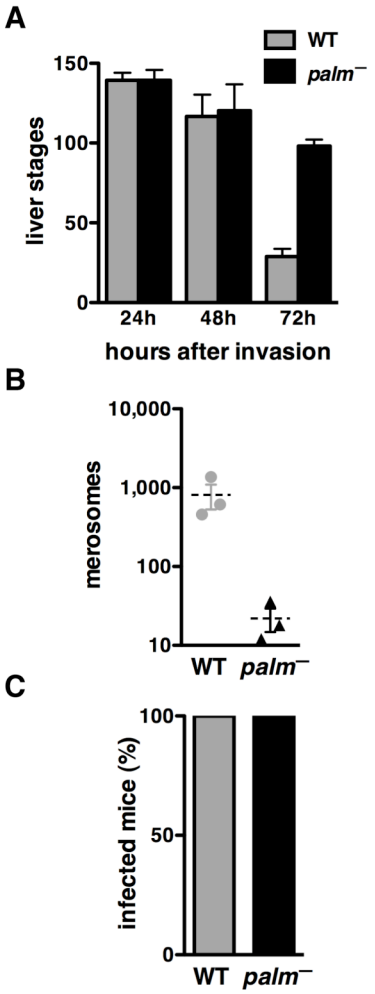

Figure 3.8: *Palm*$^{-}$ parasites display a defect in liver-stage maturation.

(**A**) Quantification of liver stages in cultured hepatoma cells at 24, 48 and 72 h after infection with 10 000 *P. berghei* WT ANKA-GFP and *palm*$^{-}$ ANKA-GFP sporozoites. Infected cells were fixed and stained with mouse anti-*Pb*HSP70 antibodies. Note that in contrast to WT ANKA-GFP parasites, *palm*$^{-}$ ANKA-GFP parasites remain inside the host cells even at 72 h after infection. Data are from two independent experiments done in triplicate. Shown are mean numbers (±SD). (**B**) Quantification of merosomes obtained from cultured hepatoma cells infected with WT ANKA-GFP and *palm*$^{-}$ ANKA-GFP parasites at 72 h after inoculation with 100 000 sporozoites. (**C**) Complete merosome- containing supernatants harvested under (**B**) were injected into recipient C57BL/6 mice (WT ANKA-GFP, n= 5; *palm*$^{-}$, n= 4) and monitored for malaria infections by examination of Giemsa-stained blood-smears.

3.1.12 *Palm*$^{-}$ parasites express the merozoite signature protein merozoite surface protein 1 (MSP1)

To further pinpoint the developmental arrest of *palm*$^{-}$ parasites, *in vitro* infections of hepatoma cells and immunofluorescence assays were repeated with anti-UIS4 antibodies, staining the parasitophorous vacuole surrounding the parasite, and antibodies against MSP1, a merozoite signature protein. It was described previously that *Plasmodium yoelii* liver-stage arrested parasites missing the pyruvate

dehydrogenase (PDH) subunit E1α (Pei et al., 2010) or the FASII enzyme FabB/F (Vaughan et al., 2009) do not show any MSP1 expression during liver-stage development. Similarly, *Plasmodium berghei* parasites missing the FASII enzyme FabI only show negligible MSP1 expression during liver-stage development (Yu et al., 2008). MSP1 staining offered the possibility to compare PALM knockout parasites to these other late liver-stage arrested parasites.

Hepatoma cells were infected with WT ANKA-GFP and *palm*$^-$ ANKA-GFP sporozoites and development was stopped at 24, 48, 60, 72 and 94 hours after infection (Fig. 3.9). At 24 h and 48 h after infection WT ANKA-GFP and *palm*$^-$ ANKA-GFP parasites were indistinguishable, surrounded by the UIS4- containing parasitophorous vacuole membrane. Typically, at 24 h after infection parasites do not show any MSP1 staining and at around 48 h after infection MSP1 expression starts at the rim of the developing schizont, which then invaginates around parasite material during the cytomere stage (Sturm et al., 2009). During merozoite formation around 60 to 72h after infection, however, striking differences were observed between WT ANKA-GFP and *palm*$^-$ ANKA-GFP parasites (Fig. 3.9 A). While WT parasites formed merozoites surrounded by a MSP1 containing membrane, *palm*$^-$ parasites seemed unable to form individual merozoites. At this stage, and even more pronounced at 94h after infection, numerous *palm*$^-$ ANKA-GFP parasites showed unusual MSP1 staining outside the parasitophorous vacuole, maybe indicating disintegration of parasites (Fig. 3.9 A). To quantify liver merozoite formation liver stages from WT ANKA-GFP and *palm*$^-$ ANKA-GFP parasites were scored at 48, 60, 72 and 94h after infection (WT ANKA-GFP n = 105, 94, 82, 25; *palm*$^-$ n = 99, 124, 107, 53) according to five categories, namely: no MSP1, rim staining of MSP1, intracellular schizont staining of MSP1, formation of MSP1-positive merozoites, and aberrant, external MSP1 staining. This quantification revealed a slight developmental delay of *palm*$^-$ parasites at 48h after infection as seen by the lower percentage of intracellular schizont staining of MSP1. At 60h after infection levels of parasites with no MSP1 or rim staining of MSP1 were equal in WT ANKA-GFP and *palm*$^-$ ANKA-GFP parasites, but in contrast to WT ANKA-GFP, *palm*$^-$ ANKA-GFP parasites seemed to be almost unable to form merozoites, which became even more apparent at 60h after infection. At 94h after infection *palm*$^-$ ANKA-GFP parasites had not been able to catch up on merozoite formation, excluding a simple developmental delay. Instead, over 40% of *palm*$^-$ ANKA-GFP parasites showed an aberrant extracellular MSP1 staining (Fig. 3.9 B).

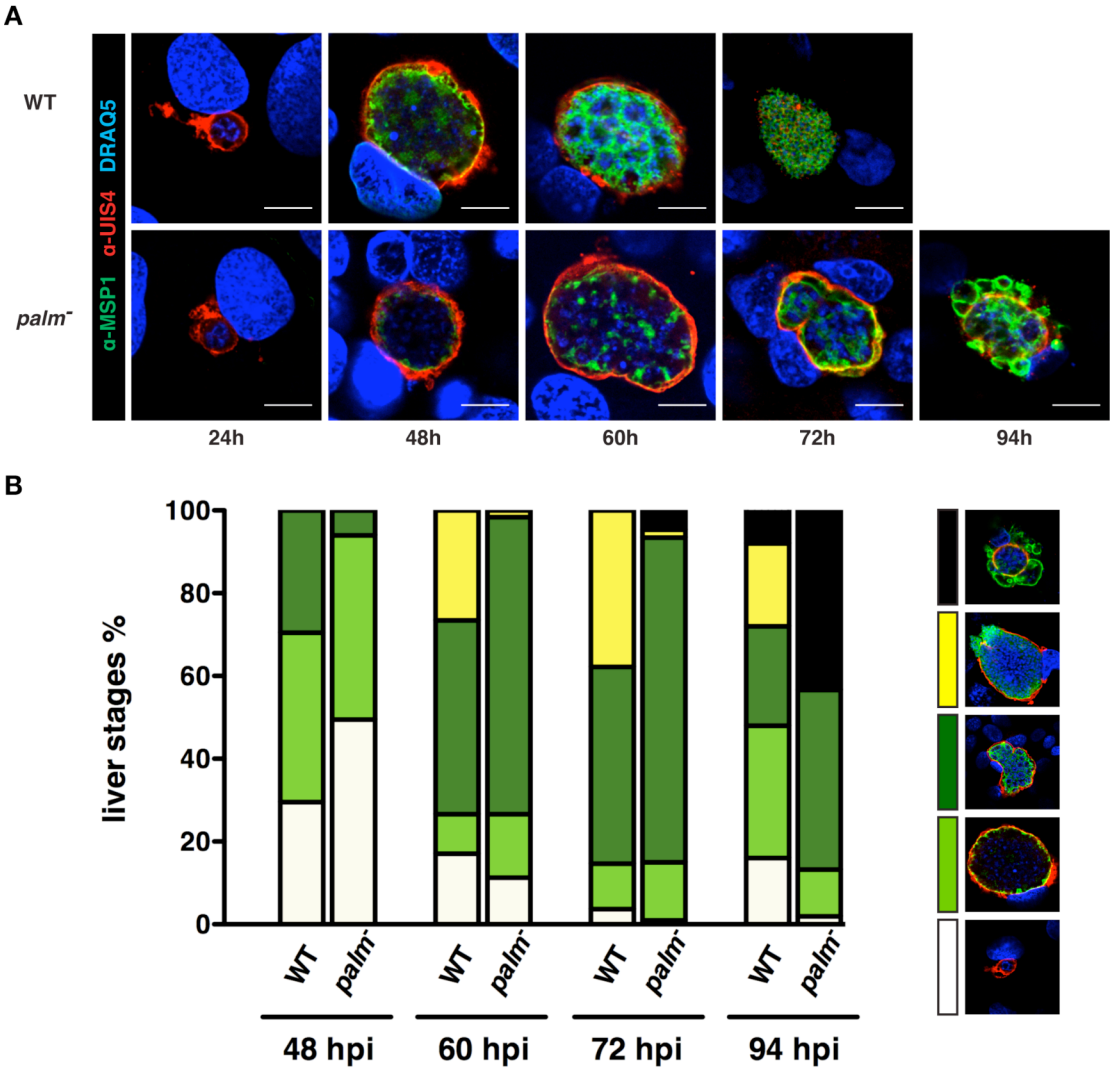

Figure 3.9: *Palm*$^{-}$ parasites cannot form liver merozoites efficiently.

(**A**) Defect in liver-stage merozoite segregation in *palm*$^{-}$ parasites. *In vitro* cultured *P. berghei* WT ANKA-GFP and *palm*$^{-}$ ANKA-GFP liver stages, were fixed at various time points after sporozoite infection and visualized by immunofluorescence using monoclonal mouse anti-*P. yoelii* MSP1 and rabbit anti-*P. berghei* UIS4 antibodies. Nuclei were stained with the DNA-dye DRAQ5 (blue). *Palm*$^{-}$ ANKA-GFP parasites develop normally until late liver stages, but rarely form merozoites. Shown are representative images of WT ANKA-GFP and *palm*$^{-}$ ANKA-GFP parasites at various time points. Bars, 10 μm. (**B**) Quantification of productive liver merozoite formation. Liver stages from WT ANKA-GFP and *palm*$^{-}$ ANKA-GFP parasites were scored at 48, 60, 72 and 94h after infection (WT ANKA-GFP $n = 105, 94, 82, 25$; *palm*$^{-}$ $n = 99, 124, 107, 53$) according to the five categories indicated by the representative images in the inset. The categories are: no MSP1 (white), rim staining of MSP1 (light green), intracellular schizont staining of MSP1 (dark green), formation of MSP1-positive merozoites (yellow), and aberrant, external MSP1 staining (black). Note the high proportion of MSP1-positive schizonts in *palm*$^{-}$ parasites, which correlates with a low production of MSP1-positive pathogenic merozoites.

Together, these findings revealed attenuation of *palm*$^{-}$ parasites at the final steps of liver merozoite formation. This clearly distinguishes the time of liver-stage arrest of *palm*$^{-}$ parasites from early genetically arrested parasites, such as UIS3 and UIS4 knockout parasites. MSP1 expression in *palm*$^{-}$ parasites might also suggest a later arrest compared to the above mentioned *Pye1*α^{-}, *Pyfabb/f*$^{-}$ and *Pbfabl*$^{-}$ parasites, where the expression of this merozoite signature protein is absent.

3.1.13 Apicoplast morphology appears to be normal in *palm*$^{-}$ parasites

To test whether *PALM* ablation affects the structure of the apicoplast, the organelle harboring PALM, the *palm*$^{-}$*-NT-tag* parasite line was generated. In this parasite line the N-terminal part of PALM containing the signal peptide and the apicoplast-targeting signal was fused to mCherry and a quadruple c-myc tag, and the protein coding part of PALM was deleted by double-homologous recombination. This should allow visualizing the apicoplast in *PALM* knockout parasites by targeting mCherry to the apicoplast while simultaneously deleting PALM. However, no live mCherry could be observed, probably due to the low expression driven by the *PALM* promoter (data not shown).

Therefore, apicoplast morphology in *palm*$^{-}$ parasites was monitored by immunofluorescence assay on fixed parasites (Fig. 3.10). To this end hepatoma cells were infected with *PALM-mCherry-myc* and *palm*$^{-}$*-NT-tag* parasites. At 48 hours after sporozoite infection the cells were fixed and stained with anti-ACP antibodies to visualize the apicoplast. As exemplified for the *palm*$^{-}$*-NT-tag* line, mutant liver stages showed no obvious difference in apicoplast morphology when compared with the transgenic control, i.e. *PALM-mCherry-myc* at 48h and 60h after infection (Fig. 3.10).

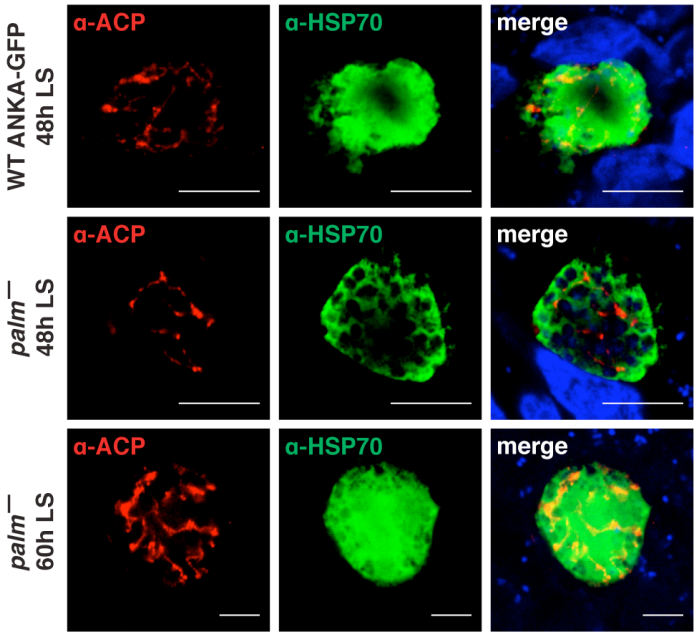

Figure 3.10: Apicoplast morphology appears normal in *palm*⁻ liver stages.

Hepatoma cells infected with WT and *palm*⁻ parasites were fixed at 48 or 60h after infection and stained for parasite cytoplasm and the apicoplast using anti-HSP70 and anti-ACP antibodies respectively. The merge includes an additional DRAQ5 nuclear stain. Bars, 10 μm.

3.1.14 *Palm*⁻ parasites are severely impaired in initiation of a blood stage infection *in vivo*

The rodent malaria model offers the possibility of not only following liver-stage development *in vitro*, but also *in vivo* by infection of susceptible C57BL/6 mice. To analyze if attenuation of *palm*⁻ parasites also occurs *in vivo*, C57BL/6 mice were infected by natural bite of five mosquitoes infected with either WT ANKA-GFP (n= 11) or *palm*⁻ ANKA-GFP (n= 13) (Fig. 3.11 A). All WT ANKA-GFP infected mice became parasite positive in Giemsa-stained blood smears 4 days after infection, whereas ~50% of mice exposed to *palm*⁻ ANKA-GFP-infected mosquitoes remained completely malaria-free, while the other half showed a severe delay in patency ranging from 3 to 8 days.

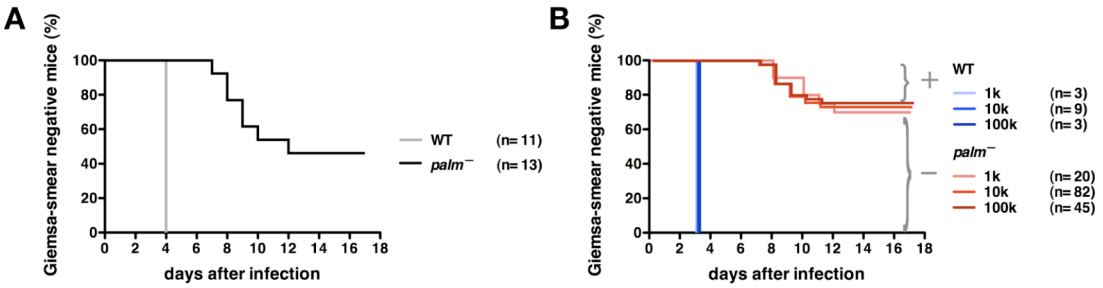

Figure 3.11: Infection with *palm*⁻ sporozoites leads to attenuated liver-stage development *in vivo*.

(**A**) Kaplan–Meier analysis of time to malaria blood-stage infection. C57BL/6 mice were infected by natural bite with five mosquitoes infected with WT ANKA-GFP (grey, n= 11) or *palm*⁻ ANKA-GFP (black, n= 13). Animals were monitored daily for presence of parasites in Giemsa-stained blood smears. (**B**) Kaplan–Meier analysis of time to malaria blood-stage infection. C57BL/6 mice were infected with 1,000, 10,000, or 100,000 WT ANKA-GFP (blue, n= 3, 9, 3) or *palm*⁻ ANKA-GFP (red, n= 20, 82, 45) sporozoites by intravenous injection. Animals were monitored daily for presence of parasites in Giemsa-stained blood smears. Next, C57BL/6 mice were infected by intravenous injection of increasing doses of WT ANKA-GFP or *palm*⁻ sporozoites (Fig. 3.11 B). All mice injected with WT ANKA-GFP sporozoites became patent on day 3 after infection as monitored by daily Giemsa-stained blood smears. In sharp contrast, patency of mice injected with sporozoites of either of the three *palm*⁻ lines was severely delayed by at least 4 days. Most importantly, a large proportion (~70%) of mice remained entirely malaria-free at day 17 after infection independent of the dose of injected *palm*⁻ sporozoites. In the rodent malaria model system, a delay of 1 day in patency corresponds to a 10-fold reduction in initial asexual blood-stage parasite load.

The prolonged pre-patent period in case of *palm*⁻ breakthrough infections could be either due to the release of less merozoites from hepatocytes or a prolonged time of merozoite formation of *palm*⁻ parasites and hence a retardation of merozoite release. To test this, C57BL/6 mice were infected by natural bite of five mosquitoes infected with WT ANKA-GFP (n= 2) or *palm*⁻ ANKA-GFP (n=5) and 30µl of blood were obtained from the tail 3, 4 and 5 days after per bite infection and injected into naive C57BL/6 mice (Fig. 3.12). The parasitemia was followed by daily Giemsa-stained blood smears. All recipient mice that received blood transfusions of either of the WT ANKA-GFP infected mice became blood-stage positive.

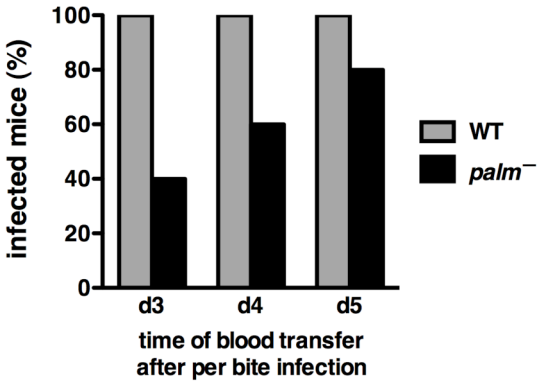

Figure 3.12: *Palm*$^{-}$ parasites are present in the blood of mice three days after per bite infection.

C57BL/6 mice were infected by bites of WT ANKA-GFP (n= 2) or *palm*$^{-}$ ANKA-GFP (n= 5) infected mosquitoes. At the indicated time points after infection, blood was transfused to recipient mice and parasitemia was followed by microscopic examination of Giemsa-stained blood smears.

Recipient mice that were infected with *palm*$^{-}$ ANKA-GFP parasites also became positive with transfusion from day 3 on after per bite infection, although this was only the case for a fraction of the animals. Blood transfers at later time points led to a higher proportion of infected animals. This suggests that at least in some mice infected with *palm*$^{-}$ ANKA-GFP, parasites are already present in the blood at day 3 after per bite infection. It is possible that this is not the case for all animals because some mice only become blood-stage positive later or that the amount of blood that was transfused was too small to harbor the few infected erythrocytes. Taken together, the delay in patency seen with *in vivo* infections with *palm*$^{-}$ ANKA-GFP parasites is probably primarily due to a lower number of merozoites released from hepatocytes and not to a general delay in development.

The results of *palm*$^{-}$ *in vivo* infections are in good agreement with the phenotype during *in vitro* liver-stage development. In a large proportion of cases *palm*$^{-}$ parasites are not able to complete liver merozoite formation and therefore are not able to initiate erythrocyte infection. In the rather rare event of merozoite formation of *palm*$^{-}$ parasites, only very few merozoites are released into the bloodstream, hence the delay in the onset of patency.

3.1.15 Impaired liver stage development leads to reduced incidence of experimental cerebral malaria (ECM)

The clinical symptoms of population '+', i.e. those mice that became *palm*$^{-}$-blood-stage-positive were followed. Only few *palm*$^{-}$-infected mice developed symptoms of experimental cerebral malaria (ECM), a fatal outcome of an acute *Plasmodium* infection (de Souza and Riley, 2002), as compared with WT ANKA-GFP-infected animals (Fig. 3.13 A). Signature signs of ECM are sudden onset of ataxia, paralysis, convulsion or coma (de Souza et al., 2010). Symptoms of ECM typically develop on the fourth day after patency in sporozoite-induced infections. Of note, none of the mice that were infected by bite of *palm*$^{-}$-infected mosquitoes developed ECM. It is important to exclude any impairment in parasite virulence due to the genetic manipulation. Previously, normal blood-stage growth of *palm*$^{-}$ parasites was detected (Fig. 3.7 A). To confirm that *palm*$^{-}$ parasites are as virulent as WT parasites, mice were inoculated with 1,000 erythrocytes infected with either *palm*$^{-}$ ANKA-GFP or, as controls, WT ANKA-GFP parasites via blood transfusion, thus bypassing the liver merozoite phase. All animals developed the signature ECM symptoms (Fig. 3.13 A). Therefore, the reduced ECM incidence of *palm*$^{-}$-infected mice can be attributed to the altered pre-erythrocytic development of these parasites.

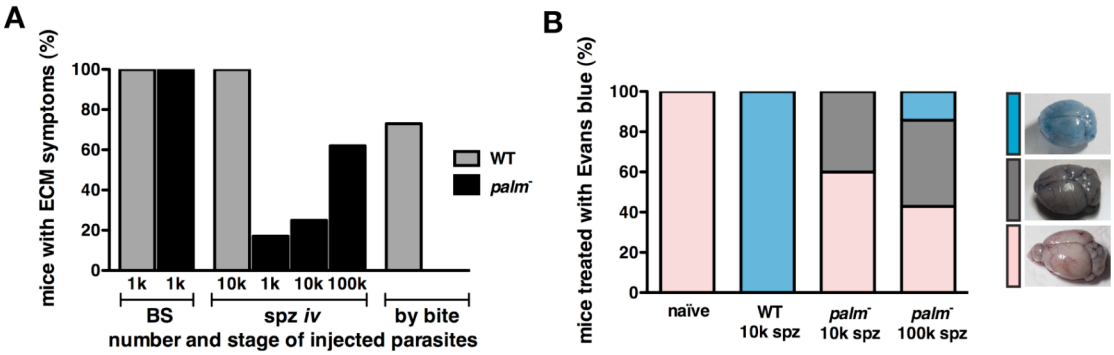

Figure 3.13: Development of symptoms of ECM is reduced in *palm*$^{-}$ sporozoite- infected animals.

(**A**) Shown is the percentage of parasite-positive C57BL/6 mice that develop signature symptoms of ECM (i.e. mice showing sudden onset of ataxia, paralysis, convulsion or coma, or a minimum of three behavioral and functional abnormalities) after injection of 1000 blood-stage parasites (WT ANKA-GFP, grey, n= 15; *palm*$^{-}$ ANKA-GFP, black, n= 15), injection of sporozoites [10,000 ANKA-GFP, grey, n= 9; *palm*$^{-}$ ANKA-GFP, black, 1,000 (n= 6), 10,000 (n= 20), or 100,000 (n= 13)], or infection by natural bite with five mosquitoes infected with WT ANKA-GFP (grey, n=

11) or *palm*$^{-}$ ANKA-GFP (black, n= 13). (**B**) Integrity of the blood–brain barrier is preserved in most *palm*$^{-}$ sporozoite-infected mice. Mice were infected with 10 000 WT ANKA-GFP sporozoites (n= 4), or 10 000 (n= 5) or 100 000 (n= 7) *palm*$^{-}$ ANKA-GFP sporozoites. Evans blue was injected intravenously at day 4 after appearance of blood-stage parasites and brains removed for documentation. One mouse infected with 100 000 *palm*$^{-}$ ANKA-GFP sporozoites showed behavioral abnormalities and breakdown of the blood–brain barrier.

Finally, the integrity of the blood-brain barrier was determined in sporozoite-injected animals by Evans blue stain at the peak of clinical symptoms, in WT-infected animals typically day 4 after patency. This experiment was done in collaboration with Dr. Taco Kooij and Carolin Nahar. If the integrity of the blood-brain barrier is disrupted, the intravenously injected dye is able to the reach the brain as seen by the blue staining (Fig. 3.13 B). In good agreement with the reduced number of *palm*$^{-}$-infected mice with behavioral abnormalities when compared to WT controls, only one *palm*$^{-}$-infected mouse showed blue staining of the brain. This analysis further corroborated the strongly reduced cases and severity of ECM-related pathology in the *palm*$^{-}$-positive mice.

3.2 Immunizations with *palm*$^{-}$ parasites

Mice were immunized with genetically arrested *palm*$^{-}$ parasites in order to analyze long-term protection potential and mechanisms of protection. Lymphocyte isolations, peptide stimulations and immunological flow cytometry experiments were done in collaboration with Jan Burgold, MPI-IB, Berlin.

3.2.1 Immunizations with *palm*$^{-}$ parasites confer potent protection against re-infection

Next, it was tested whether immunization with *palm*$^{-}$ parasites can confer protection against sporozoite challenge in population '-'. Previous work with either irradiated sporozoites or genetically arrested parasites showed that in the *P. berghei*-C57BL/6 model three consecutive doses of attenuated parasites are needed to induce sterile immunity (Douradinha et al., 2007; Mueller et al., 2005a; Nussenzweig et al., 1967). In addition, two studies reported sterile protection of between 25% and 70% of mice up to 10 days following immunization using two immunizations (Mueller et al., 2005b; van Dijk et al., 2005). Anticipating comparable levels of protection using three immunization rounds, a two-dose immunization protocol was attempted, with 10,000 *palm*$^{-}$ ANKA-GFP sporozoites each (Tab 3.2).

Table 3.2: Immunization with *palm*$^{-}$ sporozoites confers potent protection against re-infection.

Challenge	*palm*$^{-}$ immunization[a]	# Protected/ # Challenged[b]	Prepatency (days)[c]
Exposure to five infected mosquitoes	2 X 10,000 spz	20/20 (100%)	-
	2 X 1,000 spz	0/2 (0%)	6.0
	naïve	0/10 (0%)[d]	4.0
Intravenous injection of 10,000 sporozoites	2 X 10,000 spz	5/5 (100%)	-
	naïve	0/6 (0%)	3.0
Intravenous injection of 10,000 sporozoites (day 110)[e]	2 X 10,000 spz	6/7 (86%)	8.0
	naïve	0/3 (0%)	3.0
Intravenous injection of 10 blood-stage parasites[f]	2 X 10,000 spz	0/4 (0%)	6.0
	naïve	0/5 (0%)	6.0

[a] Age-matched female C57BL/6 mice were immunized with palm- sporozoites (spz) in the numbers indicated. The immunization protocol is described in the methods chapter.
[b] Animals were checked for parasitemia by daily examination of Giemsa-stained blood smears.
[c] Prepatency is the time until detection of the first parasite in the peripheral blood.
[d] One additional naive mouse (not included) stayed initially malaria-free but became positive at day 3 after intravenous re-challenge.
[e] Challenge at 110 days after the last immunization.
[f] The immunized mice were previously shown to be fully protected against 'by bite' challenge.

When the immunizations were reduced to two doses of 1,000 sporozoites, sterilizing immunity and protection from development of signs of ECM were lost, but infections became patent with a two-day delay, indicative of a substantial degree of protective immune responses (Tab. 3.2).

To study stage-specificity of protection, four mice were re-challenged with ten WT ANKA-GFP blood-stage parasites. These mice had previously been immunized twice with 10,000 *palm*$^{-}$ ANKA-GFP sporozoites and challenged by WT ANKA-GFP-infected mosquito bites and were shown to be completely protected from sporozoite challenge. However, no protection or delay in prepatency with blood-stage challenge in comparison with naive control mice was observed, indicating that protection is restricted to pre-erythrocytic stages (Tab. 3.2).

Together, these findings demonstrate that *palm*$^{-}$parasites can elicit potent protective liver stage-specific immune responses against re-infection with as few as two immunizations.

3.2.2 Long-term protection in *palm*$^{-}$ immunized mice

Palm^{-} immunized C57BL/6 mice showed potent protection, even after a period of more than 100 days (Tab. 3.2). To further corroborate the long-term protection potential of genetically arrested *palm*$^{-}$ parasites a 3 to 4 dose immunization protocol was applied, with a challenge of more than 13 months after the last immunization (Fig. 3.14 A).

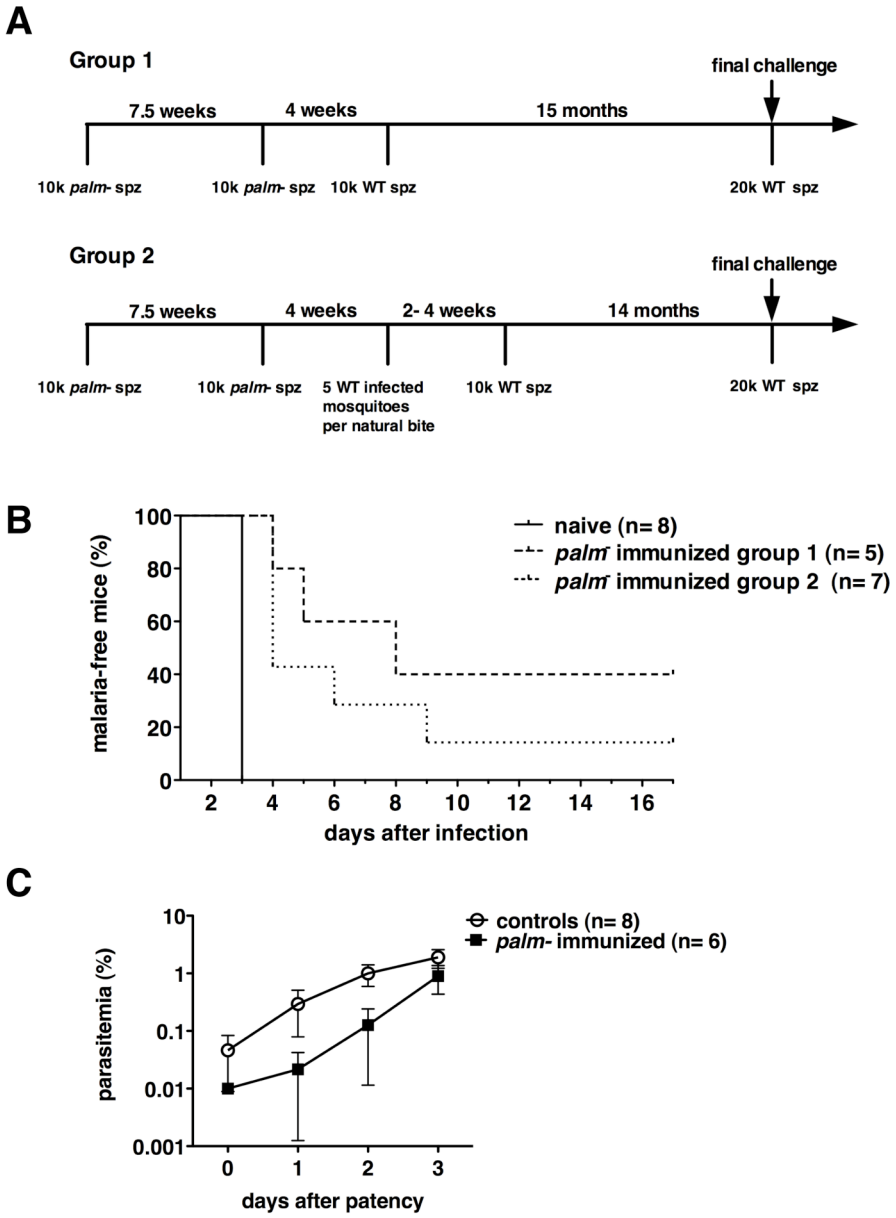

Figure 3.14: Vaccination with *palm*⁻ sporozoites elicits protracted, partial protection beyond one year.

(**A**) Experimental design and time scale of vaccination and challenge in two experimental groups. During the immunization phase, C57BL/6 mice were immunized twice by intravenous injection of 10,000 *palm*⁻ sporozoites. Sterile immunity was validated by early challenge infections by exposure to five WT-infected *Anopheles stephensi* mosquitoes and/or intravenous injection of 10,000 WT sporozoites. Mice were left untreated for 14 or 15 months and challenged by intravenous injection of 20,000 WT sporozoites, followed by monitoring of Giemsa-stained thin blood smears. (**B**) Kaplan-Meier analysis of vaccinated and age-matched control animals after final challenge as depicted in (**A**). **(C)** Parasitemia of control and immunized mice after final challenge was determined by daily microscopic examination of Giemsa-stained thin blood smears and grouped as days after detection of the first blood stage parasite (patency). Shown are means (±S.D.).

3 of 12 *palm*$^{-}$ immunized animals showed sterile protection against challenge with 20,000 WT ANKA-GFP sporozoites. The remaining 9 animals became blood-stage positive between days 4 and 9 after infection with a mean delay of 2.3 days compared to naive control mice (Fig. 3.14 B). A delay of 1 day in patency corresponds to a 10-fold reduction in initial asexual blood-stage parasite load in the rodent malaria model system. These results show that even in unprotected *palm*$^{-}$ immunized mice the initial blood stage parasite load was highly reduced. Whenever blood stage parasites could be detected in blood smears, the parasitemia was quantified (Fig. 3.14 C). A slightly reduced parasite growth was observed in *palm*$^{-}$ immunized animals. However, 3 days after patency similar high parasitemias were reached in immunized and control animals (Fig. 3.14C).

3.2.3 Liver parasite loads one year after *palm*$^{-}$ vaccination

To determine if the long-term protection against WT challenge is also reflected by a reduced relative liver infection load, livers of a third group of mice (n=4) were analyzed. These animals previously received two intravenous immunizations with 10,000 *palm*$^{-}$ sporozoites and one intravenous challenge/boost of 10,000 WT sporozoites was analyzed. Immunized and non-immunized mice (n=4 each) were challenged with 10,000 WT ANKA-GFP sporozoites one year after the last boost. The livers of these animals were isolated 41 hours after infection to determine relative parasite liver loads by quantitative real-time RT-PCR (Bruna-Romero et al., 2001). Livers of immunized animals showed a significantly lower relative liver infection load when compared to non-immunized, challenged control animals (Fig. 3.15). The variation of the parasite load in immunized mice was also substantial, ranging over 3 orders of magnitude. This variance reflects the differences in the initiation of blood-stage development after sporozoite challenge (Fig. 3.14 B). Presumably, animals with very low liver loads would be protected against WT challenge. Animals with higher liver loads would show a shift towards shorter pre-patent periods.

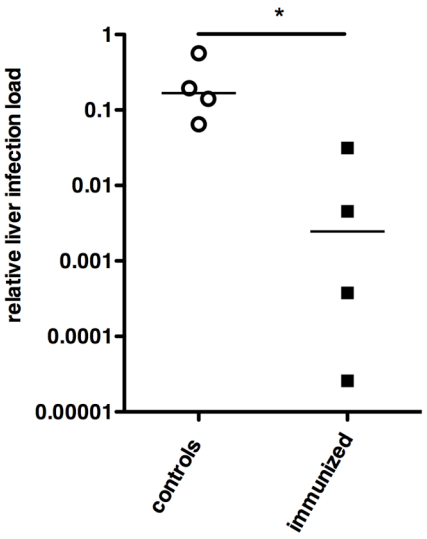

Figure 3.15: Protective efficacy of *palm*$^{-}$-sporozoite vaccination after one year as measured by liver parasite load.

Relative parasite liver infection load was determined in control and *palm*$^{-}$-immunized mice by quantitative real-time RT-PCR 41 hours after challenge by intravenous injection of 10,000 WT sporozoites one year after the last immunization. Shown are medians. Statistical significance was assessed using the two-tailed Mann-Whitney test. A *P* value of $P < 0.05$ was taken as significant (*).

3.2.4 Antigen-experienced T cells one year after *palm*$^{-}$ vaccination

To evaluate if differences in the amount of antigen-experienced $CD8^+$ T cells ($CD8\alpha^{lo}$ $CD11a^{hi}$) and $CD4^+$ T cells ($CD4^{lo}$ $CD11a^{hi}$) can still be found in the liver of immunized and control mice, liver lymphocytes were isolated and FACS analysis was employed after surface staining. A small, but significant increase of antigen-experienced $CD4^+$ T cells as well as $CD8^+$ T cells could be observed (Fig. 3.16 A, B). However, overall levels of $CD8\alpha^{lo}$ $CD11a^{hi}$ T cells were very high, which is probably due to the old age of the mice. The high baseline level renders this activation marker inappropriate for older mice.

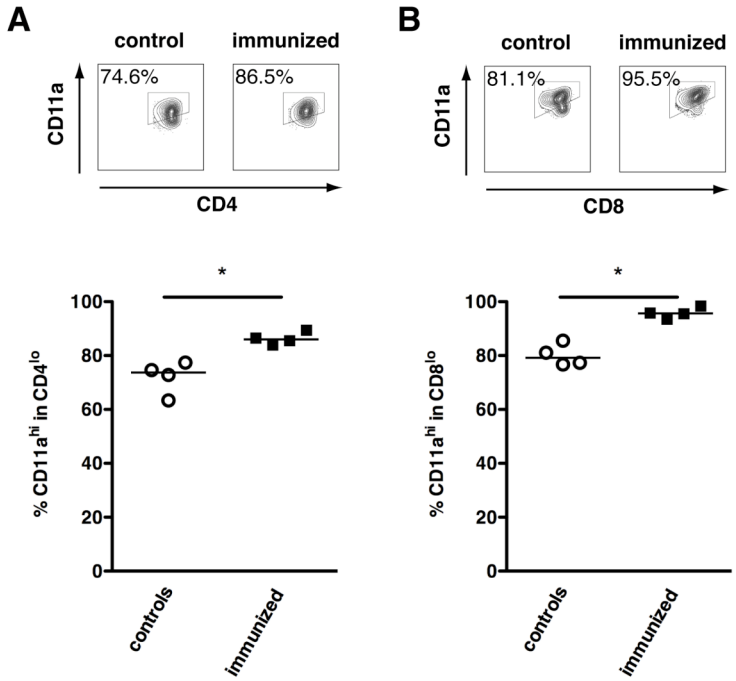

Figure 3.16: Levels of antigen-experienced CD4$^+$ T cells (CD4^{lo} CD11a^{hi}) T cells and CD8$^+$ (CD8α^{lo} CD11a^{hi}) in livers of *palm*$^-$-immunized mice.

C57BL/6 mice were immunized twice by intravenous injections with 10,000 *palm*$^-$ sporozoites and received one intravenous challenge/boost of 10,000 WT sporozoites. Immunized and non-immunized mice (n=4 each) were challenged with 10,000 WT ANKA-GFP sporozoites one year after the last boost. Livers were isolated 41hour after challenge and single cell suspensions were generated. Cells were stained with anti-mouse CD4, anti-mouse CD8 and anti-mouse CD11a antibodies and analyzed by flow cytometry. (**A**) Representative FACS plots and quantitation of antigen-experienced CD4$^+$ T cells (CD4^{lo} CD11a^{hi}) in livers of control and *palm*$^-$-immunized mice. (**B**) Representative FACS plots and quantitation of antigen-experienced CD8$^+$ T cells (CD8^{lo} CD11a^{hi}) in livers of control and *palm*$^-$-immunized mice. Medians are shown. Statistical significance was assessed using the Mann-Whitney test for nonparametric samples. *, $P < 0.05$.

3.2.5 Intracellular cytokine production after *ex vivo* stimulations

INFγ is long known to play an important role in malaria immunity (Schofield et al., 1987). A pathogen-unspecific CD3/CD28 stimulation and *Plasmodium*-specific *ex vivo* stimulations were employed to quantify INFγ production in T cells of *palm*$^-$-immunized mice.

The CSP-derived peptide P1 has been described previously as a CD4$^+$ epitope in the C57BL/6 model (Boscardin et al., 2006). Stimulations with the P1 peptide resulted in slightly, but significantly more INFγ-producing CD4$^+$ lymphocytes in the livers of *palm*$^-$-immunized mice (Fig. 3.17 B), whereas pathogen-unspecific stimulation with

CD3/CD28 antibodies revealed no significant difference between control and immunized mice (Fig. 3.17 A).

Two P. berghei peptides, termed S and T peptides, were recentlyshown to be immunodominant $CD8^+$ epitopes (Hafalla *et al.*, unpublished data). Pathogen-unspecific stimulation with CD3/CD28 antibodies resulted in more INFγ-producing $CD8^+$ lymphocytes in the livers, but not the spleens, of *palm*$^-$-immunized mice when compared to control animals (Fig. 3.17 A). In contrast, stimulation with the S and T peptides (Fig. 3.18 B, C, respectively) resulted in more INFγ-producing $CD8^+$ lymphocytes in both the spleens and livers of *palm*$^-$-immunized mice (Fig. 3.18 B, C).

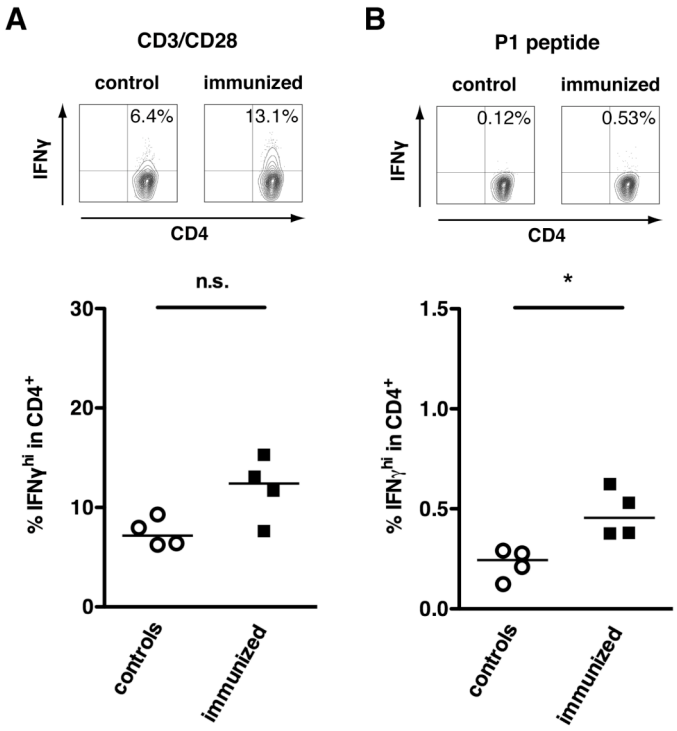

Figure 3.17: Slight increase of INFγ-producing $CD4^+$ liver lymphocytes in *palm*$^-$-immunized mice as compared to naive mice after *ex vivo* stimulation with a CD4 epitope.

Representative FACS plots and percentage of $INF\gamma^{hi}$ $CD4^+$ lymphocytes after *ex vivo* stimulation with CD3/CD28 antibodies (**A**) and with the *Plasmodium*-specific P1 peptide, a CD4 epitope (**B**). Medians are shown. Statistical significance was assessed using the Mann-Whitney test for nonparametric samples. *, $P < 0.05$.

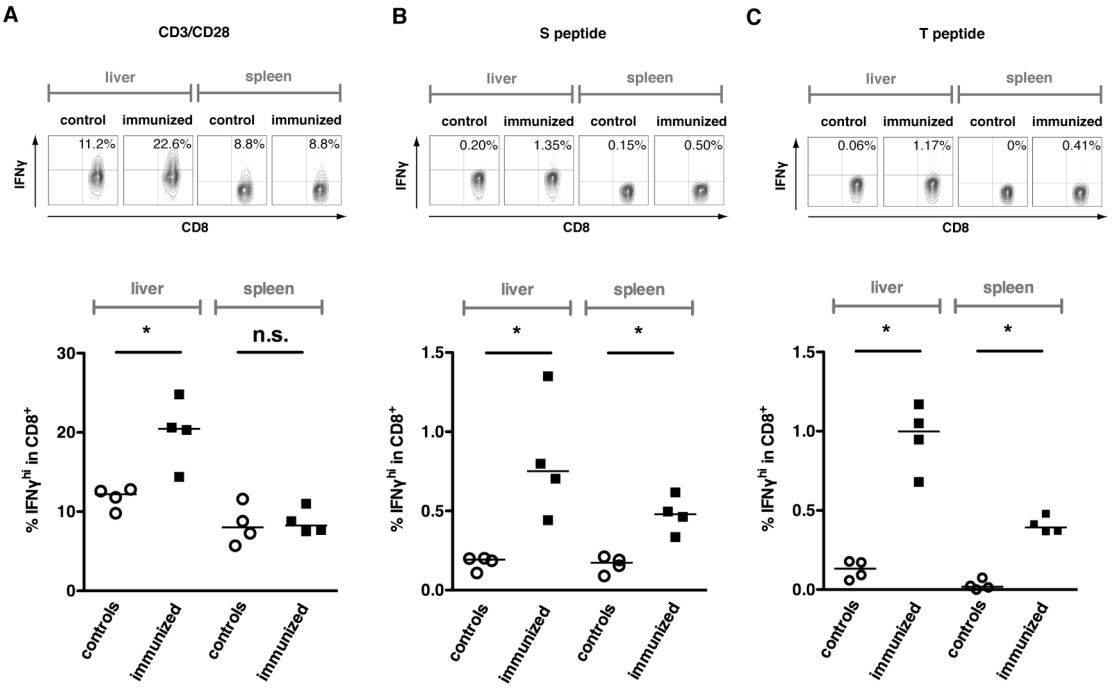

Figure 3.18: *Plasmodium*-specific *ex vivo* stimulations resulted in more CD8$^+$ INFγ^{hi} lymphocytes in livers and spleens of *palm*$^-$-immunized mice.

Representative FACS plots and quantifications of INFγ^{hi} CD8$^+$ lymphocytes after *ex vivo* stimulation with (**A**) CD3/CD28 antibodies, *Plasmodium*-specific peptides S (**B**) and T (**C**) are shown for livers and spleens of control and *palm*$^-$-immunized mice. Levels of CD8$^+$ INFγ^{hi} are significantly higher in spleens and livers of *palm*$^-$-immunized mice with all used *ex vivo* stimulations, except for spleen lymphocytes following CD3/CD28 stimulation. Statistical significance was assessed using the Mann-Whitney test for nonparametric samples. *, $P < 0.05$.

No significant differences in IL-2 and TNF production in the liver CD8$^+$ lymphocytes of control and *palm*$^-$-immunized mice could be observed with either of the 3 different stimulations (Fig. 3.19).

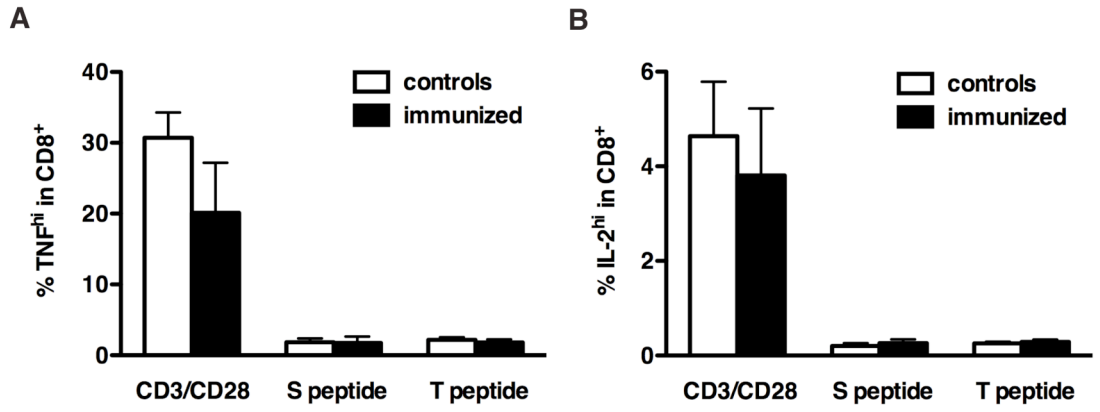

Figure 3.19: Proportions of TNF- and IL-2-producing CD8$^+$ liver lymphocytes remain unchanged in *palm*$^-$-immunized mice.

Single-cell suspensions of livers of control and *palm*$^-$-immunized mice were stimulated *ex vivo* with CD3/CD28 antibodies, or one of the CD8 epitope peptides S or T. Flow cytometry revealed no significant differences in the proportions of either TNF- (**A**) or IL-2-producing (**B**) CD8$^+$ lymphocytes. Shown are the means ±S.D. of control and *palm*$^-$-immunized mice (each n= 4).

Together, the results of the long-term protection experiments revealed a correlation of higher frequencies of antigen-specific INFγ-secreting CD8$^+$ and CD4$^+$ T cells, particularly in the target organ, i.e. the liver, and partial, albeit quantifiable protection in *palm*$^-$-immunized mice.

3.3 *In silico* analysis of genes involved in the [Fe-S] cluster biogenesis pathway in Apicomplexa

The characterization of PALM indicated that additional proteins in the apicoplast might be attractive targets for experimental genetics. The expression profile of *NFUapi*, a protein involved in [Fe-S] cluster biogenesis in the apicoplast, showed a similar upregulation in late liver stages as *PALM* (Tarun et al., 2008). Therefore, the components of the [Fe-S] cluster pathway in the apicoplast were genetically characterized.

3.3.1 Identification of *SUF* genes of the [Fe-S] cluster biogenesis pathway in the apicoplast

Previous studies described the identification of genes involved in the [Fe-S] cluster biogenesis pathway in the apicoplast (Ellis et al., 2001; Kumar et al., 2011; Seeber, 2002). However, since genome annotations of *Apicomplexa* are still ongoing and additional genes are continuously identified, an updated overview of the [Fe-S] cluster biogenesis pathway in the apicoplast was warranted. Various *Apicomplexa* species were compared using the OrthoMCL database (Chen et al., 2006; Li et al., 2003) and BLAST analysis.

The recently published ApicoAP prediction tool for apicoplast targeting sequences in *Apicomplexa* (Cilingir et al., 2012a) was also included to complement the established tools PlasmoAP (Foth et al., 2003a), PlasMitII (Bender et al., 2003a) and MitoProtII (Claros and Vincens, 1996). This offered the unprecedented possibility for *in silico* predictions of apicoplast targeting sequences in *T. gondii* and *B. bovis*. The genomes of the following species were interrogated: *P. falciparum*, *P. berghei*, *P. yoelii*, *T. gondii*, *B. bovis*, *T. annulata* and *C. parvum*.

In *P. falciparum*, *P. berghei* and *P. yoelii* a full set of *SufA*, *SufB*, *SufC*, *SufD*, *SufE*, *SufS* and *NFUapi* genes could be identified (Tab. 3.3). In *P. yoelii* the sequence of *SufB* was not yet assigned to a genomic location, but is likely to be encoded in the apicoplast genome, as it is in *P. falciparum* and *P. berghei*. *P. yoelii SufC* is not yet annotated, but EST blastn revealed various *P. yoelii* ESTs with high similarity to the nucleotide sequence of *P. berghei SufC*.

In *T. gondii SufB*, *SufC*, *SufD*, *SufE*, *SufS* and *NFUapi*, but no orthologs of *SufA* were identified (Tab. 3.4).

Table 3.3: *SUF* genes of the [Fe-S] cluster biogenesis pathway in the *Plasmodium* apicoplast.

Gene name	Predicted function	*P. berghei*[a]	*P. falciparum*[a]	ApicoAP[b]	PlasmoAP[b]	PATS[b]	PlasMit[b]	MitoProtII[b]
SufA	[Fe–S] cluster transfer protein	PBANKA_123740	PF3D7_0522700	ATP	++/++	0.951	99% non-mito	0.9862
SufB	Sulfur mobilization scaffold protein	PBANKA_API0012	PFC10_API0012	-	-	-	-	-
SufC	Sulfur mobilization scaffold protein	PBANKA_102920	PF3D7_1413500	no SP	0/++	0.862	91% possibly	0.5104
SufD	Sulfur mobilization, complexed with SUFB & C	PBANKA_094350	PF3D7_1103400	ATP	++/++	0.930	99% non-mito	0.5501
SufE	Desulfurase activator and sulfide "transferase"	PBANKA_030380	PF3D7_0206100	ATP	++/++	0.947	99% non-mito	0.9182
SufS	Cysteine desulfurase	PBANKA_061430	PF3D7_0716600	ATP	++/++	0.977	99% non-mito	0.2619
NFUapi	NifU-like scaffold protein	PBANKA_082230	PF3D7_0921400	ATP	++/++	0.972	99% non-mito	0.2084

[a] Gene IDs of the *P. berghei* and *P. falciparum* orthologs (http://PlasmoDB.org).
[b] Putative targeting of the *P. falciparum* SUF pathway proteins to the apicoplast or mitochondrion was predicted using four different algorithms. ApicoAP (Cilingir et al., 2012b) predicts whether a given protein lacks the required signal peptide ("No SP"), contains a signal peptide but no transit peptide ("non-ATP"), or is an apicoplast targeted protein ("ATP") that uses the bipartite signaling mechanism. PlasmoAP (Foth et al., 2003b) indicates the likelihood of the presence of the required signal peptide followed by the likelihood of an apicoplast localization ("-" = unlikely, "0" = undecided, "+" = likely, "++" = very likely). PlasMit (Bender et al., 2003b) predicts the likelihood of a mitochondrial localization for *P. falciparum* proteins ("99% non-mito", "91% mito", and "99% mito"). MitoProtII (Claros, 1995) gives a probability score for the likelihood of mitochondrial localization but is not optimized for *Plasmodium* sequences. No analysis was done for *SUFB* as the gene is encoded on the apicoplast genome and hence needs no targeting sequences.

B. bovis and *T. annulata* only possess a minimal set of Fe-S cluster biosynthesis genes in the apicoplast, namely *SufS* and *SufE*. In addition, *T. annulata* contains a copy of NFUapi (Tab. 3.4). The orthologs in *B. bovis* and *T. annulata* were verified by reciprocal BLAST searches, i.e. blastp of amino acid sequence of *P. falciparum* against *T. annulata* and *B. bovis* and vice versa was performed. Through the search for Pfam domain PF02657-containing orthologs with OrthoMCL, two previously unrecognized *SufE* orthologs, namely BBOV_III005960 and TA12620, were identified that were also briefly mentioned in a recent review (Seeber and Soldati-Favre, 2010). These genes were previously grouped genes containing an unrelated tRNA methyltransferase domain (PF03054). It appears, that in *B. bovis* and *T. annulata* the tRNA methyltransferase and the *SufE* genes are fused to just one gene, presuming the annotation is correct. The *B. bovis SufE/* tRNA methyltransferase gene BBOV_III005960 as well as the tRNA methyltransferases PF3D7_1019800 and TGME49_109110 are predicted by ApicoAP (Cilingir et al., 2012a) to localize to the

apicoplast, which favors the interesting hypothesis that in *B. bovis* both genes could indeed be fused. In *T. annulata* apicoplast-targeting prediction is not yet possible.

Table 3.4: *SUF* genes of the [Fe-S] cluster biogenesis pathway in the apicoplast of *T. gondii*, *B. bovis* and *T. annulata*.

Gene name	*T. gondii*	ApicoAP	MitoProtII	*B. bovis*	ApicoAP	MitoProtII	*T. annulata*	MitoProtII
SufA	-			-			-	
SufB	TogoCp26			-			-	
SufC	TGME49_025800	no SP	0.0034	-			-	
SufD	TGME49_073450	no SP	0.1716	-			-	
SufE	TGME49_077010	no SP	0.8741	BBOV_III005960	ATP	0.9217	TA12620	0.4508
SufS	TGME49_016170	no SP	0.9301	BBOV_IV003350	ATP	0.9658	TA16295	0.4653
NFUapi	TGME49_021920	no SP	0.3656	-			TA19885	0.5979

C. parvum probably does not posses an apicoplast (Zhu et al., 2000) and therefore it is not surprising that the [Fe-S] cluster genes in the apicoplast could not be identified. The only exception is a publlcation where cgd2_30 was listed as *SUFS* gene for *C. parvum* (Fleige et al., 2010). However, this gene does not cluster with the *Plasmodium SUFS* in OrthoMCL and experimental evidence would be necessary to draw a final conclusion.

As annotations of *Apicomplexa* species are not yet finished, absence of an ortholog might be either due to missing sequencing and/or annotation (as for *SufC* in *P. yoelii*) or actual absence in the genome.

3.3.2 Identification of NifU und NifU-like domain-containing genes

Since *NFUapi* stands out as a likely regulatory component without an assigned direct role in [Fe-S] cluster biosynthesis, an overview of all NifU und NifU-like domain-containing genes was generated (Tab. 3.5).

Table 3.5: Predicted localization of NifU und NifU-like domain proteins in *Apicomplexa*.

	Gene ID	PlasmoAP	ApicoAP	PlasMit	MitoProtII
NFUapi	PBANKA_082230	+/++	NA	non-mito 99%	0.8097
	PF3D7_0921400	++/++	ATP	non-mito 99%	0.2084
	TA19885	++/++	NA		0.5979
	TGME49_021920	-/-	no SP		0.3656
NFUmito	PBANKA_083170	-/++	NA	mito 91%	0.9792
	PF3D7_0930900	-/++	no SP	mito 91%	0.9977
	TGME49_012930	-/-	no SP		0.0046
	BBOV_III006970	-/-	no SP		0.5477
	TA10900	-/++	NA		0.9316
ISU	PBANKA_131820	-/++	NA	mito 91%	0.9957
	PF3D7_1454500	-/++	no SP	mito 91%	0.6647
	TGME49_037560	-/-	no SP		0.9318
	BBOV_IV004050	-/-	no SP		0.9652
	TA19345	-/++	NA		0.4726

T. gondii encodes a NifU-like domain-containing protein (TGME49_012930) with unclear localization and a putative NFU protein (TGME49_037560), which might localize to the mitochondrion (PlasmoDB comment). Recently, a hypothetical protein with a NifU-like domain (TGME49_021920) was shown to localize to the apicoplast by IFA (Sheiner et al., 2011). Although its sequence is not very similar to *Plasmodium NFUapi*, it might serve a related function in the apicoplast (Tab. 3.5 and Fig. 3.20).

B. bovis has two orthologs of the mitochondrial NifU-like genes, but no NFU that localizes to the apicoplast. In contrast, all three NifU-like genes can be found in *T. annulata* (Tab. 3.5).

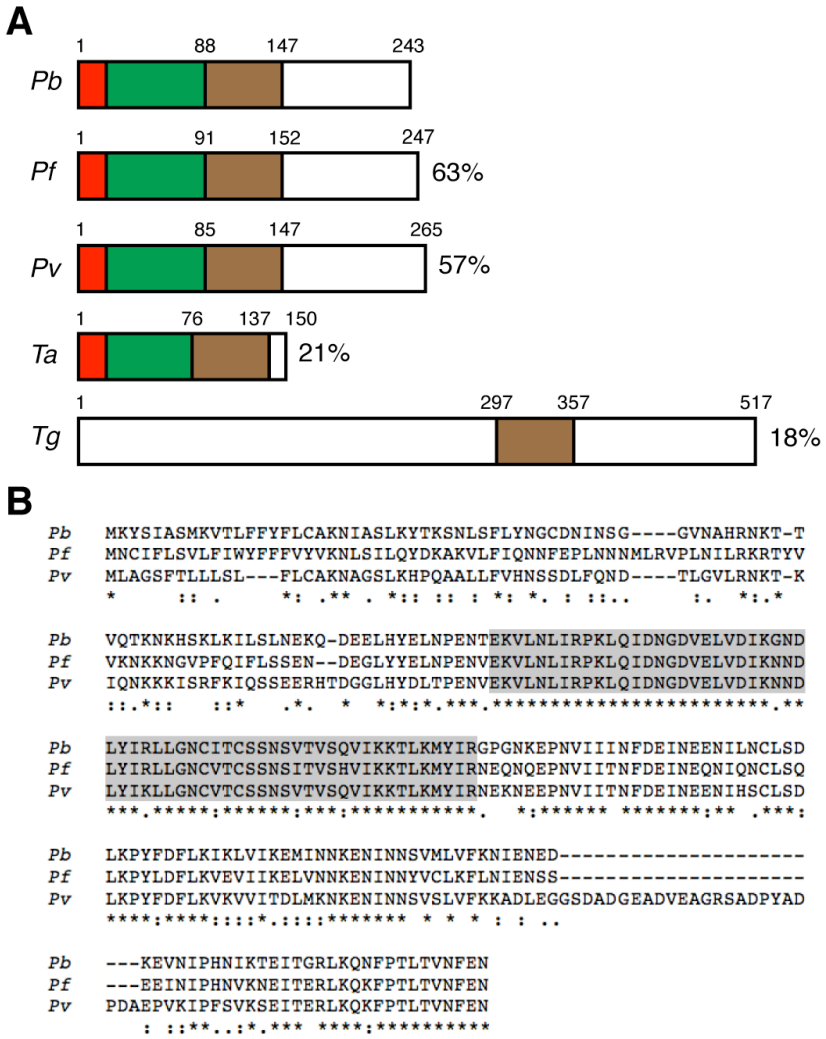

Figure 3.20: Apicomplexan NFUapi proteins.

(**A**) Primary structure of representative apicomplexan NFUapi proteins. Shown are the overall sequence structures and amino acid sequence identities of NFUapi orthologs in *P. falciparum* (PF3D7_0921400), *P. vivax* (PVX_099490), *Theileria annulata* (TA19885), and *Toxoplasma gondii* (TGME49_021920) compared with *P. berghei* NFUapi (PBANKA_082230). Signal peptide (red), apicoplast-targeting sequence (green), and the NifU-like domain (brown) are shown. (**B**) Sequence alignment of three *Plasmodium* NFUapi proteins. The NifU-like domain (gray shading) is well conserved.

3.3.3 Identification of [Fe-S] cluster-containing proteins

The list of [Fe-S] cluster-containing proteins is constantly expanding. In order to clarify where these proteins are localized and in which pathways they might be involved, the currently identified [Fe-S] cluster-containing proteins in *Plasmodium* and their possible functions were retrieved from PlasmoDB (Aurrecoechea et al.,

2009) and their localization predicted with PlasmoAP (Foth et al., 2003a), ApicoAP (Cilingir et al., 2012a), PlasMit (Bender et al., 2003a) and MitoProtII (Claros and Vincens, 1996) (Tab. 3.6). Not all predictions for cellular localizations are conclusive and therefore this list only represents an estimate and might have to be revised with new experimental data and optimized prediction tools. Furthermore, *Plasmodium* orthologs of *A. thaliana* [Fe-S] cluster-containing proteins (Balk and Pilon, 2011) were searched and added to the list as possible candidates of [Fe-S] cluster-containing proteins that might be considered for further analysis (Tab. 3.6).

Table 3.6: Confirmed and potential [Fe-S] cluster-containing proteins in *Plasmodium.*

P. berghei	*P. falciparum*	Annotation	PlasmoAP	ApicoAP	PlasMit	MitoProtII
APICOPLAST						
PBANKA_020870	PF3D7_0104400	IspH 4-hydroxy-3-methyl-but-2-enyl diphosphate reductase	-/-	no SP	possibly 91%	0.5404
PBANKA_050700	PF3D7_1022800	IspG 4-hydroxy-3-methyl-but-2-enyl diphosphate synthase	+/++	ATP	non-mito 99%	0.8285
PBANKA_070700	PF3D7_0823600	LipB, lipoate-protein ligase	+/++	no SP	non-mito 99%	0.9748
PBANKA_081190	PF3D7_0910800	nucleotide binding protein, putative	++/++	ATP	non-mito 99%	0.9760
PBANKA_112110	PF3D7_0622200	MiaB ?, radical SAM protein, putative?	+/++	ATP	non-mito 99%	0.9952
PBANKA_135750	PF3D7_1344600	LipA, lipoyl synthase	++/++	ATP	non-mito 99%	0.6838
PBANKA_141660	PF3D7_1318100	ferredoxin, putative	++/++	ATP	non-mito 99%	0.8117
MITOCHONDRION						
PBANKA_061790	PF3D7_0720400	ferrodoxin reductase-like protein	-/++	no SP	possibly 91%	0.8670
PBANKA_082810	PF3D7_0927300	fumarat hydratase, putative	-/++	no SP	non-mito 99%	0.8939
PBANKA_090930	PF3D7_1139700	adrenodoxin reductase, putative	-/+	no SP	possibly 91%	0.0610
PBANKA_122950	PF3D7_0614800	endonuclease III homologue, putative	-/++	no SP	non-mito 99%	0.5453
PBANKA_130330	PF3D7_1439400	ubiquinol-cytochrome c reductase iron-sulfur subunit, putative	-/++	no SP	possibly 91%	0.9782
PBANKA_135520	PF3D7_1342100	aconitase hydratase	-/++	no SP	possibly 91%	0.8460
PBANKA_142880	PF3D7_1212800	iron-sulfur subunit of succinate dehydrogenase	-/++	no SP	possibly 91%	0.1521
PBANKA_143040	PF3D7_1214600	adrenodoxin-type ferredoxin, putative	-/++	no SP	possibly 91%	0.8299
NUCLEUS or CYTOPLASM						
PBANKA_011240	PF3D7_0614200	conserved Plasmodium protein, unknown function	-/-	no SP	non-mito 99%	0.0141
PBANKA_083490	PF3D7_0934100	DNA excision-repair helicase, putative	-/-	no SP	non-mito 99%	0.0106
PBANKA_091970	PF3D7_1128500	conserved protein, unknown function	-/-		non-mito 99%	0.1301
PBANKA_101520	PF3D7_1429500	diphthamide synthesis protein, putative	-/-	no SP	non-mito 99%	0.2517
PBANKA_102890	PF3D7_1413800	diphthamide synthesis protein, putative	-/-	no SP	possibly 91%	0.0176
PBANKA_103410	PF3D7_1408400	DNA-repair helicase, putative	-/-	no SP	possibly 91%	0.0139
PBANKA_103530	PF3D7_1406900	radical SAM protein, putative	-/+	no SP	possibly 91%	0.1722
PBANKA_133970	PF3D7_1324500	DEAD box helicase, putative	-/-	no SP	non-mito 99%	0.4691
SUBCELLULAR LOCALIZATION NOT PREDICTED						
PBANKA_011230	PF3D7_0614100	conserved Plasmodium protein, unknown function	-/++	no SP	possibly 91%	0.2399
PBANKA_070600	PF3D7_0824600	anamorsin related protein, putative	-/-	no SP	non-mito 99%	0.1138
PBANKA_081200	PF3D7_0910900	DNA primase large subunit, putative	-/++	no SP	possibly 91%	0.0509
PBANKA_090570	PF3D7_1143300	DNA-directed RNA polymerase I, putative	-/-	no SP	non-mito 99%	0.0677
PBANKA_100950	PF3D7_1435300	NAD(P)H-dependent glutamate synthase, putative	-/-	no SP	non-mito 99%	0.0131
PBANKA_114410	PF3D7_1368200	RNAse L inhibitor protein, putative	-/-	no SP	possibly 91%	0.0535
PBANKA_123970	PF3D7_0524900	tRNA-YW synthesizing protein, putative	-/0	no SP	non-mito 99%	0.0527
PBANKA_144250	PF3D7_1227800	histone S-adenosyl methyltransferase, putative	-/-	no SP	non-mito 99%	0.0660

All proteins were either retrieved from PlasmoDB or based on similarity to *A. thaliana* [Fe-S] cluster proteins (Balk and Pilon, 2011).

3.4 Systematic experimental genetics of the iron-sulfur [Fe-S] cluster biogenesis pathway in the apicoplast of *Plasmodium berghei*

3.4.1 *SUF* genes are refractory to targeted gene deletion

[Fe-S] cluster-containing proteins in the apicoplast are involved in essential biosynthesis pathways (Fig. 1.8). Therefore, genes involved in the formation and assembly of [Fe-S] clusters in the apicoplast are likely to be vital, too. However, it is possible that not all components of the SUF-system are strictly required for the generation of [Fe-S] clusters, but rather fulfill auxiliary roles, at least in parts of the *Plasmodium* life cycle. To address these possibilities, systematic generation of loss-of-function mutants of the five genome-encoded *SUF* genes was attempted (Fig. 3.21).

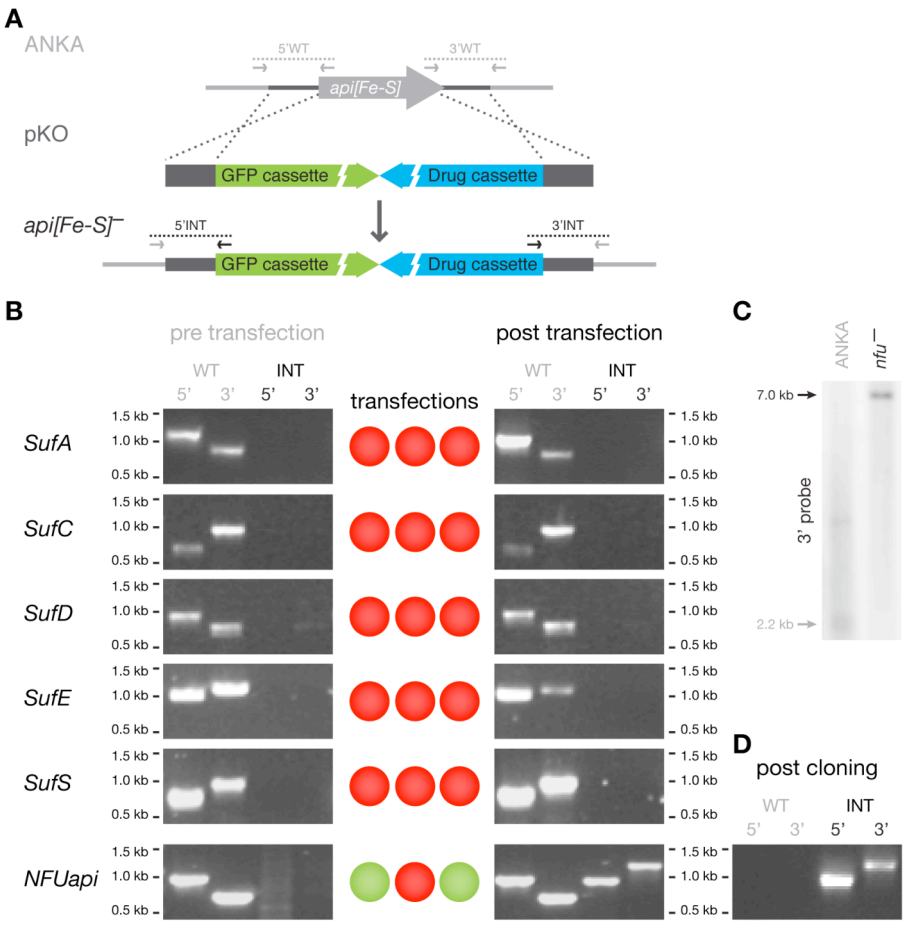

Figure 3.21: Targeted gene deletion of *SUF* genes and *NFU*.

(**A**) Replacement strategy to delete nuclear-encoded *PbSUF* genes. The respective loci (*api[Fe-S]*) were targeted with replacement plasmids containing 5' and 3' regions

(dark gray bars) flanking the open reading frames (light gray arrow), a high expressing GFP cassette (green), and the *hDHFR-yFcu* drug-selectable cassette (blue). Integration- and WT-specific primer combinations (see section 2.XXX) and expected fragments are indicated. (**B**) Overview of all transfection experiments. For each target gene, a diagnostic PCR of the WT locus, the outcome of three independent transfection experiments (green circle; successful gene deletion; red circle; unsuccessful gene deletion), and diagnostic PCR of the drug-selected parasites are shown. (**C**) Southern blot analysis of the clonal *nfu*–parasite line used in all phenotypic assays. gDNAs were restriction-digested with NdeI. The 3' homologous sequence used for targeted integration was used as the probe. (**D**) PCR-based genotyping of clonal *nfu*–parasites to verify successful deletion of *NFUapi*. Absence of WT signals confirms the purity of the clonal population.

Upon successful double cross-over recombination events, recombinant parasites are predicted to contain high-expressing GFP- and drug-selectable cassettes in place of the respective genes.

For targeted gene deletion of the *P. berghei SUF* genes, fragments of the 5'UTR and of the 3'UTR were amplified from gDNA. PCR fragments were cloned into the pBART-SIL6 transfection vector (Kooij et al., 2012), which contains the human dihydrofolatereductase (hDHFR) gene that confers resistance to pyrimethamine and the antifolate W99210. The resulting plasmids were linearized and *P. berghei* WT ANKA parasites were transfected (Fig. 3.21 A). Each KO was attempted in three independent transfection experiments. In none of the transfections integration of the targeting plasmid into the parasite genome could be achieved, as tested by diagnostic PCR (Fig. 3.21 B).

This finding lends genetic evidence for the importance of the five [Fe-S] cluster assembly proteins in the apicoplast.

3.4.2 Generation of *P. berghei nfu*$^{-}$ parasites

For targeted gene deletion of *P. berghei NFUapi*, a plasmid was generated, following the same principles as the *SUF* targeting plasmids (Fig. 3.21 A).

Integration-specific PCR amplification of the *NFU* locus to confirm the predicted deletion of *NFU* was done using the following primers: 5'HSP70rev and GT-5'NFU-F (5' integration, 958 bp), and GT-3'NFU-R and 5'DHFRrev (3' integration,1,210 bp) (Fig. 3.21 B). After successful integration a clonal *nfu*$^{-}$ parasite line was generated by intravenous injection of limiting parasite dilutions into mice. Absence of WT-

specific PCR products using primers GT-5'NFU-F and GT-5'NFU-R (5' WT ANKA control, 960 bp), and GT-3'NFU-F and GT-3'NFU-R (3' WT ANKA control, 702 bp) confirmed the purity of the clonal *nfu*⁻ parasite line (Fig. 3.21 D). The genotype of the clonal *nfu*⁻ parasite line was also confirmed by Southern blot analysis. For amplification of the hybridization probe, primers TV-3'NFU-F and TV-3'NFU-R were used. The hybridization probe was annealed to NdeI digested gDNA resulting in bands of 2.2kb (WT) and 7.0kb (*nfu*⁻) (Fig. 3.21 C).

3.4.3 *NFU* is dispensable for life cycle progression

In marked contrast to the *SUF* genes, *NFUapi* was readily replaced (Fig. 3.21 B)). Successful generation of a clonal *nfu*– parasite line permitted detailed *in vivo* phenotyping of parasite fitness during life cycle progression.

First, transmission to the *Anopheles* vector and sporogony was tested. Mosquito infectivity, numbers of mosquito midgut- and salivary gland-associated sporozoites of *nfu*⁻ parasites were within the WT phenotypic range (Fig. 3.22 A).

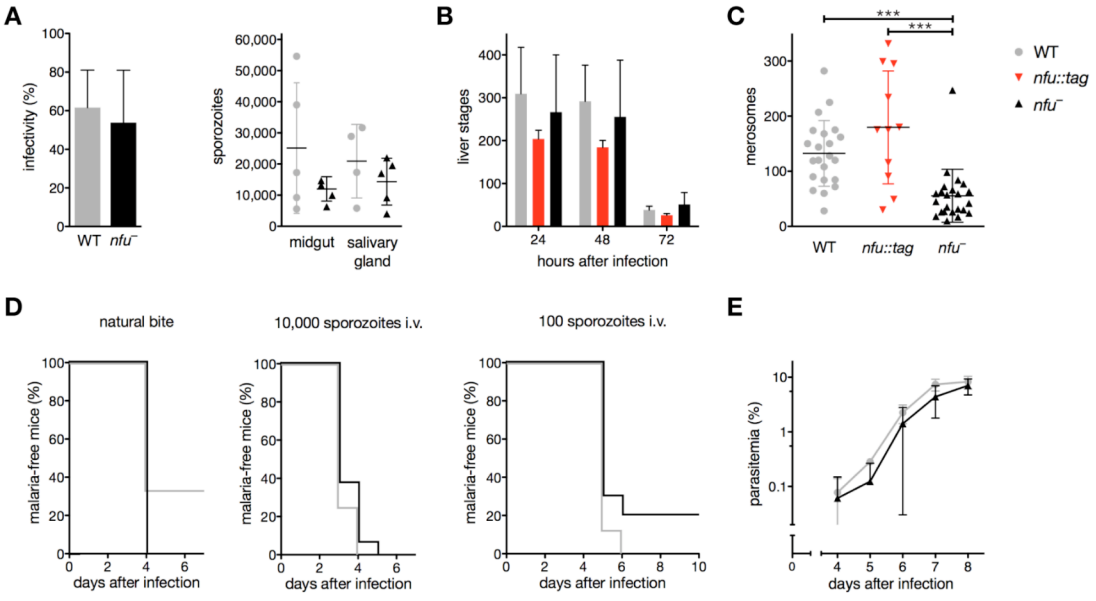

Figure 3.22: *NFUapi* assists onset of *Plasmodium* blood stage infection *in vivo*.

(**A**) Infectivity and mean sporozoite numbers (± S.D.) in midgut-associated oocysts (day 14 after infection) and salivary glands (day 17-21 after infection) of WT and *nfu*⁻-infected mosquitoes (n=5). (**B**) Liver stage development of *nfu*– 529 parasites in

cultured hepatoma cells. Shown are mean numbers (± S.D.) 24, 48, and 72 hours after infection from four independent experiments (n=3 each). Data for *nfu::tag* parasites are from a single experiment (n=3). (**C**) Merosome formation at 72 hours after inoculation of cultured hepatoma cells with 10,000 sporozoites. Shown are mean values (± S.D.). Data are from two (*nfu::tag*) or four (WT and *nfu*$^{-}$) independent experiments. Merosome formation of *nfu*$^{-}$ liver stage parasites was significantly reduced compared to WT and *nfu::tag* parasites (Kruskal-Wallis test followed by Dunn's multiple comparison test. ***, $p < 0.001$). (**D**) Kaplan-Meier analysis of time to malaria blood stage infection. C57BL/6 mice were infected with WT (gray) or *nfu*$^{-}$ (black) parasites by natural bite by 5-7 infected mosquitoes (single experiment; WT, n=3; *nfu*$^{-}$, n=7) or by intravenous injection of 10,000 (three independent experiments; WT, n=8; *nfu*$^{-}$, n=16) or 100 (two independent experiments; WT, n=8; *nfu*$^{-}$, n=10) isolated sporozoites. Animals were monitored daily for presence of parasites in Giemsa stained thin blood smears. (**E**) Asexual blood stage development following intravenous injection of 1,000 infected erythrocytes. Parasitemia of recipient mice (n=10, from three independent experiments) was monitored daily by examination of Giemsa-stained thin blood smears. Shown are mean values (± S.D.). Except for merosome formation, differences observed between WT and *nfu*$^{-}$ parasite development were non-significant.

Next, cultured hepatoma cells were infected with isolated sporozoites (Fig. 3.22 B). Numbers of *nfu*$^{-}$ liver stage parasites were similar to those of WT and *nfu::tag* parasites. However, when merosome development was quantified, a significant (~60%) reduction as compared to WT parasites (Fig. 3.22 C) was apparent. The *in vivo* development of *nfu*$^{-}$ parasites in mice was followed. Consistent with the observed reduction of *nfu*$^{-}$ merosome formation (Fig. 3.22 C), a trend towards a delay in prepatency following intravenous injection of 100 sporozoites was observed. Two mice injected with 100 *nfu*$^{-}$ sporozoites stayed malaria-free (Fig. 3.22D). However, these differences were non-significant and when mice were infected by bite of 5-7 infected mosquitoes the prepatent period was identical in *nfu*$^{-}$ and WT-infected animals (Fig. 3.22 C). Finally, naive NMRI mice were infected by transfusion of 1,000 infected erythrocytes. In good agreement with the data from sporozoite-induced infections, mice infected with *nfu*$^{-}$ parasites displayed a small but non-significant delay in blood stage expansion (Fig. 3.22 D). After 8 days this difference was completely abrogated and *nfu*$^{-}$-infected animals displayed high parasitemia.

Together, this phenotyping establishes an auxiliary role of NFU for the onset of the blood stage infection, particularly for the release of liver stage merozoites into the mammalian host bloodstream.

3.4.4 Generation of *P. berghei nfu::tag* parasites

To verify the predicted apicoplast targeting of NFUapi, a transgenic parasite line that expresses NFUapi with a combined fluorescent protein-epitope tag was generated (Fig. 3.23 A).

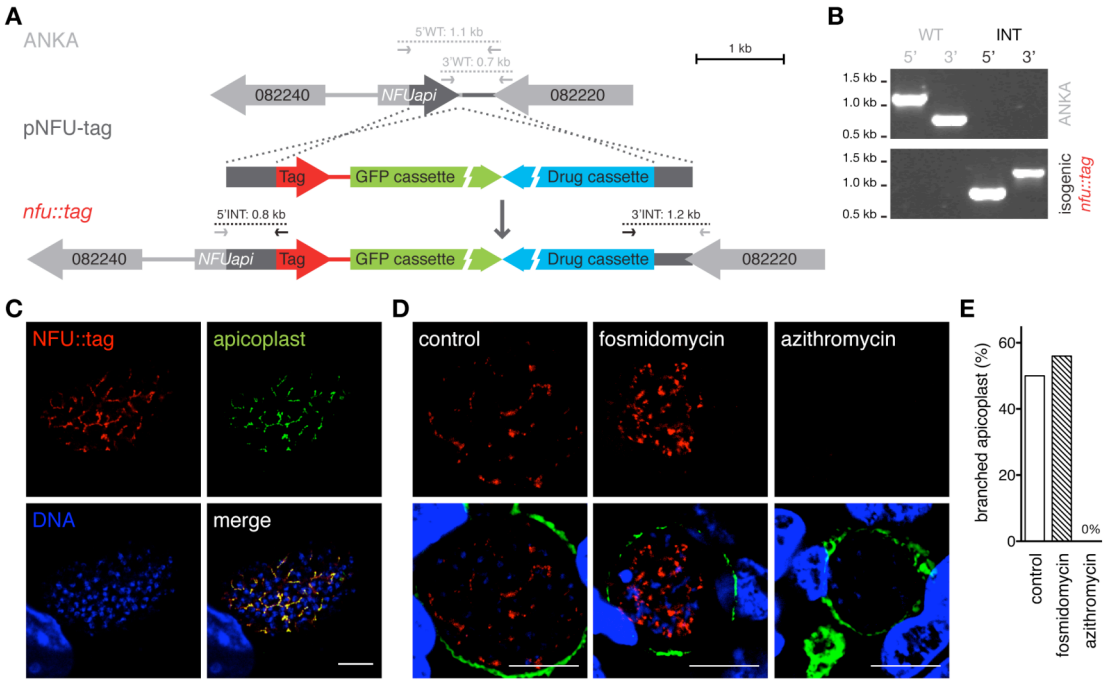

Figure 3.23: Apicoplast localization of NFU.

(**A**) Replacement strategy to generate stable parasite lines that express the endogenous *NFUapi* fused to the mCherry-3xMyc tag (red). In addition, recombinant parasites contain the high-expressing GFP cassette (green) and the drug-selectable *hDHFR yFcu* cassette (blue). Integration-specific (5'INT and 3'INT) and wild type-specific (5'WT and 3'WT) primer combinations (Tab. 2.1) are indicated by arrows and expected fragments as dotted lines. (**B**) PCR-based genotyping of *nfu::tag* parasites to verify successful fusion of *NFUapi* with the mCherry-3xMyc tag. Absence of WT signals confirms the purity of the isogenic parasite line. (**C**) Co-staining of fixed, *nfu::tag* parasite-infected hepatoma cells 48 hours after sporozoite infection using anti-myc and anti-ACP antibodies. Note substantial overlap between NFUapi and the signature apicoplast protein. Bar, 10 µm. (**D**) Drug treatment of *nfu::tag*-infected hepatoma cells to corroborate apicoplast localization of NFUapi. During liver stage development *nfu::tag*-infected cells were left untreated (control), treated with 100 µM fosmidomycin, or 1µM azithromycin. Liver stages were stained with anti-myc antibodies and anti-sera against upregulated in infective sporozoite protein 4 (UIS4), a signature protein of the parasitophorous vacuolar membrane. Bars, 10 µm. (**E**) Quantification of the percentage of control (n=70), fosmidomycin- (n=100), or azithromycin-treated (n=100) *nfu::tag* liver stages from panel (**D**) with branched apicoplasts.

For this purpose the C-terminal part and the 3'UTR of *NFU* were amplified by PCR and cloned into the pBART-SIL6 vector (Kooij et al., 2012), which contains the mCherry coding region fused to a triple c-myc tag sequence and the human dihydrofolatereductase (hDHFR) gene for positive selection (Fig. 3.23 A). *Plasmodium berghei* WT ANKA parasites were transfected with the linearized plasmid and correct integration by double homologous recombination of the replacement construct was confirmed by integration-specific PCR using primers GT-C-NFU-F and A70 (5' integration, 758 bp), and GT-3'NFU-R and 5'DHFRrev (3' integration, 1,210 bp). After successful integration, flow cytometric isolation of green fluorescent parasites resulted in an isogenic parasite line (Kenthirapalan et al., 2012). Absence of WT-specific PCR products using primers GT-C-NFU-F and TV-3'NFU-R (5' WT ANKA control, 1,106 bp), and GT-3'NFU-F and GT-3'NFU-R (3' WT ANKA control, 702 bp) confirmed the purity of the isogenic *nfu::tag* parasite line (Fig. 3.23 B).

3.4.5 Localization of NFU

Live *nfu::tag* parasites only produced faint undefined signals in developing midgut-associated oocysts and cultured liver stage parasites. To enhance the NFU::tag signal, fixed liver stage parasites at 48 hours after infection were stained with antibodies against the myc epitope tag. The extended branched structure was reminiscent of the apicoplast. This was further supported by co-localization with a signature apicoplast protein, acyl carrier protein (ACP (Friesen et al., 2010)) (Fig. 3.23 C).

To further corroborate these findings, *nfu::tag* liver stage parasites were treated with azithromycin, which led to apicoplast disintegration and a complete loss of NFUapi signal (Fig. 3.23 D and E). When parasites were treated with fosmidomycin, the NFUapi signal showed a healthy looking branched apicoplast at levels comparable to control cultures (Fig. 3.23 D and E).

4 Discussion

4.1 PALM - a novel *Plasmodium* apicoplast protein important for liver merozoite formation

In this study, a previously uncharacterized hypothetical gene, later named *Plasmodium*-specific Apicoplast protein important for Liver Merozoite formation (*PALM*), was analyzed. *In silico* analysis revealed that *PALM* is conserved in *Plasmodium* species, and no orthologs in any other organism were identified (Fig. 3.1). Further, the presence of a signal peptide and an apicoplast-targeting signal was revealed, strongly suggesting apicoplast localization of PALM. No functional domain could be identified that might hint at the function of PALM. However, a highly conserved region with a pair of conserved cysteine residues was apparent. It is tempting to speculate that these cysteine residues might play a functional role, but it is also conceivable that they have structural or other functions. Partial gene deletions of the conserved region and mutation of the conserved cysteins might reveal, if this sequence is essential for PALM function.

The predicted apicoplast localization of PALM was confirmed by generation of parasites that express fluorescently tagged PALM (Fig. 3.2). *PALM-mCherry-myc* parasites behaved undistinguishable from wildtype (WT) parasites, suggesting that function of PALM was not impeded by the protein tag. It was previously published that *PALM* expression is especially high in late liver-stage parasites (Tarun et al., 2008). Liver-stage expression and apicoplast localization could be confirmed. As a clearer and more reliable visualization of the apicoplast was obtained by α-myc antibodies in combination with *PALM-mCherry-myc* parasites than by α-ACP antibodies, *PALM-mCherry-myc* parasites provide a good opportunity to test apicoplast localization of other proteins via co-localization with α-myc antibodies. In addition, *PALM-mCherry-myc* parasites might also be used as a tool to test the effect of further drugs on the apicoplast.

Generation of *palm*$^-$ parasite lines by targeted gene deletion offered the possibility to study the role of *PALM* during the whole life cycle. Blood- and mosquito-stage development of *palm*$^-$ parasites was indistinguishable from WT parasites. In contrast, transition from liver- to blood-stage infection was severely impaired in *palm*$^-$ parasites. A large proportion of mice infected with *palm*$^-$ sporozoites did not

develop any blood-stage infection. When breakthrough infections occurred, blood-stage patency was delayed by at least four days, which can either be a sign of delayed liver-stage development or release of less merozoites. However, blood transfers from mice that were infected with *palm*$^{-}$ sporozoites showed that, at least in some mice, *palm*$^{-}$ parasites were already present in the blood at day 3 after per bite infection. It is possible that this is not the case for all animals because some mice only became blood-stage positive later. It is also possible that the amount of blood that was transfused was too small to harbor the few infected erythrocytes. Together, the results indicate that the delay in patency seen with *in vivo* infections with *palm*$^{-}$ parasites is probably primarily due to a lower number of merozoites released from hepatocytes and not to a general delay in development.

Assuming that breakthroughs of *palm*$^{-}$ parasites that establish a blood stage infection are due to a threshold that is passed, for example in terms of nutrient availability, or maybe even mechanical release of merozoites, it would be expected that injections with increasing doses of *palm*$^{-}$ sporozoites would also lead to increasing amounts of breakthrough infections. Surprisingly, injections of 1,000, 10,000 and 100,000 *palm*$^{-}$ sporozoites lead to comparable numbers of blood-stage positive mice, which currently cannot be explained (Fig. 3.11). There does not seem to be a limiting factor, e.g. nutrient availability, or a mechanical restriction. In these scenarios, a linear relationship between inoculum size and pre-patency would be expected.

Furthermore, it is interesting to note that passage of *palm*$^{-}$ parasites through more than one life cycle did not result in an increase of breakthrough infections in mice (data not shown). Thus, *palm*$^{-}$ parasites do not seem to adapt rapidly to the loss of *PALM*, for instance by gene mutations or upregulation of other genes.

Mice that became blood-stage positive after infection with *palm*$^{-}$ sporozoites only rarely showed symptoms of experimental cerebral malaria (ECM) and breaching of the blood-brain barrier and in this case a dose-dependent increase was observed. However, when infection occurred through injection of blood-stage *palm*$^{-}$ parasites, bypassing the liver phase, all mice showed symptoms of ECM and blue staining of the brain after Evans Blue injection. Instead of a direct role of PALM, it seems rather likely that a liver-stage infection resulting in a particularly slow onset of blood-stage infection influences the host defense and provides an advantage that prevents the development of ECM symptoms. A similar effect was also observed for other

knockout parasites that led to a delay in blood-stage patency, such as *sera4*$^{-}$ parasites (Putrianti et al., unpublished data).

A second, independent method to evaluate ECM development confirmed that *palm*$^{-}$ sporozoites lead to a reduced incidence of ECM (Fig. 3.13). Mice were infected with WT or *palm*$^{-}$ sporozoites and when WT infected mice started showing ECM symptoms, the mice were injected with Evans Blue, a dye that stains the brain, if the blood-brain barrier is breached. One hour later, WT-infected mice showed a blue brain, whereas only with a higher dose of injected sporozoites a single *palm*$^{-}$-infected mouse showed blue staining of the brain.

In vitro infection of hepatoma cells with *palm*$^{-}$ sporozoites revealed that 24 and 48 hours after infection the parasite numbers were in the WT range, suggesting that host cell invasion and early liver-stage development of *palm*$^{-}$ are not impeded. Strikingly, at 72 hours after infection significantly more *palm*$^{-}$ than WT parasites could still be detected inside host hepatocytes, suggesting that they are not able to efficiently leave the host cells. This was independently corroborated by lower numbers of *in vitro* merosome formation of *palm*$^{-}$ parasites when compared to WT. When total numbers of merosomes were injected intravenously into mice, all mice injected with *palm*$^{-}$ merosomes became blood-stage positive. These results revealed that once merozoites and merosomes can be formed by *palm*$^{-}$ parasites, they are infectious and capable of establishing a blood-stage infection.

The time point of developmental arrest was further characterized by immunofluorescence assays with α-MSP1 and α-UIS4 antibodies of liver-stage parasites (Fig. 3.9). *Palm*$^{-}$ parasites were able to form schizonts, as was seen by the nuclear division visualized by the DNA stain with DRAQ5. Quantification of different staining patterns of the merozoite signature protein MSP1 revealed that *palm*$^{-}$ parasites express MSP1, but are almost completely incapable of forming merozoites, which in WT parasites are clearly surrounded by MSP1. Furthermore, prolonged *in vitro* cultivation of *palm*$^{-}$ parasites for 94 hours did not result in more merozoites. This finding suggests, that merozoite formation is not simply delayed in *palm*$^{-}$, but instead a rare event. Strikingly, at 72 hours, and even more so at 94 hours, after infection a large proportion of *palm*$^{-}$ parasites showed aberrant MSP1 outside of the parasitophorous membrane. This might hint at leakage of the parasitophorous membrane and might be a sign of parasite death. Expression of MSP1 in *palm*$^{-}$ parasites is also different from mutants of the FASII pathway, which mostly lack

expression of this merozoite signature protein and therefore seem to be attenuated at an earlier developmental stage (Vaughan et al., 2009; Yu et al., 2008).
Staining of developing liver-stage *palm*$^{-}$ parasites with antibodies against a signature apicoplast-targeted protein (ACP) demonstrated that apicoplast growth, branching and protein import of ACP are unaffected in the absence of *PALM* (Fig. 3.10). Therefore, a structural role for apicoplast maintenance, branching and growth can be excluded.

It was shown that PALM is expressed throughout the parasite life cycle in the same structured pattern that was previously observed for other apicoplast proteins (Stanway et al., 2009) (Fig. 3.3). A puzzling question is why PALM is not equally important for other replicative *Plasmodium* life cycle stages, in particular blood-stage trophozoites and during mosquito midgut sporozoite formation, where the presence of the myc-tagged PALM protein was clearly demonstrated. Apparently, specific requirements for the development of malaria parasites are clearly needed in hepatocytes. This has previously been suggested by the generation of FASII pathway mutants that progress normally through the life cycle and only lead to growth arrests in late liver-stage development (Vaughan et al., 2009; Yu et al., 2008). Based on the distinct later time point of arrested development in comparison with FASII pathway mutants, a metabolic role in the biogenesis of fatty acids seems unlikely.
Remarkably, no *PALM* ortholog was found in *Plasmodium gallinaceum*. This raises the intriguing possibility that *PALM* emerged in response to specific requirements for the development of malaria parasites in hepatocytes, as exo-erythrocytic development of avian malaria species, such as *P. gallinaceum*, mainly occurs in leukocytes and endothelial cells of the brain (Frevert et al., 2008a; James, 1938; Macchi Bde et al., 2010). The enormous number of merozoites that are produced during liver-stage schizogeny may require a yet unidentified synthetic pathway in the apicoplast that is dispensable for other life cycle stages and related apicomplexan parasites. As the sequencing of the complete genome of *P. gallinaceum* is still ongoing, cloning and sequencing of the orthologous region of *P. gallinaceum* needs to be awaited to reveal whether *P. gallinaceum* harbours a *PALM* gene or not.
Application of a recently developed extended similarity group method (Chitale et al., 2009) revealed protein binding and metal ion binding among the top hits of probable molecular function of both *Pf*PALM and *Pb*PALM. Although these predictions are rather vague, it is tempting to speculate that PALM might be involved in iron

metabolism and maybe even in [Fe-S] cluster biogenesis. Preliminary tests using different media for injection of *palm*$^{-}$ sporozoites suggest that the medium used for dissection and injection of parasites might influence the amount of breakthrough infections (data not shown). Interestingly, the medium with higher iron content seemed to increase the amount of breakthrough infections.

Altogether, this study demonstrates a distinct and important role of PALM in full maturation of liver merozoites. In the absence of PALM, efficient formation of liver merozoites is the limiting step in *Plasmodium* life cycle progression.

4.2 *Palm*$^{-}$ parasites as whole-organism vaccine

Despite the efforts undertaken in the past decades to develop a safe and efficient vaccine against malaria, no vaccine has been licensed, yet. Clinical trials with the RTS,S/AS01 vaccine only show partial, short-lived protection (Agnandji et al., 2011) and demonstrate that there is still a long way to go until a vaccine that induces robust and lasting protection against *Plasmodium* infection vaccine will be commercially available. Various alternative approaches have been developed, including a vaccine using radiation-attenuated sporozoites (RAS) (Nussenzweig et al., 1967), genetically attenuated parasites (GAPs) (Mueller et al., 2005b; van Schaijk et al., 2008) and non-attenuated sporozoites under prophylactic drug cover (Belnoue et al., 2004). Each of these approaches bears advantages and disadvantages concerning safety, costs, efficacy, mode of application and storage.

In this thesis *palm*$^{-}$ parasites were generated, which, to date, are the latest liver-stage arrested GAPs. In contrast to several genetically arrested parasites deficient in apicoplast-targeted proteins of the FASII pathway (Pei et al., 2010; Vaughan et al., 2009; Yu et al., 2008), *palm*$^{-}$ parasites develop to a later time point, as indicated by the expression of the merozoite signature protein MSP1 (Fig. 3.9). At late time points in liver-stage development *in vitro*, MSP1 staining was frequently observed outside of *palm*$^{-}$ parasites. It would be interesting to see, if this holds true for *in vivo* infections and if the protection efficacy might benefit from broader antigen presentation.

Important improvements could be achieved by the generation of *palm*$^{-}$ parasites. Complete sterilizing immunity by only two doses of genetically arrested *P. berghei* parasites is unprecedented thus far. Two studies have reported protection in a fraction of mice by two consecutive immunizations (Mueller et al., 2005b; van Dijk et al., 2005). In addition to incomplete protection, in both cases challenges were

performed already after 7 (Mueller et al., 2005b) or 10 days (van Dijk et al., 2005) following the final boost, and in one case the immunization doses were also substantially higher (van Dijk et al., 2005).

A recent study using the *P. yoelii*/ Balb/c model showed that late arrested *fabb/f*$^{-}$ parasites mount superior antimalarial immunity compared to early arrested and non-efficient *sap1*$^{-}$ parasites, suggesting enhanced protection of late liver-stage arrested GAPs, probably due to a broader set of presented antigens (Butler et al., 2011). These results indicate that advanced liver-stage development may correlate with more potent immune responses. This notion is further supported in experimental human trials by the potent long-term protection against re-infection induced by delivery of low-dose sporozoite inocula under chloroquine cover (Roestenberg et al., 2009; Roestenberg et al., 2011).

Immunizations with *palm*$^{-}$ parasites corroborate the superior protection of late liver-stage arrested parasites (Tab. 3.2). Even after a period of more than 100 days, six of seven mice were completely protected from challenge of 10,000 intravenously injected WT sporozoites by only two immunizations with *palm*$^{-}$ sporozoites. The single mouse that developed a blood-stage malaria infection showed a substantial delay in patency of 5 days, suggestive of the presence of strong pre-erythrocytic immunity, and did not develop any ECM-associated symptoms.

It is interesting to note that, although *palm*$^{-}$ parasites express the merozoite surface marker MSP1, and might also express other blood-stage antigens, immunization with *palm*$^{-}$ parasites did not lead to a protection against challenge with blood-stage parasites. The only report that a GAP also induced protection against blood-stage challenge was achieved in the *P. yoelii*/ BALB/c model using *fabb/f*$^{-}$ parasites (Butler et al., 2011). Again, the reason for this difference might be that the *P. bergheil* C57BL/6 model is the rodent malaria model most difficult to protect against (Doolan and Hoffman, 2000; Ngonseu et al., 1998).

The longevity of protection with whole-organism vaccines against *Plasmodium* re-challenge was previously analyzed for up to 1 year (Douradinha et al., 2011; Douradinha et al., 2007; Jobe et al., 2007; Nganou-Makamdop et al., 2012). So far, one study describes long-term protection of 118 days using the *P. berghei*-C57BL/6 model with genetically arrested *Pbuis3* $^{-}$/*uis4* $^{-}$ parasites (Jobe *et al.*, 2007). The protocol employed three subsequent immunization rounds and it is unclear, but unlikely in the light of incomplete short-term protection acquired using *uis4* - parasites, that a single booster would suffice. In another study, long-term protection of up to 9

months following *P. berghei* immunization of C57BL/6 mice with RAS or infection with sporozoites under chloroquine cover was assessed (Nganou-Makamdop et al., 2012). Challenges 9 months after the last immunization showed superior protective efficacy of RAS, as 100% of RAS immunized mice were still protected against re-infection whereas only 50% of mice immunized with sporozoites under chloroquine chemoprophylaxis were sterilely protected. Douradinha and colleagues analyzed protection of RAS and *p52*$^{-}$ parasites for up to one year (Douradinha et al., 2007). However, in this study 6 immunizations were applied before final challenge after 365 days. Only 2 out of 4 *p52*$^{-}$ immunized mice were protected (Douradinha et al., 2007). Challenge of more than 13 months after the last boost revealed sterile protection in 25% of *palm*$^{-}$ immunized animals, after a 3 to 4 dose immunization protocol, and a mean delay of blood-stage patency of 2.3 days compared to naive control mice in the rest of the *palm*$^{-}$ immunized animals. Such long-term protection is unprecedented with malaria whole-organism vaccines in the rodent model and encourages further optimization attempts.

Development of immunization protocols with lower and fewer doses is particularly important in the context of integrating a safe, affordable and accessible malaria vaccine into the expanded program of immunization for infants. Although still elusive, such a vaccine should ideally have the capacity to induce potent immune responses after as few postnatal care visits as possible.

Livers of *palm*$^{-}$ immunized animals showed a significantly lower relative liver infection load, even when challenged one year after the last boost, indicating that protection against WT challenge also is reflected in lower liver loads (Fig. 3.15). The liver loads of immunized mice ranged over three orders of magnitude, which is consistent with the variance that was also seen in the initiation of blood-stage development after sporozoite challenge (Fig. 3.14). It seems likely that animals with very low liver loads correspond to those protected against WT challenge, whereas animals with increasing liver loads reflect the shift towards shorter pre-patent periods.

A small, but significant increase of antigen-experienced CD11a^{hi} CD8^{+} T and CD4^{+} T cells was observed in the livers of *palm*$^{-}$-immunized mice (Fig. 3.16). However, overall levels of CD11a^{hi} T cells were very high, rendering this activation marker inappropriate. This is probably due to the old age of the mice and might, for instance, be caused by unwanted exposure of mice to other pathogens over the long time of the experiment.

The findings of long-term protection experiments showed that antigen-specific effector T cells persist in the target organ even in aging mice. The results also corroborate previous findings that $CD8^+$ lymphocytes and IFNγ production, but not TNF and IL-2 (Fig. 3.19), play a major role in pre-erythrocytic immunity (Jobe et al., 2007; Mueller et al., 2007). More IFNγ-producing lymphocytes were found in the liver, the site of the first stages of *Plasmodium* infection, than the spleen. Antigen-specific stimulations with the three epitopes revealed that even one year after the last immunization, *palm*$^-$-immunized mice showed higher levels of $CD8^+$ and $CD4^+$ IFNγ-producing liver lymphocytes, emphasizing the long-lasting protection achieved by immunization with *palm*$^-$ sporozoites. However, total numbers of IFNγ-producing lymphocytes stimulated with the applied peptide stimulations were overall very low. This might be explained by vanishing pathogen-specific lymphocytes over this long period or generally small *Plasmodium*-specific IFNγ-producing lymphocyte populations activated by immunization with liver-attenuated, metabolically active parasites.

Due to substantial breakthrough infections, direct translation of *palm*$^-$ parasites as genetically arrested parasites for human vaccine trials is currently not possible. However, *palm*$^-$ parasites illustrate the advantages of tailor-made mutant parasites that arrest at a very last moment in liver development, before merozoite release from hepatocytes. This likely results in the broadest possible presentation of parasite antigens from sporozoite injection until liver merozoite formation. Complete attenuation of *palm*$^-$ parasites might be achieved by additional deletions of genes that are important for late liver-stage development. Deletion of several genes involved in different pathways might have a synergistic effect, preventing merozoite release from hepatocytes in multiple ways and thus making GAPs safer. Ideal additional gene deletion candidates would also arrest at a very late time point in liver-stage development and also show expression of late liver-stage and merozoite signature proteins. One such candidate might be the cysteine-type protease sera repeat antigen 4 (SERA4). *Pbsera4*$^-$ parasites display a two-day delay in establishing blood-stage patency and show expression of MSP1 of *in vitro* cultured liver stages (Putrianti et al., unpublished results). Another hypothetical candidate gene (PBANKA_110500) that encodes a protein, which is predicted to localize to the apicoplast, and was reported to have increased expression in late liver stages (Tarun

et al., 2008) was refractory to gene deletion. Therefore, it could not be considered for generation of a double knockout (data not shown).

A tight attenuation would also be important for follow-up immunization studies, because no mice would have to be discarded due to breakthrough infections. Once late liver-stage arrested parasites have been generated that do not show any breakthrough infections in the *P. berghei*/ C57BL/6 model, side-by-side studies could be performed with early arrested GAPs, where immunization doses, boosts, and duration of protection could be directly compared. This would then also offer the possibility of analyzing the underlying molecular and immunological mechanisms of protection, to evaluate if some protective mechanisms are shared between early and late arrested GAPs, as it was shown for early arrested GAPs and radiation-attenuated sporozoites (Kumar et al., 2009).

However, in addition, safety, production, route of delivery, and storage of genetically arrested parasites still need to be optimized before they can realistically be considered as malaria vaccines.

Altogether, I could show that immunizations with *palm*$^{-}$ parasites induce unprecedented potent, long-lasting protection against re-infection in the *P. berghei*/ C57/BL/6 model. These findings suggest that generation of a safe, MSP1-positive, genetically arrested parasite line may be an important improvement over first generations, which are arrested during onset of liver-stage development.

4.3 [Fe-S] cluster biogenesis in the apicoplast of *P. berghei*

[Fe-S] cluster biogenesis has been well studied in bacteria and yeast, and to a lesser extent in other eukaryotes (Balk and Pilon, 2011; Johnson et al., 2005a; Lill and Muhlenhoff, 2006; Seeber, 2002; Xu and Moller, 2011). However, very little functional data are yet available for apicomplexan parasites.

In this study I applied *in silico* analysis to identify nuclear-encoded components of the SUF system in various *Apicomplexa* and analyzed their predicted localization with a recently published program (Cilingir et al., 2012a). I then targeted the components of the *P. berghei* SUF system systematically by double-homologous recombination to test whether they are essential or not during blood infection *in vivo*. In *T. gondii*, *NFUapi* and a complete set of *SUF* genes, with the exception of *SufA,* were identified (Tab. 3.4). *B. bovis* and *T. annulata* only possess a reduced set of Fe-S cluster biosynthesis genes in the apicoplast, namely *SufS* and, *SufS* and *NFUapi*,

respectively. However, through the search for Pfam domain PF02657-containing genes with OrthoMCL, I could identify two previously unrecognized *SufE* orthologs, namely BBOV_III005960 and TA12620, which were also briefly mentioned in a recent review (Seeber and Soldati-Favre, 2010).

Of note, none of the annotated *Toxoplasma gondii* SUF proteins contain an apicoplast-targeting sequence. For one of the components, TgNFUapi, apicoplast localization has been shown experimentally (Sheiner et al., 2011). Assuming that gene and protein annotation in the *T. gondii* genome database is correct, this might suggest that the other components of the SUF pathway [Fe-S] cluster biogenesis also localize to the apicoplast, despite the uniform absence of a signal peptide and apicoplast-targeting sequence. It remains elusive how this alternative targeting to the apicoplast might have evolved and if there are specific reasons why all of the SUF components in *T. gondii* are targeted through this alternative pathway. Clearly, other apicomplexan parasites target these components through a classical signal peptide and apicoplast-targeting sequence-dependent import pathway.

In *Plasmodium* spp. a complete set of SUF genes and NFU is present (Seeber and Soldati-Favre, 2010). Interestingly, the avian malaria parasite *P. gallinaceum* appears to lack a gene encoding NFUapi, while all SUF elements were readily identified (data not shown). As for PALM, this might be easily explained by incomplete sequence data available for this *Plasmodium* species, nevertheless it is striking that another gene encoding a *Plasmodium* apicoplast protein is also missing from its genome.

Moreover, searching published [Fe-S] cluster-containing proteins in *A. thaliana* for orthologs in *Plasmodium* spp., new potential [Fe-S] cluster-containing proteins were identified (Tab. 3.6). These candidates can now be considered for biochemical analysis and evaluation of the possible impact on [Fe-S] cluster biogenesis or unrelated metabolic pathways.

Three independent transfection experiments using the most recent and efficient techniques available for experimental genetics in *P. berghei* showed that the *SUF* genes were refractory to gene deletions. Positive selection of pyrimethamine-resistant parasites *in vivo* only yielded WT parasites. This finding suggested that the malarial SUF system is critical for survival during blood stage growth (Fig. 3.21). However, definitive proof would require additional experimentation, including gene complementation and conditional gene ablation strategies, which are unfortunately not established in the *P. berghei* system. Cross-species complementation could

prove, that the gene locus can be targeted and might also provide information on functional conservation of these proteins in other species.

Presence of [Fe-S] clusters in the penultimate and ultimate enzymes of the DOXP pathway of isoprenoid biosynthesis, ISPG and ISPH, respectively, make it plausible that the components of the SUF assembly machinery are refractory to targeted gene deletion. In a recent publication it was shown that apicoplast destruction by antibiotics treatment in cultured *P. falciparum* parasites could be compensated for by supplementation with IPP, one of the endproducts of the DOXP pathway of isoprenoid biosynthesis (Yeh and DeRisi, 2011). However, it remains unclear what happens to nuclear-encoded apicoplast proteins upon azithromycin treatment. Are these proteins still present in the cytoplasm and can partially fulfill their biological functions? In such a scenario apicoplast proteins might fulfill other essential functions in blood-stage parasites that are simply not affected by azithromycin treatment. This also raises the question if [Fe-S] cluster biosynthesis is essential because of the presence of [Fe-S] clusters in enzymes of the DOXP pathway of isoprenoid biosynthesis. This hypothesis can be tested in *P. falciparum* where gene deletions of SUF pathway components might be feasible under IPP supplementation. This would show whether the DOXP pathway of isoprenoid biosynthesis is the sole reason for the essentiality of [Fe-S] cluster biogenesis in the apicoplast in *Plasmodium* blood stages or not. *P. berghei* parasites cannot be kept in *in vitro* culture for multiple rounds of replication and, hence, this experiment cannot be performed in this model. Since transfections are currently not possible in other life cycle stages IPP complementation cannot be tested directly.

The assembly of results presented in this thesis and previously published data on apicoplast gene deletion experiments can provide a basis for the evaluation of the significance of specific apicoplast pathways and interdependences of these pathways, as for the [Fe-S] cluster biosynthesis pathway and [Fe-S] cluster-containing proteins of other pathways (Fig. 4.1). It is evident that the various pathways do not have equal importance for different life cycle stages, as some components are refractory to gene deletion in blood stages, such as the *SUF* genes, whereas others can be deleted, but reveal significance for liver stages, as observed with *PALM* and genes involved in fatty acid biosynthesis (Vaughan et al., 2009; Yu et al., 2008), or seem to have redundant or non-essential functions, as *LipB* (Gunther et al., 2007), for instance.

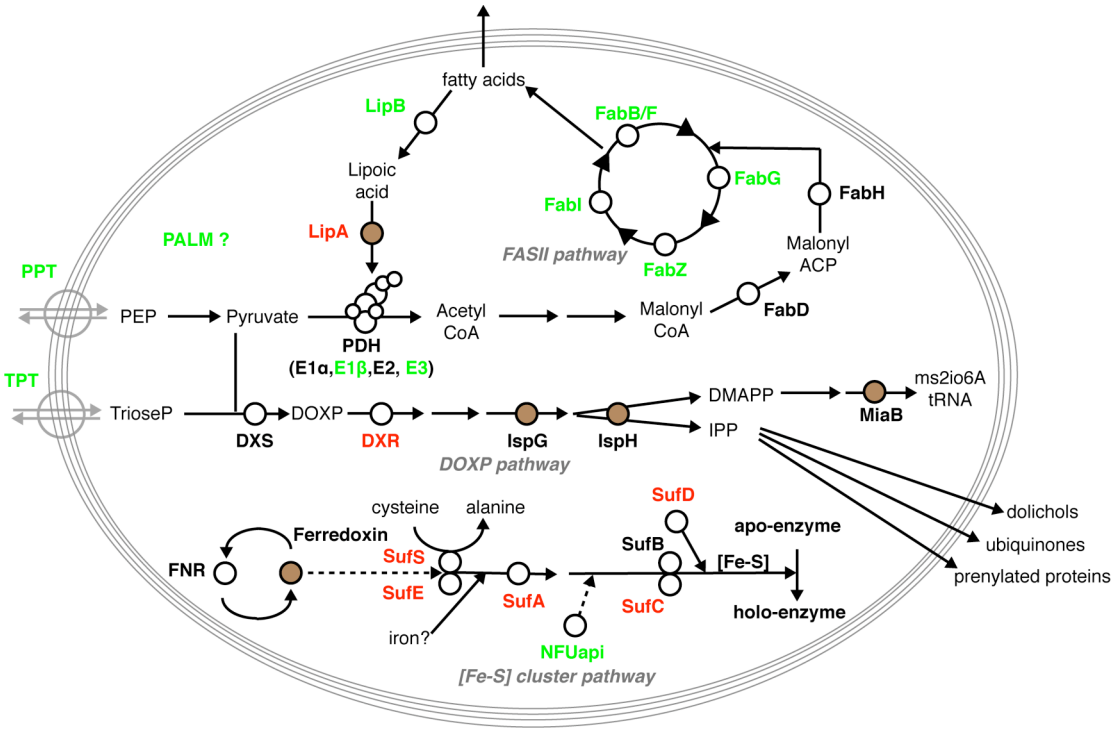

Figure 4.1: Updated overview of *Plasmodium* apicoplast genes targeted for gene deletion.

Shown is an updated overview of apicoplast localized biosynthesis pathways that have been targeted for gene deletions in *Plasmodium*. Apicoplast enzymes successfully targeted by transfection plasmids and enzymes refractory to gene deletion are depicted in green and red, respectively. Apicoplast proteins that contain a [Fe-S] cluster are depicted as brown circles. For references see text in sections 1.4.2, 1.5 and 1.6. (PPT= phospho-enolpyruvate transporter, PEP= phospho-enolpyruvate, PDH= pyruvate dehydrogenase, CoA= coenzyme A, FabD= malonyl-CoA:ACP transacylase, ACP= acyl carrier protein, FabH= b-ketoacyl-ACP synthase III, FabG= β-ketoacyl-ACP reductase, FabZ= β-hydroxyacyl-ACP dehydratase, FabI= trans-2-enoyl-ACP reductase, FabB/F= β-ketoacyl-acyl-carrier-protein synthase , LipB= lipoate protein ligase, LipA= lipoate synthase, Suf= sulfur utiliuzation factor, NFU= nitrogen fixation factor U, TPT= triose phosphate transporter, TrioseP= triose-phosphate, DXS= DOXP synthase, DXR= DOXP reductosiomerase, IspG= GcpE; 4-hydroxy-3-methyl-but-2-enyl-diphosphate (HMBPP)-synthase, IspH= LytB; HMBPP-reductase, DMAPP= dimethylallyl pyrophosphate, IPP= isopentenyl pyrophosphate, MiaB= (Dimethylallyl)adenosine-tRNA-methylthiotransferase), DOXP= 1-deoxy-D-xylulose-5-phosphate)

In contrast, to the SUF genes a *PbNFUapi* loss-of-function mutant was readily obtained (Fig. 3.21). Through the generation of *nfu::tag* parasites it was possible to verify the localization of NFUapi to the apicoplast (Fig. 3.23). During *in vitro* liver-stage development *nfu::tag* parasites were treated with azithromycin to exclude mitochondrial targeting, similar to the experiments with *PALM-mCherry-myc* parasites. In this experiment fosmidomycin was also tested. High doses (100μM) of fosmidomycin did not abolish apicoplast structures. This finding is in perfect

agreement with a recent publication by Baumeister and colleagues, where it was shown that up to 100*µ*M of the fosmidomycin derivate FR900098 does not inhibit growth of *P. berghei* liver stages *in vitro* at 48 hours after infection (Baumeister et al., 2011). FR900098 activity was also tested *in vivo* by infection of C57BL/6 mice with 10,000 *P. berghei* sporozoites and subsequent treatment with four high doses of 250 mg/kg FR900098 at 12 hours intervals. Again, no significant difference in parasite load could be observed 42 hours after infection. However, others reported that fosmidomycin can kill *Plasmodium* liver-stages (Nair et al., 2011). This apparent discrepancy is difficult to reconcile and argues for follow-up experimentation, including heterologous expression of a transporter in hepatoma cells and synthesis of membrane-permeable derivates of fosmidomycin.

The only available functional data for NifU-like domain containing proteins in apicomplexan parasites to date, is the confirmation of the apicoplast subcellular localization of *T. gondii* NFUapi (TGME49_021920) (Sheiner et al., 2011). Furthermore, Sheiner *et al.* were apparently able to delete *TgNFUapi* by experimental genetics, as the authors listed the gene as non-essential. Yet, no phenotypical data on *Tgnfuapi*$^{-}$ were provided.

As the *P. berghei* malaria model allows in depth analysis of the entire life cycle, life cycle progression of *nfu*$^{-}$ parasites was carefully observed (Fig. 3.22). Despite not being critical, *PbNFUapi* seems to fulfill an auxiliary function. Presence of NFUapi results in a more efficient release of merosomes and thus a slightly faster onset of blood stage infection following sporozoite inoculation. In other organisms NifU-like proteins have been shown to act as [Fe-S] cluster scaffolds (Touraine et al., 2004; Yabe et al., 2004) and NFUapi might present an alternative scaffold to SufA. The plant-type ferredoxin, a [Fe-S] cluster-containing protein in the apicoplast of *Plasmodium* (Vollmer et al., 2001), was proposed to function as a reductant in a light-independent manner, for example in the desaturation of fatty acids (Schmidt and Heinz, 1990; Wada et al., 1993). If deletion of *NFUapi* would influence ferredoxin activity, this hypothesis might explain the observed defect in merosome formation where high amounts of fatty acids are required for the membranes of tens of thousands of invasive merozoites. Interestingly, it was shown that the [2Fe-2S] cluster-containing NifU of cyanobacterium *Synechocystis* PCC6803 possesses the ability to deliver its [2Fe-2S] cluster to apoferredoxin (Nishio and Nakai, 2000) and thus provides a rationale for further investigations on the role of *Plasmodium* NFUapi on the maturation of the plant-type ferredoxin.

It should also be considered that all analyses of *nfu*$^{-}$ parasites were performed *in vivo* or under optimal culture conditions. In *Escherichia coli* deficiencies in the SUF pathway do not result in phenotypes under normal growth conditions. However, when cultured in low iron (Outten et al., 2004) or increased oxidative stress conditions (Nachin et al., 2003; Zheng et al., 2001), bacteria demonstrate marked growth problems. Another NifU-like protein in *E. coli*, NfuA, was also shown to be required for maturing of [Fe-S] cluster proteins under oxidative stress and iron starvation conditions (Angelini et al., 2008). Therefore it would be interesting to test *nfu*$^{-}$ parasites under stress conditions. One possibility would be to study *in vitro* liver stage development in the presence of iron chelators or in medium with decreased iron content. It is tempting to speculate that under such suboptimal conditions *nfu*$^{-}$ parasites might reveal a stronger deficiency in development.

In conclusion, the results of this study and the absence of a plastid-like SUF system in humans, provide the first genetic evidence for the importance of the *Plasmodium* apicoplast [Fe-S] biosynthetic pathway and validate its potential as antimalarial drug targets.

4.4 Outlook

In the presented study I could characterize a previously unrecognized *Plasmodium*-specific apicoplast protein, termed PALM. The distinct and important role of *PALM* for full development of liver-stage merozoites and establishment of blood-stage infection in the vertebrate host are important findings. However, the biochemical function of PALM remains to be determined.

Recombinant expression and purification of PALM in *E. coli* would be required to initiate biochemical studies. Crystallization and successful x-ray structure determination might reveal possible functions, assuming that it displays structural similarity to previously described proteins. Purified PALM protein might also indicate if PALM binds iron, as other iron-binding proteins display a distinct brown color upon purification (Raux-Deery et al., 2005).

The search for proteins that interact with PALM might provide information on the biological function(s) and involvement in metabolic pathways. To find interaction partners, complementary methods can be applied including co-immunoprecipitation of *Plasmodium* liver-stage lysates with *PALM-mCherry-myc* parasites or

recombinantly expressed PALM and a yeast-2-hybrid screen with PALM as bait against a *Plasmodium* liver-stage library. However, biochemical studies with *Plasmodium* liver stages are not trivial as the parasite material is very limited and development of biochemical assays and metabolome profiling has not been established yet. Microarray analysis in *palm*$^{-}$ parasites could give additional indications if genes are upregulated to compensate for the loss of *PALM*.

As an alternative approach, PALM could be transgenically expressed in *T. gondii* were no PALM ortholog is present. This could reveal if its presence alters parasite growth or egress. Similarly, PALM could also be overexpressed in *P. berghei* by placing it under a strong liver-stage promoter. Possible scenarios might be larger liver-stage parasites, growth deficiencies because of toxic effects, and/or premature merozoite formation.

Altogether, the characterization of *PALM* knockout mutants provides an exciting opportunity to discover missing pieces in the puzzle of *Plasmodium* liver-stage development. Identification of PALM functions might reveal new apicoplast pathways that are tailor-made for efficient pre-erythrocytic development in the liver.

Immunizations with *palm*$^{-}$ sporozoites as whole-organism vaccine yielded promising improvements over previous studies, including fewer immunization doses and long-term protection. These results encourage the development of late liver-stage genetically arrested parasites that express blood-stage antigens. To achieve safe attenuation without breakthrough infections, multiple genes should be deleted. Differential gene expression with upregulation in late liver stages might be a helpful tool to identify additional candidates for genetic targeting. However, it should be kept in mind that it would only be a first indication as another candidate with a similar expression profile to *PALM* was refractory to gene deletion in blood stages (PBANKA_110500). Moreover, one candidate (NFUapi) could be deleted, but did not show an essential function during liver-stage development. In addition, late liver-stage arrested parasites in the rodent malaria model are needed to be rigorously tested in pre-clinical research before advancing to clinical trials.

My experimental findings argue for the essential role of [Fe-S] cluster biogenesis in the apicoplast of *Plasmodium*. Expression analysis of [Fe-S] cluster biogenesis genes in different parasite life cycle stages can provide additional indications, whether [Fe-S] cluster biogenesis and all proteins involved are equally important in

all life cycle stages. Higher or reduced expression levels would suggest critical and less important roles. Generation of conditional knockout mutants in *T.gondii* could provide additional proof for the proposed central role of [Fe-S] cluster biogenesis in parasite survival. Follow-up analysis of [Fe-S] cluster biogenesis could also include cross-species complementation with bacterial, plant or other apicomplexan orthologs to analyze if protein function is conserved among these species.

A recent study provided the first biochemical analysis of SUF proteins (Kumar et al., 2011). Certainly further analyses will help to unravel specific functions of the proteins involved in [Fe-S] cluster biogenesis in *Plasmodium*. This may or may not confirm functions that have been already described for orthologs in other species.

The proposed auxiliary function of NFUapi might be connected to the desaturation of fatty acids through the [Fe-S] cluster-containing plant-type ferredoxin. In another organism, the cyanobacterium *Synechocystis*, NFU was shown to transfer the [Fe-S] cluster to apoferredoxin (Nishio and Nakai, 2000). This provides an exciting hypothesis for the role of *Pb*NFUapi in the formation of liver-stage merozoites where high amounts of fatty acids are required for the membranes of the merozoites. Future investigations on the functions of *Pb*NFUapi should consider this possibility. As a first step, a possible direct interaction of *Pb*NFUapi and plan-type ferredoxin could be tested.

The biogenesis of [Fe-S] clusters in the mitochondrion and the cytoplasm remains to be investigated. It will be interesting to see if they are equally important as in the apicoplast and if assembly in the cytosol is dependent on one of the organellar [Fe-S] clusters biosynthesis pathways.

Many mysteries, such as the source of iron for [Fe-S] clusters and the exact functions of all components, are yet to be unraveled and the presented results on [Fe-S] cluster biogenesis may serve as a starting point to kick off future studies on this exciting, yet for so long mostly disregarded, pathway.

5 Bibliography

Agnandji, S.T., Lell, B., Soulanoudjingar, S.S., Fernandes, J.F., Abossolo, B.P., Conzelmann, C., Methogo, B.G., Doucka, Y., Flamen, A., Mordmuller, B., Issifou, S., Kremsner, P.G., Sacarlal, J., Aide, P., Lanaspa, M., Aponte, J.J., Nhamuave, A., Quelhas, D., Bassat, Q., Mandjate, S., Macete, E., Alonso, P., Abdulla, S., Salim, N., Juma, O., Shomari, M., Shubis, K., Machera, F., Hamad, A.S., Minja, R., Mtoro, A., Sykes, A., Ahmed, S., Urassa, A.M., Ali, A.M., Mwangoka, G., Tanner, M., Tinto, H., D'Alessandro, U., Sorgho, H., Valea, I., Tahita, M.C., Kabore, W., Ouedraogo, S., Sandrine, Y., Guiguemde, R.T., Ouedraogo, J.B., Hamel, M.J., Kariuki, S., Odero, C., Oneko, M., Otieno, K., Awino, N., Omoto, J., Williamson, J., Muturi-Kioi, V., Laserson, K.F., Slutsker, L., Otieno, W., Otieno, L., Nekoye, O., Gondi, S., Otieno, A., Ogutu, B., Wasuna, R., Owira, V., Jones, D., Onyango, A.A., Njuguna, P., Chilengi, R., Akoo, P., Kerubo, C., Gitaka, J., Maingi, C., Lang, T., Olotu, A., Tsofa, B., Bejon, P., Peshu, N., Marsh, K., Owusu-Agyei, S., Asante, K.P., Osei-Kwakye, K., Boahen, O., Ayamba, S., Kayan, K., Owusu-Ofori, R., Dosoo, D., Asante, I., Adjei, G., Chandramohan, D., Greenwood, B., Lusingu, J., Gesase, S., Malabeja, A., Abdul, O., Kilavo, H., Mahende, C., Liheluka, E., Lemnge, M. et al. (2011) First results of phase 3 trial of RTS,S/AS01 malaria vaccine in African children. The New England journal of medicine 365, 1863-75.

Ali, V., Shigeta, Y., Tokumoto, U., Takahashi, Y. and Nozaki, T. (2004) An intestinal parasitic protist, Entamoeba histolytica, possesses a non-redundant nitrogen fixation-like system for iron-sulfur cluster assembly under anaerobic conditions. The Journal of biological chemistry 279, 16863-74.

Altschul, S.F., Gish, W., Miller, W., Myers, E.W. and Lipman, D.J. (1990) Basic local alignment search tool. Journal of molecular biology 215, 403-10.

Aly, A.S., Lindner, S.E., MacKellar, D.C., Peng, X. and Kappe, S.H. (2011) SAP1 is a critical post-transcriptional regulator of infectivity in malaria parasite sporozoite stages. Molecular microbiology 79, 929-39.

Aly, A.S., Mikolajczak, S.A., Rivera, H.S., Camargo, N., Jacobs-Lorena, V., Labaied, M., Coppens, I. and Kappe, S.H. (2008) Targeted deletion of SAP1 abolishes the expression of infectivity factors necessary for successful malaria parasite liver infection. Molecular microbiology 69, 152-63.

Amino, R., Giovannini, D., Thiberge, S., Gueirard, P., Boisson, B., Dubremetz, J.F., Prevost, M.C., Ishino, T., Yuda, M. and Menard, R. (2008) Host cell traversal is important for progression of the malaria parasite through the dermis to the liver. Cell host & microbe 3, 88-96.

Amino, R., Thiberge, S., Blazquez, S., Baldacci, P., Renaud, O., Shorte, S. and Menard, R. (2007) Imaging malaria sporozoites in the dermis of the mammalian host. Nature protocols 2, 1705-12.

Amino, R., Thiberge, S., Martin, B., Celli, S., Shorte, S., Frischknecht, F. and Menard, R. (2006) Quantitative imaging of Plasmodium transmission from mosquito to mammal. Nature medicine 12, 220-4.

Angelini, S., Gerez, C., Ollagnier-de Choudens, S., Sanakis, Y., Fontecave, M., Barras, F. and Py, B. (2008) NfuA, a new factor required for maturing Fe/S proteins in Escherichia coli under oxidative stress and iron starvation conditions. The Journal of biological chemistry 283, 14084-91.

Annoura, T., Ploemen, I.H., van Schaijk, B.C., Sajid, M., Vos, M.W., van Gemert, G.J., Chevalley-Maurel, S., Franke-Fayard, B.M., Hermsen, C.C., Gego, A., Franetich, J.F., Mazier, D., Hoffman, S.L., Janse, C.J., Sauerwein, R.W. and Khan, S.M. (2012) Assessing the adequacy of attenuation of genetically modified malaria parasite vaccine candidates. Vaccine 30, 2662-70.

Aurrecoechea, C., Brestelli, J., Brunk, B.P., Dommer, J., Fischer, S., Gajria, B., Gao, X., Gingle, A., Grant, G., Harb, O.S., Heiges, M., Innamorato, F., Iodice, J., Kissinger, J.C., Kraemer, E., Li, W., Miller, J.A., Nayak, V., Pennington, C., Pinney, D.F., Roos, D.S., Ross, C., Stoeckert, C.J., Jr., Treatman, C. and Wang, H. (2009) PlasmoDB: a functional genomic database for malaria parasites. Nucleic acids research 37, D539-43.

Aurrecoechea, C., Heiges, M., Wang, H., Wang, Z., Fischer, S., Rhodes, P., Miller, J., Kraemer, E., Stoeckert, C.J., Jr., Roos, D.S. and Kissinger, J.C. (2007) ApiDB: integrated resources for the apicomplexan bioinformatics resource center. Nucleic acids research 35, D427-30.

Baer, K., Klotz, C., Kappe, S.H., Schnieder, T. and Frevert, U. (2007) Release of hepatic Plasmodium yoelii merozoites into the pulmonary microvasculature. PLoS pathogens 3, e171.

Balk, J. and Pilon, M. (2011) Ancient and essential: the assembly of iron-sulfur clusters in plants. Trends in plant science 16, 218-26.

Banerjee, T., Jaijyan, D.K., Surolia, N., Singh, A.P. and Surolia, A. (2012) Apicoplast triose phosphate transporter (TPT) gene knockout is lethal for Plasmodium. Molecular and biochemical parasitology.

Baumeister, S., Wiesner, J., Reichenberg, A., Hintz, M., Bietz, S., Harb, O.S., Roos, D.S., Kordes, M., Friesen, J., Matuschewski, K., Lingelbach, K., Jomaa, H. and Seeber, F. (2011) Fosmidomycin uptake into Plasmodium and Babesia-infected erythrocytes is facilitated by parasite-induced new permeability pathways. PloS one 6, e19334.

Beck, H.P., Blake, D., Darde, M.L., Felger, I., Pedraza-Diaz, S., Regidor-Cerrillo, J., Gomez-Bautista, M., Ortega-Mora, L.M., Putignani, L., Shiels, B., Tait, A. and Weir, W. (2009) Molecular approaches to diversity of populations of apicomplexan parasites. International journal for parasitology 39, 175-89.

Beeson, J.G. and Brown, G.V. (2002) Pathogenesis of Plasmodium falciparum malaria: the roles of parasite adhesion and antigenic variation. Cellular and molecular life sciences : CMLS 59, 258-71.

Belnoue, E., Costa, F.T., Frankenberg, T., Vigario, A.M., Voza, T., Leroy, N., Rodrigues, M.M., Landau, I., Snounou, G. and Renia, L. (2004) Protective T cell immunity against malaria liver stage after vaccination with live sporozoites under chloroquine treatment. Journal of immunology 172, 2487-95.

Bender, A., van Dooren, G.G., Ralph, S.A., McFadden, G.I. and Schneider, G. (2003a) Properties and prediction of mitochondrial transit peptides from Plasmodium falciparum. Molecular and biochemical parasitology 132, 59-66.

Bender, A., van Dooren, G.G., Ralph, S.A., McFadden, G.I. and Schneider, G. (2003b) Properties and prediction of mitochondrial transit peptides from Plasmodium falciparum. Mol Biochem Parasitol 132, 59-66.

Billker, O., Lindo, V., Panico, M., Etienne, A.E., Paxton, T., Dell, A., Rogers, M., Sinden, R.E. and Morris, H.R. (1998) Identification of xanthurenic acid as the putative inducer of malaria development in the mosquito. Nature 392, 289-92.

Billker, O., Shaw, M.K., Margos, G. and Sinden, R.E. (1997) The roles of temperature, pH and mosquito factors as triggers of male and female gametogenesis of Plasmodium berghei in vitro. Parasitology 115 (Pt 1), 1-7.

Bishop, R., Musoke, A., Morzaria, S., Gardner, M. and Nene, V. (2004) Theileria: intracellular protozoan parasites of wild and domestic ruminants transmitted by ixodid ticks. Parasitology 129 Suppl, S271-83.

Blandin, S.A., Wang-Sattler, R., Lamacchia, M., Gagneur, J., Lycett, G., Ning, Y., Levashina, E.A. and Steinmetz, L.M. (2009) Dissecting the genetic basis of resistance to malaria parasites in Anopheles gambiae. Science 326, 147-50.

Borrmann, S., Adegnika, A.A., Matsiegui, P.B., Issifou, S., Schindler, A., Mawili-Mboumba, D.P., Baranek, T., Wiesner, J., Jomaa, H. and Kremsner, P.G. (2004) Fosmidomycin-clindamycin for Plasmodium falciparum Infections in African children. The Journal of infectious diseases 189, 901-8.

Boscardin, S.B., Hafalla, J.C., Masilamani, R.F., Kamphorst, A.O., Zebroski, H.A., Rai, U., Morrot, A., Zavala, F., Steinman, R.M., Nussenzweig, R.S. and Nussenzweig, M.C. (2006) Antigen targeting to dendritic cells elicits long-lived T cell help for antibody responses. The Journal of experimental medicine 203, 599-606.

Bruna-Romero, O., Hafalla, J.C., Gonzalez-Aseguinolaza, G., Sano, G., Tsuji, M. and Zavala, F. (2001) Detection of malaria liver-stages in mice infected through the bite of a single Anopheles mosquito using a highly sensitive real-time PCR. International journal for parasitology 31, 1499-502.

Butler, N.S., Schmidt, N.W., Vaughan, A.M., Aly, A.S., Kappe, S.H. and Harty, J.T. (2011) Superior antimalarial immunity after vaccination with late liver stage-arresting genetically attenuated parasites. Cell host & microbe 9, 451-62.

Bych, K., Kerscher, S., Netz, D.J., Pierik, A.J., Zwicker, K., Huynen, M.A., Lill, R., Brandt, U. and Balk, J. (2008) The iron-sulphur protein Ind1 is required for effective complex I assembly. The EMBO journal 27, 1736-46.

Carlton, J.M., Hayton, K., Cravo, P.V. and Walliker, D. (2001) Of mice and malaria mutants: unravelling the genetics of drug resistance using rodent malaria models. Trends in parasitology 17, 236-42.

Cavalier-Smith, T. (2000) Membrane heredity and early chloroplast evolution. Trends in plant science 5, 174-82.

Chahal, H.K., Dai, Y., Saini, A., Ayala-Castro, C. and Outten, F.W. (2009) The SufBCD Fe-S scaffold complex interacts with SufA for Fe-S cluster transfer. Biochemistry 48, 10644-53.

Chako, C.Z., Tyler, J.W., Schultz, L.G., Chiguma, L. and Beerntsen, B.T. (2010) Cryptosporidiosis in people: it's not just about the cows. Journal of veterinary internal medicine / American College of Veterinary Internal Medicine 24, 37-43.

Chaudhari, R., Narayan, A. and Patankar, S. (2012) A novel trafficking pathway in Plasmodium falciparum for the organellar localization of glutathione peroxidase-like thioredoxin peroxidase. The FEBS journal 279, 3872-88.

Chen, F., Mackey, A.J., Stoeckert, C.J., Jr. and Roos, D.S. (2006) OrthoMCL-DB: querying a comprehensive multi-species collection of ortholog groups. Nucleic acids research 34, D363-8.

Chitale, M., Hawkins, T., Park, C. and Kihara, D. (2009) ESG: extended similarity group method for automated protein function prediction. Bioinformatics 25, 1739-45.

Cilingir, G., Broschat, S.L. and Lau, A.O. (2012a) ApicoAP: the first computational model for identifying apicoplast-targeted proteins in multiple species of Apicomplexa. PloS one 7, e36598.

Cilingir, G., Broschat, S.L. and Lau, A.O.T. (2012b) ApicoAP: the first computational model for identifying apicoplast-targeted proteins in multiple species of Apicomplexa. PLoS ONE 7, e36598.

Claros, M.G. (1995) MitoProt, a Macintosh application for studying mitochondrial proteins. Comput Appl Biosci 11, 441-7.

Claros, M.G. and Vincens, P. (1996) Computational method to predict mitochondrially imported proteins and their targeting sequences. European journal of biochemistry / FEBS 241, 779-86.

Clyde, D.F. (1975) Immunization of man against falciparum and vivax malaria by use of attenuated sporozoites. The American journal of tropical medicine and hygiene 24, 397-401.

Cogswell, F.B. (1992) The hypnozoite and relapse in primate malaria. Clinical microbiology reviews 5, 26-35.

Creasey, A., Mendis, K., Carlton, J., Williamson, D., Wilson, I. and Carter, R. (1994) Maternal inheritance of extrachromosomal DNA in malaria parasites. Molecular and biochemical parasitology 65, 95-8.

Davidson, E.A. and Gowda, D.C. (2001) Glycobiology of Plasmodium falciparum. Biochimie 83, 601-4.

de Souza, J.B., Hafalla, J.C., Riley, E.M. and Couper, K.N. (2010) Cerebral malaria: why experimental murine models are required to understand the pathogenesis of disease. Parasitology 137, 755-72.

de Souza, J.B. and Riley, E.M. (2002) Cerebral malaria: the contribution of studies in animal models to our understanding of immunopathogenesis. Microbes and infection / Institut Pasteur 4, 291-300.

Doolan, D.L. and Hoffman, S.L. (2000) The complexity of protective immunity against liver-stage malaria. Journal of immunology 165, 1453-62.

Douradinha, B., van Dijk, M., van Gemert, G.J., Khan, S.M., Janse, C.J., Waters, A.P., Sauerwein, R.W., Luty, A.J., Silva-Santos, B., Mota, M.M. and Epiphanio, S. (2011) Immunization with genetically attenuated P52-deficient Plasmodium berghei

sporozoites induces a long-lasting effector memory CD8+ T cell response in the liver. Journal of immune based therapies and vaccines 9, 6.

Douradinha, B., van Dijk, M.R., Ataide, R., van Gemert, G.J., Thompson, J., Franetich, J.F., Mazier, D., Luty, A.J., Sauerwein, R., Janse, C.J., Waters, A.P. and Mota, M.M. (2007) Genetically attenuated P36p-deficient Plasmodium berghei sporozoites confer long-lasting and partial cross-species protection. International journal for parasitology 37, 1511-9.

Driss, A., Hibbert, J.M., Wilson, N.O., Iqbal, S.A., Adamkiewicz, T.V. and Stiles, J.K. (2011) Genetic polymorphisms linked to susceptibility to malaria. Malaria journal 10, 271.

Edgar, R.C. (2004) MUSCLE: multiple sequence alignment with high accuracy and high throughput. Nucleic acids research 32, 1792-7.

Ellis, K.E., Clough, B., Saldanha, J.W. and Wilson, R.J. (2001) Nifs and Sufs in malaria. Molecular microbiology 41, 973-81.

Fichera, M.E., Bhopale, M.K. and Roos, D.S. (1995) In vitro assays elucidate peculiar kinetics of clindamycin action against Toxoplasma gondii. Antimicrobial agents and chemotherapy 39, 1530-7.

Fichera, M.E. and Roos, D.S. (1997) A plastid organelle as a drug target in apicomplexan parasites. Nature 390, 407-9.

Fidock, D.A., Rosenthal, P.J., Croft, S.L., Brun, R. and Nwaka, S. (2004) Antimalarial drug discovery: efficacy models for compound screening. Nature reviews. Drug discovery 3, 509-20.

Fleige, T., Limenitakis, J. and Soldati-Favre, D. (2010) Apicoplast: keep it or leave it. Microbes and infection / Institut Pasteur 12, 253-62.

Foth, B.J., Ralph, S.A., Tonkin, C.J., Struck, N.S., Fraunholz, M., Roos, D.S., Cowman, A.F. and McFadden, G.I. (2003a) Dissecting apicoplast targeting in the malaria parasite Plasmodium falciparum. Science 299, 705-8.

Foth, B.J., Ralph, S.A., Tonkin, C.J., Struck, N.S., Fraunholz, M.J., Roos, D.S., Cowman, A.F. and McFadden, G.I. (2003b) Dissecting apicoplast targeting in the malaria parasite Plasmodium falciparum. Science 299, 705-8.

Franke-Fayard, B., Fonager, J., Braks, A., Khan, S.M. and Janse, C.J. (2010) Sequestration and tissue accumulation of human malaria parasites: can we learn anything from rodent models of malaria? PLoS pathogens 6, e1001032.

Frevert, U., Engelmann, S., Zougbede, S., Stange, J., Ng, B., Matuschewski, K., Liebes, L. and Yee, H. (2005) Intravital observation of Plasmodium berghei sporozoite infection of the liver. PLoS biology 3, e192.

Frevert, U., Spath, G.F. and Yee, H. (2008a) Exoerythrocytic development of Plasmodium gallinaceum in the White Leghorn chicken. International journal for parasitology 38, 655-72.

Frevert, U., Usynin, I., Baer, K. and Klotz, C. (2006) Nomadic or sessile: can Kupffer cells function as portals for malaria sporozoites to the liver? Cellular microbiology 8, 1537-46.

Frevert, U., Usynin, I., Baer, K. and Klotz, C. (2008b) Plasmodium sporozoite passage across the sinusoidal cell layer. Sub-cellular biochemistry 47, 182-97.

Friesen, J., Silvie, O., Putrianti, E.D., Hafalla, J.C., Matuschewski, K. and Borrmann, S. (2010) Natural immunization against malaria: causal prophylaxis with antibiotics. Science translational medicine 2, 40ra49.

Funes, S., Davidson, E., Reyes-Prieto, A., Magallon, S., Herion, P., King, M.P. and Gonzalez-Halphen, D. (2002) A green algal apicoplast ancestor. Science 298, 2155.

Goodman, C.D. and McFadden, G.I. (2007) Fatty acid biosynthesis as a drug target in apicomplexan parasites. Current drug targets 8, 15-30.

Gowda, D.C., Gupta, P. and Davidson, E.A. (1997) Glycosylphosphatidylinositol anchors represent the major carbohydrate modification in proteins of intraerythrocytic stage Plasmodium falciparum. The Journal of biological chemistry 272, 6428-39.

Gueirard, P., Tavares, J., Thiberge, S., Bernex, F., Ishino, T., Milon, G., Franke-Fayard, B., Janse, C.J., Menard, R. and Amino, R. (2010) Development of the malaria parasite in the skin of the mammalian host. Proceedings of the National Academy of Sciences of the United States of America 107, 18640-5.

Gunther, S., Storm, J. and Muller, S. (2009) Plasmodium falciparum: organelle-specific acquisition of lipoic acid. The international journal of biochemistry & cell biology 41, 748-52.

Gunther, S., Wallace, L., Patzewitz, E.M., McMillan, P.J., Storm, J., Wrenger, C., Bissett, R., Smith, T.K. and Muller, S. (2007) Apicoplast lipoic acid protein ligase B is not essential for Plasmodium falciparum. PLoS pathogens 3, e189.

Gwadz, R.W., Cochrane, A.H., Nussenzweig, V. and Nussenzweig, R.S. (1979) Preliminary studies on vaccination of rhesus monkeys with irradiated sporozoites of Plasmodium knowlesi and characterization of surface antigens of these parasites. Bulletin of the World Health Organization 57 Suppl 1, 165-73.

Haile, D.J., Rouault, T.A., Tang, C.K., Chin, J., Harford, J.B. and Klausner, R.D. (1992) Reciprocal control of RNA-binding and aconitase activity in the regulation of the iron-responsive element binding protein: role of the iron-sulfur cluster. Proceedings of the National Academy of Sciences of the United States of America 89, 7536-40.

Haldar, K., Murphy, S.C., Milner, D.A. and Taylor, T.E. (2007) Malaria: mechanisms of erythrocytic infection and pathological correlates of severe disease. Annual review of pathology 2, 217-49.

He, C.Y., Shaw, M.K., Pletcher, C.H., Striepen, B., Tilney, L.G. and Roos, D.S. (2001) A plastid segregation defect in the protozoan parasite Toxoplasma gondii. The EMBO journal 20, 330-9.

Heinemann, I.U., Jahn, M. and Jahn, D. (2008) The biochemistry of heme biosynthesis. Archives of biochemistry and biophysics 474, 238-51.

Hidese, R., Mihara, H. and Esaki, N. (2011) Bacterial cysteine desulfurases: versatile key players in biosynthetic pathways of sulfur-containing biofactors. Applied microbiology and biotechnology 91, 47-61.

Hill, D.E., Chirukandoth, S. and Dubey, J.P. (2005) Biology and epidemiology of Toxoplasma gondii in man and animals. Animal health research reviews / Conference of Research Workers in Animal Diseases 6, 41-61.

Hoffman, S.L., Billingsley, P.F., James, E., Richman, A., Loyevsky, M., Li, T., Chakravarty, S., Gunasekera, A., Chattopadhyay, R., Li, M., Stafford, R., Ahumada, A., Epstein, J.E., Sedegah, M., Reyes, S., Richie, T.L., Lyke, K.E., Edelman, R., Laurens, M.B., Plowe, C.V. and Sim, B.K. (2010) Development of a metabolically active, non-replicating sporozoite vaccine to prevent Plasmodium falciparum malaria. Human vaccines 6, 97-106.

Hoffman, S.L., Goh, L.M., Luke, T.C., Schneider, I., Le, T.P., Doolan, D.L., Sacci, J., de la Vega, P., Dowler, M., Paul, C., Gordon, D.M., Stoute, J.A., Church, L.W., Sedegah, M., Heppner, D.G., Ballou, W.R. and Richie, T.L. (2002) Protection of humans against malaria by immunization with radiation-attenuated Plasmodium falciparum sporozoites. The Journal of infectious diseases 185, 1155-64.

Huang, J., Mullapudi, N., Sicheritz-Ponten, T. and Kissinger, J.C. (2004) A first glimpse into the pattern and scale of gene transfer in Apicomplexa. International journal for parasitology 34, 265-74.

Hunfeld, K.P., Hildebrandt, A. and Gray, J.S. (2008) Babesiosis: recent insights into an ancient disease. International journal for parasitology 38, 1219-37.

Hunt, N.H., Grau, G.E., Engwerda, C., Barnum, S.R., van der Heyde, H., Hansen, D.S., Schofield, L. and Golenser, J. (2010) Murine cerebral malaria: the whole story. Trends in parasitology 26, 272-4.

Hviid, L., Marinho, C.R., Staalsoe, T. and Penha-Goncalves, C. (2010) Of mice and women: rodent models of placental malaria. Trends in parasitology 26, 412-9.

Ishino, T., Boisson, B., Orito, Y., Lacroix, C., Bischoff, E., Loussert, C., Janse, C., Menard, R., Yuda, M. and Baldacci, P. (2009) LISP1 is important for the egress of Plasmodium berghei parasites from liver cells. Cellular microbiology 11, 1329-39.

Ishino, T., Chinzei, Y. and Yuda, M. (2005a) A Plasmodium sporozoite protein with a membrane attack complex domain is required for breaching the liver sinusoidal cell layer prior to hepatocyte infection. Cellular microbiology 7, 199-208.

Ishino, T., Chinzei, Y. and Yuda, M. (2005b) Two proteins with 6-cys motifs are required for malarial parasites to commit to infection of the hepatocyte. Molecular microbiology 58, 1264-75.

Ishino, T., Yano, K., Chinzei, Y. and Yuda, M. (2004) Cell-passage activity is required for the malarial parasite to cross the liver sinusoidal cell layer. PLoS biology 2, E4.

James, S.P.T., Tate, P. (1938) Exo-erythrocytic schizogony in Plasmodium gallinaceum Brumpt, 1935. Parasitology 30, pp 128-138

Janouskovec, J., Horak, A., Obornik, M., Lukes, J. and Keeling, P.J. (2010) A common red algal origin of the apicomplexan, dinoflagellate, and heterokont plastids. Proceedings of the National Academy of Sciences of the United States of America 107, 10949-54.

Janse, C.J., Franke-Fayard, B., Mair, G.R., Ramesar, J., Thiel, C., Engelmann, S., Matuschewski, K., van Gemert, G.J., Sauerwein, R.W. and Waters, A.P. (2006a) High efficiency transfection of Plasmodium berghei facilitates novel selection procedures. Molecular and biochemical parasitology 145, 60-70.

Janse, C.J., Franke-Fayard, B. and Waters, A.P. (2006b) Selection by flow-sorting of genetically transformed, GFP-expressing blood stages of the rodent malaria parasite, Plasmodium berghei. Nature protocols 1, 614-23.

Janse, C.J., Ramesar, J. and Waters, A.P. (2006c) High-efficiency transfection and drug selection of genetically transformed blood stages of the rodent malaria parasite Plasmodium berghei. Nature protocols 1, 346-56.

Jayabalasingham, B., Bano, N. and Coppens, I. (2010) Metamorphosis of the malaria parasite in the liver is associated with organelle clearance. Cell research 20, 1043-59.

Jobe, O., Lumsden, J., Mueller, A.K., Williams, J., Silva-Rivera, H., Kappe, S.H., Schwenk, R.J., Matuschewski, K. and Krzych, U. (2007) Genetically attenuated Plasmodium berghei liver stages induce sterile protracted protection that is mediated by major histocompatibility complex Class I-dependent interferon-gamma-producing CD8+ T cells. The Journal of infectious diseases 196, 599-607.

Johnson, D.C., Dean, D.R., Smith, A.D. and Johnson, M.K. (2005a) Structure, function, and formation of biological iron-sulfur clusters. Annual review of biochemistry 74, 247-81.

Johnson, D.C., Dos Santos, P.C. and Dean, D.R. (2005b) NifU and NifS are required for the maturation of nitrogenase and cannot replace the function of isc-gene products in Azotobacter vinelandii. Biochemical Society transactions 33, 90-3.

Jomaa, H., Wiesner, J., Sanderbrand, S., Altincicek, B., Weidemeyer, C., Hintz, M., Turbachova, I., Eberl, M., Zeidler, J., Lichtenthaler, H.K., Soldati, D. and Beck, E. (1999) Inhibitors of the nonmevalonate pathway of isoprenoid biosynthesis as antimalarial drugs. Science 285, 1573-6.

Kalanon, M. and McFadden, G.I. (2010) Malaria, Plasmodium falciparum and its apicoplast. Biochemical Society transactions 38, 775-82.

Kalanon, M., Tonkin, C.J. and McFadden, G.I. (2009) Characterization of two putative protein translocation components in the apicoplast of Plasmodium falciparum. Eukaryotic cell 8, 1146-54.

Kenthirapalan, S., Waters, A.P., Matuschewski, K. and Kooij, T.W. (2012) Flow cytometry-assisted rapid isolation of recombinant Plasmodium berghei parasites exemplified by functional analysis of aquaglyceroporin. International journal for parasitology.

Khan, S.M., Janse, C.J., Kappe, S.H. and Mikolajczak, S.A. (2012) Genetic engineering of attenuated malaria parasites for vaccination. Current opinion in biotechnology.

Kibbe, W.A. (2007) OligoCalc: an online oligonucleotide properties calculator. Nucleic acids research 35, W43-6.

Kispal, G., Csere, P., Prohl, C. and Lill, R. (1999) The mitochondrial proteins Atm1p and Nfs1p are essential for biogenesis of cytosolic Fe/S proteins. The EMBO journal 18, 3981-9.

Kispal, G., Sipos, K., Lange, H., Fekete, Z., Bedekovics, T., Janaky, T., Bassler, J., Aguilar Netz, D.J., Balk, J., Rotte, C. and Lill, R. (2005) Biogenesis of cytosolic ribosomes requires the essential iron-sulphur protein Rli1p and mitochondria. The EMBO journal 24, 589-98.

Kitaoka, S., Wada, K., Hasegawa, Y., Minami, Y., Fukuyama, K. and Takahashi, Y. (2006) Crystal structure of Escherichia coli SufC, an ABC-type ATPase component of the SUF iron-sulfur cluster assembly machinery. FEBS letters 580, 137-43.

Klinge, S., Hirst, J., Maman, J.D., Krude, T. and Pellegrini, L. (2007) An iron-sulfur domain of the eukaryotic primase is essential for RNA primer synthesis. Nature structural & molecular biology 14, 875-7.

Kohler, S., Delwiche, C.F., Denny, P.W., Tilney, L.G., Webster, P., Wilson, R.J., Palmer, J.D. and Roos, D.S. (1997) A plastid of probable green algal origin in Apicomplexan parasites. Science 275, 1485-9.

Kooij, T.W. and Matuschewski, K. (2007) Triggers and tricks of Plasmodium sexual development. Current opinion in microbiology 10, 547-53.

Kooij, T.W., Rauch, M.M. and Matuschewski, K. (2012) Expansion of experimental genetics approaches for Plasmodium berghei with versatile transfection vectors. Molecular and biochemical parasitology.

Kordes, M., Matuschewski, K. and Hafalla, J.C. (2011) Caspase-1 activation of interleukin-1beta (IL-1beta) and IL-18 is dispensable for induction of experimental cerebral malaria. Infection and immunity 79, 3633-41.

Kumar, B., Chaubey, S., Shah, P., Tanveer, A., Charan, M., Siddiqi, M.I. and Habib, S. (2011) Interaction between sulphur mobilisation proteins SufB and SufC: evidence for an iron-sulphur cluster biogenesis pathway in the apicoplast of Plasmodium falciparum. International journal for parasitology 41, 991-9.

Kumar, K.A., Baxter, P., Tarun, A.S., Kappe, S.H. and Nussenzweig, V. (2009) Conserved protective mechanisms in radiation and genetically attenuated uis3(-) and uis4(-) Plasmodium sporozoites. PloS one 4, e4480.

Labaied, M., Harupa, A., Dumpit, R.F., Coppens, I., Mikolajczak, S.A. and Kappe, S.H. (2007) Plasmodium yoelii sporozoites with simultaneous deletion of P52 and P36 are completely attenuated and confer sterile immunity against infection. Infection and immunity 75, 3758-68.

Lackner, P., Beer, R., Heussler, V., Goebel, G., Rudzki, D., Helbok, R., Tannich, E. and Schmutzhard, E. (2006) Behavioural and histopathological alterations in mice with cerebral malaria. Neuropathology and applied neurobiology 32, 177-88.

Lamb, T.J., Brown, D.E., Potocnik, A.J. and Langhorne, J. (2006) Insights into the immunopathogenesis of malaria using mouse models. Expert reviews in molecular medicine 8, 1-22.

Larkin, M.A., Blackshields, G., Brown, N.P., Chenna, R., McGettigan, P.A., McWilliam, H., Valentin, F., Wallace, I.M., Wilm, A., Lopez, R., Thompson, J.D., Gibson, T.J. and Higgins, D.G. (2007) Clustal W and Clustal X version 2.0. Bioinformatics 23, 2947-8.

Legrand, N., Ploss, A., Balling, R., Becker, P.D., Borsotti, C., Brezillon, N., Debarry, J., de Jong, Y., Deng, H., Di Santo, J.P., Eisenbarth, S., Eynon, E., Flavell, R.A., Guzman, C.A., Huntington, N.D., Kremsdorf, D., Manns, M.P., Manz, M.G., Mention, J.J., Ott, M., Rathinam, C., Rice, C.M., Rongvaux, A., Stevens, S., Spits, H., Strick-Marchand, H., Takizawa, H., van Lent, A.U., Wang, C., Weijer, K., Willinger, T. and Ziegler, P. (2009) Humanized mice for modeling human infectious disease: challenges, progress, and outlook. Cell host & microbe 6, 5-9.

Leibundgut, M., Maier, T., Jenni, S. and Ban, N. (2008) The multienzyme architecture of eukaryotic fatty acid synthases. Current opinion in structural biology 18, 714-25.

Leon, S., Touraine, B., Ribot, C., Briat, J.F. and Lobreaux, S. (2003) Iron-sulphur cluster assembly in plants: distinct NFU proteins in mitochondria and plastids from Arabidopsis thaliana. The Biochemical journal 371, 823-30.

Li, L., Stoeckert, C.J., Jr. and Roos, D.S. (2003) OrthoMCL: identification of ortholog groups for eukaryotic genomes. Genome research 13, 2178-89.

Lill, R. (2009) Function and biogenesis of iron-sulphur proteins. Nature 460, 831-8.

Lill, R. and Muhlenhoff, U. (2006) Iron-sulfur protein biogenesis in eukaryotes: components and mechanisms. Annual review of cell and developmental biology 22, 457-86.

Lim, L. and McFadden, G.I. (2010) The evolution, metabolism and functions of the apicoplast. Philosophical transactions of the Royal Society of London. Series B, Biological sciences 365, 749-63.

Loiseau, L., Ollagnier-de-Choudens, S., Nachin, L., Fontecave, M. and Barras, F. (2003) Biogenesis of Fe-S cluster by the bacterial Suf system: SufS and SufE form a new type of cysteine desulfurase. The Journal of biological chemistry 278, 38352-9.

Macchi Bde, M., Quaresma, J.A., Herculano, A.M., Crespo-Lopez, M.E., DaMatta, R.A. and do Nascimento, J.L. (2010) Pathogenic action of Plasmodium gallinaceum in chickens: brain histology and nitric oxide production by blood monocyte-derived macrophages. Veterinary parasitology 172, 16-22.

Malkin, R. and Rabinowitz, J.C. (1966) The reconstitution of clostridial ferredoxin. Biochemical and biophysical research communications 23, 822-7.

Marsh, K., Forster, D., Waruiru, C., Mwangi, I., Winstanley, M., Marsh, V., Newton, C., Winstanley, P., Warn, P., Peshu, N. and et al. (1995) Indicators of life-threatening malaria in African children. The New England journal of medicine 332, 1399-404.

Martin, W., Stoebe, B., Goremykin, V., Hapsmann, S., Hasegawa, M. and Kowallik, K.V. (1998) Gene transfer to the nucleus and the evolution of chloroplasts. Nature 393, 162-5.

Martinsen, E.S., Perkins, S.L. and Schall, J.J. (2008) A three-genome phylogeny of malaria parasites (Plasmodium and closely related genera): evolution of life-history traits and host switches. Molecular phylogenetics and evolution 47, 261-73.

Matuschewski, K. (2006) Getting infectious: formation and maturation of Plasmodium sporozoites in the Anopheles vector. Cellular microbiology 8, 1547-56.

Matuschewski, K., Ross, J., Brown, S.M., Kaiser, K., Nussenzweig, V. and Kappe, S.H. (2002) Infectivity-associated changes in the transcriptional repertoire of the malaria parasite sporozoite stage. The Journal of biological chemistry 277, 41948-53.

McConkey, G.A., Rogers, M.J. and McCutchan, T.F. (1997) Inhibition of Plasmodium falciparum protein synthesis. Targeting the plastid-like organelle with thiostrepton. The Journal of biological chemistry 272, 2046-9.

McFadden, G.I. (1999) Plastids and protein targeting. The Journal of eukaryotic microbiology 46, 339-46.

McFadden, G.I., Reith, M.E., Munholland, J. and Lang-Unnasch, N. (1996) Plastid in human parasites. Nature 381, 482.

Menard, R. (2001) Gliding motility and cell invasion by Apicomplexa: insights from the Plasmodium sporozoite. Cellular microbiology 3, 63-73.

Menard, R. and Janse, C. (1997) Gene targeting in malaria parasites. Methods 13, 148-57.

Meunier, B., de Visser, S.P. and Shaik, S. (2004) Mechanism of oxidation reactions catalyzed by cytochrome p450 enzymes. Chemical reviews 104, 3947-80.

Mikolajczak, S.A., Sacci, J.B., Jr., De La Vega, P., Camargo, N., VanBuskirk, K., Krzych, U., Cao, J., Jacobs-Lorena, M., Cowman, A.F. and Kappe, S.H. (2011) Disruption of the Plasmodium falciparum liver-stage antigen-1 locus causes a differentiation defect in late liver-stage parasites. Cellular microbiology 13, 1250-60.

Moore, R.B., Obornik, M., Janouskovec, J., Chrudimsky, T., Vancova, M., Green, D.H., Wright, S.W., Davies, N.W., Bolch, C.J., Heimann, K., Slapeta, J., Hoegh-Guldberg, O., Logsdon, J.M. and Carter, D.A. (2008) A photosynthetic alveolate closely related to apicomplexan parasites. Nature 451, 959-63.

Mota, M.M., Pradel, G., Vanderberg, J.P., Hafalla, J.C., Frevert, U., Nussenzweig, R.S., Nussenzweig, V. and Rodriguez, A. (2001) Migration of Plasmodium sporozoites through cells before infection. Science 291, 141-4.

Mueller, A.K., Camargo, N., Kaiser, K., Andorfer, C., Frevert, U., Matuschewski, K. and Kappe, S.H. (2005a) Plasmodium liver stage developmental arrest by depletion of a protein at the parasite-host interface. Proceedings of the National Academy of Sciences of the United States of America 102, 3022-7.

Mueller, A.K., Deckert, M., Heiss, K., Goetz, K., Matuschewski, K. and Schluter, D. (2007) Genetically attenuated Plasmodium berghei liver stages persist and elicit sterile protection primarily via CD8 T cells. The American journal of pathology 171, 107-15.

Mueller, A.K., Labaied, M., Kappe, S.H. and Matuschewski, K. (2005b) Genetically modified Plasmodium parasites as a protective experimental malaria vaccine. Nature 433, 164-7.

Muhlenhoff, U. and Lill, R. (2000) Biogenesis of iron-sulfur proteins in eukaryotes: a novel task of mitochondria that is inherited from bacteria. Biochimica et biophysica acta 1459, 370-82.

Nachin, L., Loiseau, L., Expert, D. and Barras, F. (2003) SufC: an unorthodox cytoplasmic ABC/ATPase required for [Fe-S] biogenesis under oxidative stress. The EMBO journal 22, 427-37.

Nair, S.C., Brooks, C.F., Goodman, C.D., Sturm, A., McFadden, G.I., Sundriyal, S., Anglin, J.L., Song, Y., Moreno, S.N. and Striepen, B. (2011) Apicoplast isoprenoid precursor

synthesis and the molecular basis of fosmidomycin resistance in Toxoplasma gondii. The Journal of experimental medicine 208, 1547-59.

Navarro-Sastre, A., Tort, F., Stehling, O., Uzarska, M.A., Arranz, J.A., Del Toro, M., Labayru, M.T., Landa, J., Font, A., Garcia-Villoria, J., Merinero, B., Ugarte, M., Gutierrez-Solana, L.G., Campistol, J., Garcia-Cazorla, A., Vaquerizo, J., Riudor, E., Briones, P., Elpeleg, O., Ribes, A. and Lill, R. (2011) A fatal mitochondrial disease is associated with defective NFU1 function in the maturation of a subset of mitochondrial Fe-S proteins. American journal of human genetics 89, 656-67.

Nganou-Makamdop, K., van Gemert, G.J., Arens, T., Hermsen, C.C. and Sauerwein, R.W. (2012) Long term protection after immunization with P. berghei sporozoites correlates with sustained IFNgamma responses of hepatic CD8+ memory T cells. PloS one 7, e36508.

Ngonseu, E., Chatterjee, S. and Wery, M. (1998) Blocked hepatic-stage parasites and decreased susceptibility to Plasmodium berghei infections in BALB/c mice. Parasitology 117 (Pt 5), 419-23.

Nishio, K. and Nakai, M. (2000) Transfer of iron-sulfur cluster from NifU to apoferredoxin. The Journal of biological chemistry 275, 22615-8.

Nussenzweig, R.S., Vanderberg, J., Most, H. and Orton, C. (1967) Protective immunity produced by the injection of x-irradiated sporozoites of plasmodium berghei. Nature 216, 160-2.

Odom, A.R. and Van Voorhis, W.C. (2010) Functional genetic analysis of the Plasmodium falciparum deoxyxylulose 5-phosphate reductoisomerase gene. Molecular and biochemical parasitology 170, 108-11.

Okamoto, N., Spurck, T.P., Goodman, C.D. and McFadden, G.I. (2009) Apicoplast and mitochondrion in gametocytogenesis of Plasmodium falciparum. Eukaryotic cell 8, 128-32.

Orlean, P. (1990) Dolichol phosphate mannose synthase is required in vivo for glycosyl phosphatidylinositol membrane anchoring, O mannosylation, and N glycosylation of protein in Saccharomyces cerevisiae. Molecular and cellular biology 10, 5796-805.

Otto, T.D., Wilinski, D., Assefa, S., Keane, T.M., Sarry, L.R., Bohme, U., Lemieux, J., Barrell, B., Pain, A., Berriman, M., Newbold, C. and Llinas, M. (2010) New insights into the blood-stage transcriptome of Plasmodium falciparum using RNA-Seq. Molecular microbiology 76, 12-24.

Outten, F.W., Djaman, O. and Storz, G. (2004) A suf operon requirement for Fe-S cluster assembly during iron starvation in Escherichia coli. Molecular microbiology 52, 861-72.

Outten, F.W., Wood, M.J., Munoz, F.M. and Storz, G. (2003) The SufE protein and the SufBCD complex enhance SufS cysteine desulfurase activity as part of a sulfur transfer pathway for Fe-S cluster assembly in Escherichia coli. The Journal of biological chemistry 278, 45713-9.

Palacpac, N.M., Hiramine, Y., Mi-ichi, F., Torii, M., Kita, K., Hiramatsu, R., Horii, T. and Mitamura, T. (2004) Developmental-stage-specific triacylglycerol biosynthesis, degradation and trafficking as lipid bodies in Plasmodium falciparum-infected erythrocytes. Journal of cell science 117, 1469-80.

Pei, Y., Tarun, A.S., Vaughan, A.M., Herman, R.W., Soliman, J.M., Erickson-Wayman, A. and Kappe, S.H. (2010) Plasmodium pyruvate dehydrogenase activity is only essential for the parasite's progression from liver infection to blood infection. Molecular microbiology.

Pfefferkorn, E.R., Nothnagel, R.F. and Borotz, S.E. (1992) Parasiticidal effect of clindamycin on Toxoplasma gondii grown in cultured cells and selection of a drug-resistant mutant. Antimicrobial agents and chemotherapy 36, 1091-6.

Ploemen, I.H., Chakravarty, S., van Gemert, G.J., Annoura, T., Khan, S.M., Janse, C.J., Hermsen, C.C., Hoffman, S.L. and Sauerwein, R.W. (2012) Plasmodium liver load following parenteral sporozoite administration in rodents. Vaccine.

Porello, S.L., Cannon, M.J. and David, S.S. (1998) A substrate recognition role for the [4Fe-4S]2+ cluster of the DNA repair glycosylase MutY. Biochemistry 37, 6465-75.

Ralph, S.A., D'Ombrain, M.C. and McFadden, G.I. (2001) The apicoplast as an antimalarial drug target. Drug resistance updates : reviews and commentaries in antimicrobial and anticancer chemotherapy 4, 145-51.

Ralph, S.A., van Dooren, G.G., Waller, R.F., Crawford, M.J., Fraunholz, M.J., Foth, B.J., Tonkin, C.J., Roos, D.S. and McFadden, G.I. (2004) Tropical infectious diseases: metabolic maps and functions of the Plasmodium falciparum apicoplast. Nature reviews. Microbiology 2, 203-16.

Ramya, T.N., Mishra, S., Karmodiya, K., Surolia, N. and Surolia, A. (2007) Inhibitors of nonhousekeeping functions of the apicoplast defy delayed death in Plasmodium falciparum. Antimicrobial agents and chemotherapy 51, 307-16.

Rangachari, K., Davis, C.T., Eccleston, J.F., Hirst, E.M., Saldanha, J.W., Strath, M. and Wilson, R.J. (2002) SufC hydrolyzes ATP and interacts with SufB from Thermotoga maritima. FEBS letters 514, 225-8.

Raux-Deery, E., Leech, H.K., Nakrieko, K.A., McLean, K.J., Munro, A.W., Heathcote, P., Rigby, S.E., Smith, A.G. and Warren, M.J. (2005) Identification and characterization of the terminal enzyme of siroheme biosynthesis from Arabidopsis thaliana: a plastid-located sirohydrochlorin ferrochelatase containing a 2FE-2S center. The Journal of biological chemistry 280, 4713-21.

Roestenberg, M., McCall, M., Hopman, J., Wiersma, J., Luty, A.J., van Gemert, G.J., van de Vegte-Bolmer, M., van Schaijk, B., Teelen, K., Arens, T., Spaarman, L., de Mast, Q., Roeffen, W., Snounou, G., Renia, L., van der Ven, A., Hermsen, C.C. and Sauerwein, R. (2009) Protection against a malaria challenge by sporozoite inoculation. The New England journal of medicine 361, 468-77.

Roestenberg, M., Teirlinck, A.C., McCall, M.B., Teelen, K., Makamdop, K.N., Wiersma, J., Arens, T., Beckers, P., van Gemert, G., van de Vegte-Bolmer, M., van der Ven, A.J., Luty, A.J., Hermsen, C.C. and Sauerwein, R.W. (2011) Long-term protection against malaria after experimental sporozoite inoculation: an open-label follow-up study. Lancet 377, 1770-6.

Rohmer, M., Knani, M., Simonin, P., Sutter, B. and Sahm, H. (1993) Isoprenoid biosynthesis in bacteria: a novel pathway for the early steps leading to isopentenyl diphosphate. The Biochemical journal 295 (Pt 2), 517-24.

Sakurai, H. and San Pietro, A. (1985) Association of Fe-S center(s) with the large subunit(s) of photosystem I particles. Journal of biochemistry 98, 69-76.

Sato, S., Clough, B., Coates, L. and Wilson, R.J. (2004) Enzymes for heme biosynthesis are found in both the mitochondrion and plastid of the malaria parasite Plasmodium falciparum. Protist 155, 117-25.

Schilke, B., Voisine, C., Beinert, H. and Craig, E. (1999) Evidence for a conserved system for iron metabolism in the mitochondria of Saccharomyces cerevisiae. Proceedings of the National Academy of Sciences of the United States of America 96, 10206-11.

Schmidt, H. and Heinz, E. (1990) Desaturation of oleoyl groups in envelope membranes from spinach chloroplasts. Proceedings of the National Academy of Sciences of the United States of America 87, 9477-80.

Schofield, L., Villaquiran, J., Ferreira, A., Schellekens, H., Nussenzweig, R. and Nussenzweig, V. (1987) Gamma interferon, CD8+ T cells and antibodies required for immunity to malaria sporozoites. Nature 330, 664-6.

Seeber, F. (2002) Biogenesis of iron-sulphur clusters in amitochondriate and apicomplexan protists. International journal for parasitology 32, 1207-17.

Seeber, F. (2003) Biosynthetic pathways of plastid-derived organelles as potential drug targets against parasitic apicomplexa. Current drug targets. Immune, endocrine and metabolic disorders 3, 99-109.

Seeber, F. and Soldati-Favre, D. (2010) Metabolic pathways in the apicoplast of apicomplexa. International review of cell and molecular biology 281, 161-228.

Sharma, A.K., Pallesen, L.J., Spang, R.J. and Walden, W.E. (2010) Cytosolic iron-sulfur cluster assembly (CIA) system: factors, mechanism, and relevance to cellular iron regulation. The Journal of biological chemistry 285, 26745-51.

Sheiner, L., Demerly, J.L., Poulsen, N., Beatty, W.L., Lucas, O., Behnke, M.S., White, M.W. and Striepen, B. (2011) A systematic screen to discover and analyze apicoplast

proteins identifies a conserved and essential protein import factor. PLoS pathogens 7, e1002392.

Sibley, L.D. (2011) Invasion and intracellular survival by protozoan parasites. Immunological reviews 240, 72-91.

Siden-Kiamos, I. and Louis, C. (2004) Interactions between malaria parasites and their mosquito hosts in the midgut. Insect biochemistry and molecular biology 34, 679-85.

Sidjanski, S. and Vanderberg, J.P. (1997) Delayed migration of Plasmodium sporozoites from the mosquito bite site to the blood. The American journal of tropical medicine and hygiene 57, 426-9.

Silvie, O., Goetz, K. and Matuschewski, K. (2008) A sporozoite asparagine-rich protein controls initiation of Plasmodium liver stage development. PLoS pathogens 4, e1000086.

Sinden, R.E. and Hartley, R.H. (1985) Identification of the meiotic division of malarial parasites. The Journal of protozoology 32, 742-4.

Sommer, M.S., Gould, S.B., Lehmann, P., Gruber, A., Przyborski, J.M. and Maier, U.G. (2007) Der1-mediated preprotein import into the periplastid compartment of chromalveolates? Molecular biology and evolution 24, 918-28.

Spork, S., Hiss, J.A., Mandel, K., Sommer, M., Kooij, T.W., Chu, T., Schneider, G., Maier, U.G. and Przyborski, J.M. (2009) An unusual ERAD-like complex is targeted to the apicoplast of Plasmodium falciparum. Eukaryotic cell 8, 1134-45.

Stanway, R.R., Mueller, N., Zobiak, B., Graewe, S., Froehlke, U., Zessin, P.J., Aepfelbacher, M. and Heussler, V.T. (2011) Organelle segregation into Plasmodium liver stage merozoites. Cellular microbiology 13, 1768-82.

Stanway, R.R., Witt, T., Zobiak, B., Aepfelbacher, M. and Heussler, V.T. (2009) GFP-targeting allows visualization of the apicoplast throughout the life cycle of live malaria parasites. Biology of the cell / under the auspices of the European Cell Biology Organization 101, 415-30, 5 p following 430.

Stewart, M.J., Parikh, S., Xiao, G., Tonge, P.J. and Kisker, C. (1999) Structural basis and mechanism of enoyl reductase inhibition by triclosan. Journal of molecular biology 290, 859-65.

Sturm, A., Amino, R., van de Sand, C., Regen, T., Retzlaff, S., Rennenberg, A., Krueger, A., Pollok, J.M., Menard, R. and Heussler, V.T. (2006) Manipulation of host hepatocytes by the malaria parasite for delivery into liver sinusoids. Science 313, 1287-90.

Sturm, A., Graewe, S., Franke-Fayard, B., Retzlaff, S., Bolte, S., Roppenser, B., Aepfelbacher, M., Janse, C. and Heussler, V. (2009) Alteration of the parasite plasma membrane and the parasitophorous vacuole membrane during exo-erythrocytic development of malaria parasites. Protist 160, 51-63.

Sullivan, D.J., Jr., Gluzman, I.Y. and Goldberg, D.E. (1996) Plasmodium hemozoin formation mediated by histidine-rich proteins. Science 271, 219-22.

Surolia, N. and Padmanaban, G. (1992) de novo biosynthesis of heme offers a new chemotherapeutic target in the human malarial parasite. Biochemical and biophysical research communications 187, 744-50.

Surolia, N. and Surolia, A. (2001) Triclosan offers protection against blood stages of malaria by inhibiting enoyl-ACP reductase of Plasmodium falciparum. Nature medicine 7, 167-73.

Takahashi, Y. and Tokumoto, U. (2002) A third bacterial system for the assembly of iron-sulfur clusters with homologs in archaea and plastids. The Journal of biological chemistry 277, 28380-3.

Tanaka, R. and Tanaka, A. (2007) Tetrapyrrole biosynthesis in higher plants. Annual review of plant biology 58, 321-46.

Tarun, A.S., Peng, X., Dumpit, R.F., Ogata, Y., Silva-Rivera, H., Camargo, N., Daly, T.M., Bergman, L.W. and Kappe, S.H. (2008) A combined transcriptome and proteome survey of malaria parasite liver stages. Proceedings of the National Academy of Sciences of the United States of America 105, 305-10.

Tarun, A.S., Vaughan, A.M. and Kappe, S.H. (2009) Redefining the role of de novo fatty acid synthesis in Plasmodium parasites. Trends in parasitology 25, 545-50.

Thomsen-Zieger, N., Schachtner, J. and Seeber, F. (2003) Apicomplexan parasites contain a single lipoic acid synthase located in the plastid. FEBS letters 547, 80-6.

Tokumoto, U. and Takahashi, Y. (2001) Genetic analysis of the isc operon in Escherichia coli involved in the biogenesis of cellular iron-sulfur proteins. Journal of biochemistry 130, 63-71.

Tong, W.H., Jameson, G.N., Huynh, B.H. and Rouault, T.A. (2003) Subcellular compartmentalization of human Nfu, an iron-sulfur cluster scaffold protein, and its ability to assemble a [4Fe-4S] cluster. Proceedings of the National Academy of Sciences of the United States of America 100, 9762-7.

Tonkin, C.J., Foth, B.J., Ralph, S.A., Struck, N., Cowman, A.F. and McFadden, G.I. (2008) Evolution of malaria parasite plastid targeting sequences. Proceedings of the National Academy of Sciences of the United States of America 105, 4781-5.

Toso, M.A. and Omoto, C.K. (2007) Gregarina niphandrodes may lack both a plastid genome and organelle. The Journal of eukaryotic microbiology 54, 66-72.

Touraine, B., Boutin, J.P., Marion-Poll, A., Briat, J.F., Peltier, G. and Lobreaux, S. (2004) Nfu2: a scaffold protein required for [4Fe-4S] and ferredoxin iron-sulphur cluster assembly in Arabidopsis chloroplasts. The Plant journal : for cell and molecular biology 40, 101-11.

Tsuji, M., Mattei, D., Nussenzweig, R.S., Eichinger, D. and Zavala, F. (1994) Demonstration of heat-shock protein 70 in the sporozoite stage of malaria parasites. Parasitology research 80, 16-21.

Upadhyay, S.K., Misra, A., Srivastava, R., Surolia, N., Surolia, A. and Sundd, M. (2009) Structural insights into the acyl intermediates of the Plasmodium falciparum fatty acid synthesis pathway: the mechanism of expansion of the acyl carrier protein core. The Journal of biological chemistry 284, 22390-400.

van der Meer, J.Y. and Hirsch, A.K. (2012) The isoprenoid-precursor dependence of Plasmodium spp. Natural product reports 29, 721-8.

van Dijk, M.R., Douradinha, B., Franke-Fayard, B., Heussler, V., van Dooren, M.W., van Schaijk, B., van Gemert, G.J., Sauerwein, R.W., Mota, M.M., Waters, A.P. and Janse, C.J. (2005) Genetically attenuated, P36p-deficient malarial sporozoites induce protective immunity and apoptosis of infected liver cells. Proceedings of the National Academy of Sciences of the United States of America 102, 12194-9.

van Dooren, G.G., Marti, M., Tonkin, C.J., Stimmler, L.M., Cowman, A.F. and McFadden, G.I. (2005) Development of the endoplasmic reticulum, mitochondrion and apicoplast during the asexual life cycle of Plasmodium falciparum. Molecular microbiology 57, 405-19.

van Dooren, G.G., Stimmler, L.M. and McFadden, G.I. (2006) Metabolic maps and functions of the Plasmodium mitochondrion. FEMS microbiology reviews 30, 596-630.

van Dooren, G.G., Su, V., D'Ombrain, M.C. and McFadden, G.I. (2002) Processing of an apicoplast leader sequence in Plasmodium falciparum and the identification of a putative leader cleavage enzyme. The Journal of biological chemistry 277, 23612-9.

van Dooren, G.G., Tomova, C., Agrawal, S., Humbel, B.M. and Striepen, B. (2008) Toxoplasma gondii Tic20 is essential for apicoplast protein import. Proceedings of the National Academy of Sciences of the United States of America 105, 13574-9.

van Schaijk, B.C., Janse, C.J., van Gemert, G.J., van Dijk, M.R., Gego, A., Franetich, J.F., van de Vegte-Bolmer, M., Yalaoui, S., Silvie, O., Hoffman, S.L., Waters, A.P., Mazier, D., Sauerwein, R.W. and Khan, S.M. (2008) Gene disruption of Plasmodium falciparum p52 results in attenuation of malaria liver stage development in cultured primary human hepatocytes. PloS one 3, e3549.

VanBuskirk, K.M., O'Neill, M.T., De La Vega, P., Maier, A.G., Krzych, U., Williams, J., Dowler, M.G., Sacci, J.B., Jr., Kangwanrangsan, N., Tsuboi, T., Kneteman, N.M., Heppner, D.G., Jr., Murdock, B.A., Mikolajczak, S.A., Aly, A.S., Cowman, A.F. and Kappe, S.H. (2009) Preerythrocytic, live-attenuated Plasmodium falciparum vaccine candidates by design. Proceedings of the National Academy of Sciences of the United States of America 106, 13004-9.

Vanderberg, J.P. (1975) Development of infectivity by the Plasmodium berghei sporozoite. The Journal of parasitology 61, 43-50.

Varadharajan, S., Dhanasekaran, S., Bonday, Z.Q., Rangarajan, P.N. and Padmanaban, G. (2002) Involvement of delta-aminolaevulinate synthase encoded by the parasite gene

in de novo haem synthesis by Plasmodium falciparum. The Biochemical journal 367, 321-7.

Vaughan, A.M., Kappe, S.H., Ploss, A. and Mikolajczak, S.A. (2012) Development of humanized mouse models to study human malaria parasite infection. Future microbiology 7, 657-65.

Vaughan, A.M., O'Neill, M.T., Tarun, A.S., Camargo, N., Phuong, T.M., Aly, A.S., Cowman, A.F. and Kappe, S.H. (2009) Type II fatty acid synthesis is essential only for malaria parasite late liver stage development. Cellular microbiology 11, 506-20.

Vaughan, A.M., Wang, R. and Kappe, S.H. (2010) Genetically engineered, attenuated whole-cell vaccine approaches for malaria. Human vaccines 6, 107-13.

Vollmer, M., Thomsen, N., Wiek, S. and Seeber, F. (2001) Apicomplexan parasites possess distinct nuclear-encoded, but apicoplast-localized, plant-type ferredoxin-NADP+ reductase and ferredoxin. The Journal of biological chemistry 276, 5483-90.

Voza, T., Miller, J.L., Kappe, S.H. and Sinnis, P. (2012) Extrahepatic exoerythrocytic forms of rodent malaria parasites at the site of inoculation: clearance after immunization, susceptibility to primaquine, and contribution to blood-stage infection. Infection and immunity 80, 2158-64.

Wada, H., Schmidt, H., Heinz, E. and Murata, N. (1993) In vitro ferredoxin-dependent desaturation of fatty acids in cyanobacterial thylakoid membranes. Journal of bacteriology 175, 544-7.

Waller, R.F., Keeling, P.J., Donald, R.G., Striepen, B., Handman, E., Lang-Unnasch, N., Cowman, A.F., Besra, G.S., Roos, D.S. and McFadden, G.I. (1998) Nuclear-encoded proteins target to the plastid in Toxoplasma gondii and Plasmodium falciparum. Proceedings of the National Academy of Sciences of the United States of America 95, 12352-7.

Waller, R.F., Keeling, P.J., van Dooren, G.G. and McFadden, G.I. (2003) Comment on "A green algal apicoplast ancestor". Science 301, 49; author reply 49.

Waller, R.F., Reed, M.B., Cowman, A.F. and McFadden, G.I. (2000) Protein trafficking to the plastid of Plasmodium falciparum is via the secretory pathway. The EMBO journal 19, 1794-802.

Waters, A.P., Thomas, A.W., van Dijk, M.R. and Janse, C.J. (1997) Transfection of malaria parasites. Methods 13, 134-47.

Wells, T.N., Burrows, J.N. and Baird, J.K. (2010) Targeting the hypnozoite reservoir of Plasmodium vivax: the hidden obstacle to malaria elimination. Trends in parasitology 26, 145-51.

White, N.J., Turner, G.D., Medana, I.M., Dondorp, A.M. and Day, N.P. (2010) The murine cerebral malaria phenomenon. Trends in parasitology 26, 11-5.

WHO (World Health Organization) (2011) World Malaria Report 2010.

Williamson, D.H., Gardner, M.J., Preiser, P., Moore, D.J., Rangachari, K. and Wilson, R.J. (1994) The evolutionary origin of the 35 kb circular DNA of Plasmodium falciparum: new evidence supports a possible rhodophyte ancestry. Molecular & general genetics : MGG 243, 249-52.

Wilson, R.J., Denny, P.W., Preiser, P.R., Rangachari, K., Roberts, K., Roy, A., Whyte, A., Strath, M., Moore, D.J., Moore, P.W. and Williamson, D.H. (1996) Complete gene map of the plastid-like DNA of the malaria parasite Plasmodium falciparum. Journal of molecular biology 261, 155-72.

Wirth, D.F. (2002) Biological revelations. Nature 419, 495-6.

Wollers, S., Layer, G., Garcia-Serres, R., Signor, L., Clemancey, M., Latour, J.M., Fontecave, M. and Ollagnier de Choudens, S. (2010) Iron-sulfur (Fe-S) cluster assembly: the SufBCD complex is a new type of Fe-S scaffold with a flavin redox cofactor. The Journal of biological chemistry 285, 23331-41.

Wrenger, C. and Muller, S. (2004) The human malaria parasite Plasmodium falciparum has distinct organelle-specific lipoylation pathways. Molecular microbiology 53, 103-13.

Wykes, M.N. and Good, M.F. (2009) What have we learnt from mouse models for the study of malaria? European journal of immunology 39, 2004-7.

Xu, X.M., Adams, S., Chua, N.H. and Moller, S.G. (2005) AtNAP1 represents an atypical SufB protein in Arabidopsis plastids. The Journal of biological chemistry 280, 6648-54.

Xu, X.M. and Moller, S.G. (2011) Iron-sulfur clusters: biogenesis, molecular mechanisms, and their functional significance. Antioxidants & redox signaling 15, 271-307.

Yabe, T., Morimoto, K., Kikuchi, S., Nishio, K., Terashima, I. and Nakai, M. (2004) The Arabidopsis chloroplastic NifU-like protein CnfU, which can act as an iron-sulfur cluster scaffold protein, is required for biogenesis of ferredoxin and photosystem I. The Plant cell 16, 993-1007.

Yeh, E. and DeRisi, J.L. (2011) Chemical rescue of malaria parasites lacking an apicoplast defines organelle function in blood-stage Plasmodium falciparum. PLoS biology 9, e1001138.

Yu, M., Kumar, T.R., Nkrumah, L.J., Coppi, A., Retzlaff, S., Li, C.D., Kelly, B.J., Moura, P.A., Lakshmanan, V., Freundlich, J.S., Valderramos, J.C., Vilcheze, C., Siedner, M., Tsai, J.H., Falkard, B., Sidhu, A.B., Purcell, L.A., Gratraud, P., Kremer, L., Waters, A.P., Schiehser, G., Jacobus, D.P., Janse, C.J., Ager, A., Jacobs, W.R., Jr., Sacchettini, J.C., Heussler, V., Sinnis, P. and Fidock, D.A. (2008) The fatty acid biosynthesis enzyme FabI plays a key role in the development of liver-stage malarial parasites. Cell host & microbe 4, 567-78.

Zhang, B., Watts, K.M., Hodge, D., Kemp, L.M., Hunstad, D.A., Hicks, L.M. and Odom, A.R. (2011) A second target of the antimalarial and antibacterial agent fosmidomycin revealed by cellular metabolic profiling. Biochemistry 50, 3570-7.

Zhang, M., Fennell, C., Ranford-Cartwright, L., Sakthivel, R., Gueirard, P., Meister, S., Caspi, A., Doerig, C., Nussenzweig, R.S., Tuteja, R., Sullivan, W.J., Jr., Roos, D.S., Fontoura, B.M., Menard, R., Winzeler, E.A. and Nussenzweig, V. (2010) The Plasmodium eukaryotic initiation factor-2alpha kinase IK2 controls the latency of sporozoites in the mosquito salivary glands. The Journal of experimental medicine 207, 1465-74.

Zheng, L., White, R.H., Cash, V.L., Jack, R.F. and Dean, D.R. (1993) Cysteine desulfurase activity indicates a role for NIFS in metallocluster biosynthesis. Proceedings of the National Academy of Sciences of the United States of America 90, 2754-8.

Zheng, M., Wang, X., Templeton, L.J., Smulski, D.R., LaRossa, R.A. and Storz, G. (2001) DNA microarray-mediated transcriptional profiling of the Escherichia coli response to hydrogen peroxide. Journal of bacteriology 183, 4562-70.

Zhu, G., Marchewka, M.J. and Keithly, J.S. (2000) Cryptosporidium parvum appears to lack a plastid genome. Microbiology 146 (Pt 2), 315-21.

Zuegge, J., Ralph, S., Schmuker, M., McFadden, G.I. and Schneider, G. (2001) Deciphering apicoplast targeting signals--feature extraction from nuclear-encoded precursors of Plasmodium falciparum apicoplast proteins. Gene 280, 19-26.

6 Appendix

6.1 Abbreviations

A	adenosine
ACP	acyl carrier protein
A. stephensi	*Anopheles stephensi*
A. thaliana	*Arabidopsis thaliana*
ATP	adenosine trisphosphate
ATS	apicoplast targeting signal
B. bovis	*Babesia bovis*
bp	base pairs
BS	blood stages
C	cytosine
°C	degrees celcius
cat.	catalogue
CD	cluster of differentiation
cDNA	complementary DNA
CIA	cytosolic iron-sulfur protein assembly
C. parvum	*Cryptosporidium parvum*
CSP	circumsporozoite protein
C-terminal	carboxy terminal
d	days
DHFR/TS	dihydrofolate reductase-thymidilate synthetase
DMEM	Dulbecco's Modified Eagle Medium
DMSO	dimethyl sulfoxide
DNA	deoxyribonucleic acid
ECM	experimental cerebral malaria
E. coli	*Escherichia coli*
EDTA	ethylendiamine-tetraacetate
dNTP	deoxynucleoside triphosphate
DOXP	1-deoxy-D-xylulose 5-phosphate
EEF	exo-erythrocytic form
ER	endoplasmatic reticulum
FACS	fluorescence activated cell sorter

FAS II	fatty acid synthesis type II
FCS	fetal calf serum
g	gram
G	guanosine
GAP	genetically attenuated parasite
GAPDH	glyceraldeyde-3-phosphate dehydrogenase
GFP	green fluorescent protein
h	hours
hpi	hours post infection
HSP70	heat shock protein 70
ID	identification
IFA	immunofluorescence assay
IFN	interferon
IL	interleukin
IPP	isopentenyl diphosphate
ISC	iron-sulfur cluster
i.v.	intravenous
kb	kilo bases
KO	knockout
l	liter
LB medium	Luria-Broth medium
LS	liver stage
m	milli
M	molar
min	minutes
mRNA	messenger ribonucleic acid
MSP1	merozoite surface protein 1
NIF	nitrogen fixation
nm	nanometer
NMRI	Naval Medical Research Institute
N-terminal	amino terminal
No.	number
ORF	open reading frame
P.	*Plasmodium*

PALM	*Plasmodium* apicoplast protein important for liver merozoite formation
pBART	*Plasmodium berghei* adaptable recyclable transfection plasmid
PBS	phosphate buffered saline
PCR	polymerase chain reaction
PDH	pyruvate dehydrogenase
pH	potentia hydrogenii
PV	parasitophorous vacuole
PVM	parasitophorous vacuole membrane
RAS	radiation attenuated sporozoites
RNA	ribonucleic acid
qPCR	quantitative real-time PCR
rpm	rotations per minute
RT	room temperature
RT-PCR	reverse transcription polymerase chain reaction
s	seconds
SD	standard deviation
sg	salivary gland
SP	signal peptide
spp.	species
spz	sporozoite
SUF	sulfur utilization factor
T	thymidine
Taq	*Thermus aquaticus*
T. gondii	*Toxoplasma gondii*
TNF	tumor necrosis factor
TP	transit peptide
UIS	upregulated in infective sporozoites
UTR	untranslated region
V	volt
WT	wildtype

6.2 List of figures

6.3 List of tables

6.4 Selbstständigkeitserklärung

Ich erkläre hiermit, dass ich die vorliegende Arbeit selbständig und nur unter Verwendung der angegebenen Literatur und Hilfsmittel angefertigt habe. Wurden Ergebnisse in Kooperation produziert, ist dies entsprechend angegeben.

Berlin, den 26.11.2012 Joana Haußig

6.5 Publications

Articles

Joana M. Haussig, Kai Matuschewski and Taco W. A. Kooij
Inactivation of a *Plasmodium* apicoplast protein attenuates formation of liver merozoites
Molecular Microbiology, Volume 81, Issue 6, September 2011, Pages: 1511–1525

Joana M. Haussig, Kai Matuschewski, Taco W.A. Kooij
Systematic Experimental Genetics of the Iron-Sulfur Cluster Biogenesis Pathway in the *Plasmodium berghei* Apicoplast
manuscript submitted

Joana M. Haussig, Jan Burgold, Julius Clemence R. Hafalla, Kai Matuschewski, and Taco W.A. Kooij
Signatures of aging murine immune memory to cell-based malaria vaccination
manuscript in preparation

Poster presentations

Joana M. Haussig, Kai Matuschewski and Taco W.A. Kooij
A *Plasmodium berghei* apicoplast-targeted protein important for liver stage merozoite formation
6th Annual Biology and Pathology of the Malaria Parasite Conference (BioMalPar), Heidelberg, Germany, 2010

Joana M. Haussig, Kai Matuschewski and Taco W.A. Kooij
A *Plasmodium berghei* apicoplast-targeted protein important for liver stage merozoite formation
9th Annual Meeting of the Malaria Group of the Branch Anti-parasitic Chemotherapy of the Paul Ehrlich Society, Heidelberg, Germany, 2011

Joana M. Haussig, Kai Matuschewski and Taco W.A. Kooij
Systematic experimental genetics of the iron-sulfur cluster biogenesis pathway in the apicoplast of *Plasmodium berghei*
23rd Annual Molecular Parasitology Meeting (MPM), Woods Hole, USA, 2012

Berlin, November 26, 2012 Joana Haußig

Oral presentations

Joana M. Haussig, Kai Matuschewski and Taco W.A. Kooij
A *Plasmodium berghei* apicoplast-targeted protein important for liver stage merozoite formation
24. Jahrestagung der Deutschen Gesellschaft für Parasitologie und 29. Jahrestagung der Deutschen Gesellschaft für Protozoologie, Düsseldorf, Germany, 2010

Joana M. Haussig, Jan Burgold, Kai Matuschewski and Taco W.A. Kooij
Late arrest in *Plasmodium berghei* liver merozoite formation induces potent, long-lasting protection against malaria re-infection
Gemeinsame Jahrestagung der Deutschen Gesellschaft für Tropenmedizin und Internationale Gesundheit (DTG) und Deutschen Gesellschaft für Parasitologie (DGP), Heidelberg, Germany, 2012

Berlin, November 26, 2012 Joana Haußig